CHARACTERIZATION OF 14-3-3 χ PHOSPHORYLATION IN PHOSPHORUS STRESS IN ARABIDOPSIS THALIANA AND INVESTIGATION OF ACETYL-COA CARBOXYLASE REGULATION USING QUANTITATIVE MASS SPECTROMETRY

A Dissertation Presented to
The Faculty of the Graduate School
At the University of Missouri

In Partial Fulfillment
Of the Requirements for the Degree
Doctor of Philosophy

By
RASHAUN SHELAE WILSON
Dr. Jay J. Thelen, Dissertation Supervisor

MAY 2016

The undersigned, appointed by the dean of the Graduate School,
have examined the Dissertation entitled

CHARACTERIZATION OF 14-3-3 χ PHOSPHORYLATION IN PHOSPHORUS STRESS IN ARABIDOPSIS THALIANA AND INVESTIGATION OF ACETYL-COA CARBOXYLASE REGULATION USING QUANTITATIVE MASS SPECTROMETRY

Presented by
RASHAUN SHELAE WILSON

A candidate for the degree of
Doctor of Philosophy

And hereby certify that, in their opinion, it is worthy of acceptance

_____

Jay J. Thelen

_____

Bruce A. McClure

_____

Shuqun Zhang

_____

Walter Gassmann

_____

Jan A. Miernyk

ACKNOWLEDGEMENTS

First of all, I'd like to thank my mother, Gerri Balthazor, for being the biggest inspiration in my life. You encouraged me to follow my dreams and never give up, and I owe all of my accomplishments to you. I would also like to thank my father, Cody Wilson, for always reminding me to have fun in life and supporting me in all of my endeavors. To Sam Fels, thank you for your unending emotional support and encouragement. You fill my life with happiness and make each day brighter. I want to thank Dr. Matthew Salie for being an incredible colleague and friend and for your guidance and support every day. It has been a pleasure to share this journey with you. To Shad Brouillette, thank you for being the father you didn't have to be and challenging me at an early age to think critically. I would also like to thank my advisor and mentor, Dr. Jay Thelen, for the time you have invested in my scientific career and helping me strive to reach my full potential. To my family and friends, thank you for being a wonderful support system throughout the years. I wouldn't be the person I am today without all of you.

TABLE OF CONTENTS

LIST OF TABLES

Table Page

LIST OF FIGURES

Figure Page

ABSTRACT

Oilseed development involves coordination and regulation of a complex metabolic network for efficient production of storage compounds, such as fatty acids, protein, and carbohydrates. Recent advances in mass spectrometry have enabled identification of thousands of proteins and post-translational modifications in a variety of oilseed species, however, much remains to be known about their regulatory roles in seed development. A current focus in oilseed research is regulatory elucidation of these proteins and modifications, which can ultimately be applied to genetic engineering applications for higher production of storage compounds.

Several large-scale proteomics studies in oilseed species have identified multiple isoforms of a family of regulatory 14-3-3 proteins, which are known to bind and modulate the activity of phosphorylated clients. Of these isoforms, 14-3-3 χ was found to be abundant and phosphorylated during seed development in the plant model organism *Arabidopsis thaliana*. Further examination of this *Arabidopsis* isoform *in vitro* identified multiple phosphorylation sites after addition of calcium-dependent protein kinases. One site, Ser^{72}, was conserved across all 14-3-3 isoforms and positioned within the dimerization domain, suggesting possible regulatory functions for this phosphorylation event. Phosphomimetic mutation at this site reduced the regulatory activity of 14-3-3 χ *in vitro*, possibly through abrogation of client interactions or dimer destabilization.

Here we describe the characterization of 14-3-3 χ and investigate the *in vivo* role of phosphorylation at Ser^{72} in the context of phosphorus stress in *Arabidopsis*. Phosphorus is a limiting nutrient in soil, and when present at low levels, has several effects on plant growth including changes in root growth, activation of plasma membrane H^+-ATPases (AHA), and increased phosphate import into the root. As 14-3-3 proteins have previous implications in phosphorus stress, we used *Arabidopsis* 14-3-3 χ T-DNA knockout lines to investigate a role for this isoform in response to phosphorus stress adaptation. We observed altered primary root lengths and root phosphate phenotypes as well as increased expression of AHA in these mutant lines when grown in media supplemented with varying phosphate concentrations. Co-immunoprecipitation assays were also used to demonstrate 14-3-3 χ interactions with AHA in the presence and absence of phosphate in the growth media. Using these established phenotypes and interactions with AHA, we sought to investigate a functional role for 14-3-3 χ phosphorylation at Ser^{72}.

To accomplish this, stable transformation of a 14-3-3 χ T-DNA knockout line was performed with both the phosphomimetic (S^{72D}) and non-mutated (native) forms of 14-3-3 χ. Phenotypic analysis of the transgenic lines resulted in the inability of the phosphomimic to complement some phenotypes under certain phosphate-dependent growth conditions, while the native transgenic lines complemented all phenotypes under all growth conditions when both lines were compared to wild-type (Col 0) plants. However, in most cases, the phosphomimic transgenic lines did not display significant differences in

phenotypes compared to the native transgenic lines. While these results were somewhat unclear, they did suggest that 14-3-3 χ activity could be altered by this mutation *in vivo*, possibly through dimer destabilization.

To further investigate the effect of this mutation on 14-3-3 χ dimer stability, gel electrophoresis under non-denaturing conditions was performed, which displayed altered monomer/dimer ratios of 14-3-3 χ^{S72D} when compared to the non-mutated form. Pull-down assays with 14-3-3 χ^{S72A} and χ^{S72D} using *Arabidopsis* T-DNA seedling lysate revealed a reduced ability of χ^{S72D} to interact with AHA. Collectively, these results suggested that phosphomimetic mutation of 14-3-3 χ at Ser^{72} alters dimer stability, which ultimately affects interactions with client proteins.

In addition to 14-3-3 proteins, many metabolic enzymes have been identified during seed development, several of which have regulatory implications on oil production. One enzyme complex, heteromeric acetyl-CoA carboxylase (ACCase) catalyzes the committed step of *de novo* fatty acid synthesis in plastids. Although several modes of regulation have been demonstrated for this complex, the effects of protein-protein interactions have yet to be fully elucidated. We hypothesized that a newly-identified family of BADC proteins are inhibitors of the ACCase complex through protein-protein interactions and displacement of a biotin carboxyl carrier (BCCP) subunit of ACCase. The platform of this hypothesis was based on established interactions between BADC and ACCase subunits, structural similarities of BADC and BCCP, and the lack of BADC biotinylation.

To investigate this hypothesis, AQUA-multiple reaction monitoring (MRM) was employed, which is a quantitative mass spectrometry technique that uses heavy-labeled AQUA peptide standards for absolute protein quantitation. Although this technique offers several advantages, it requires extensive method development procedures to ensure accurate quantitation of target proteins of interest. Using this method, stoichiometric changes of the BADC and ACCase subunits were quantified under established regulatory conditions for ACCase. These results provide insight into the stoichiometric regulation of ACCase and indicate a potential for competitive incorporation of BADC proteins into the complex. A limiting subunit was also identified, which has potential for future genetic engineering applications to increase oil yield in crop species. Overall, this study demonstrates a quantitative method with promising applications for regulatory elucidation of complex stoichiometry in a variety of biochemical pathways and species.

CHAPTER I

REGULATION OF THE REGULATORS: POST-TRANSLATIONAL MODIFICATIONS, SUBCELLULAR AND SPATIOTEMPORAL DISTRIBUTION OF PLANT 14-3-3 PROTEINS

INTRODUCTION

The 14-3-3 proteins exist in all eukaryotes and regulate protein function generally through a direct association with phosphorylated proteins. These small, acidic proteins can function as homo- or heterodimers, and each monomer is capable of interacting with phosphorylated serine or threonine residues of binding partners. This structural characteristic allows 14-3-3 proteins to act as scaffolding molecules during signal transduction events, bringing two phosphoproteins within close proximity of one another. Of all eukaryotes, plants contain the largest number of 14-3-3 gene paralogs, which increases the combinatorial possibilities for specialized roles. Plants have developed fine-tuned mechanisms for cellular control through protein-protein interactions. 14-3-3 proteins are capable of influencing their binding partners in various ways, including their subcellular localization and enzymatic activities, which can vary in different organs, from primary metabolism to phototropism. Here, we focus on three emerging areas of 14-3-3 regulation: subcellular compartmentalization, spatiotemporal expression, and post-translational modification.

EVOLUTIONARY BACKGROUND OF 14-3-3 PROTEINS

14-3-3 proteins are ancient, eukaryotic phosphobinding proteins. The discrete arginine and lysine residues that interact with the phosphate group of 14-3-3 binding partners are conserved across eukaryotes. Membrane-bound subcellular organelles are unique to eukaryotes, and 14-3-3 proteins affect binding partners

within these compartments. Cytoplasmic sequestration of transcription factors, activation of mitochondrial enzymes, and guidance of chloroplast precursor proteins are a few examples of how 14-3-3 proteins influence these organelles.

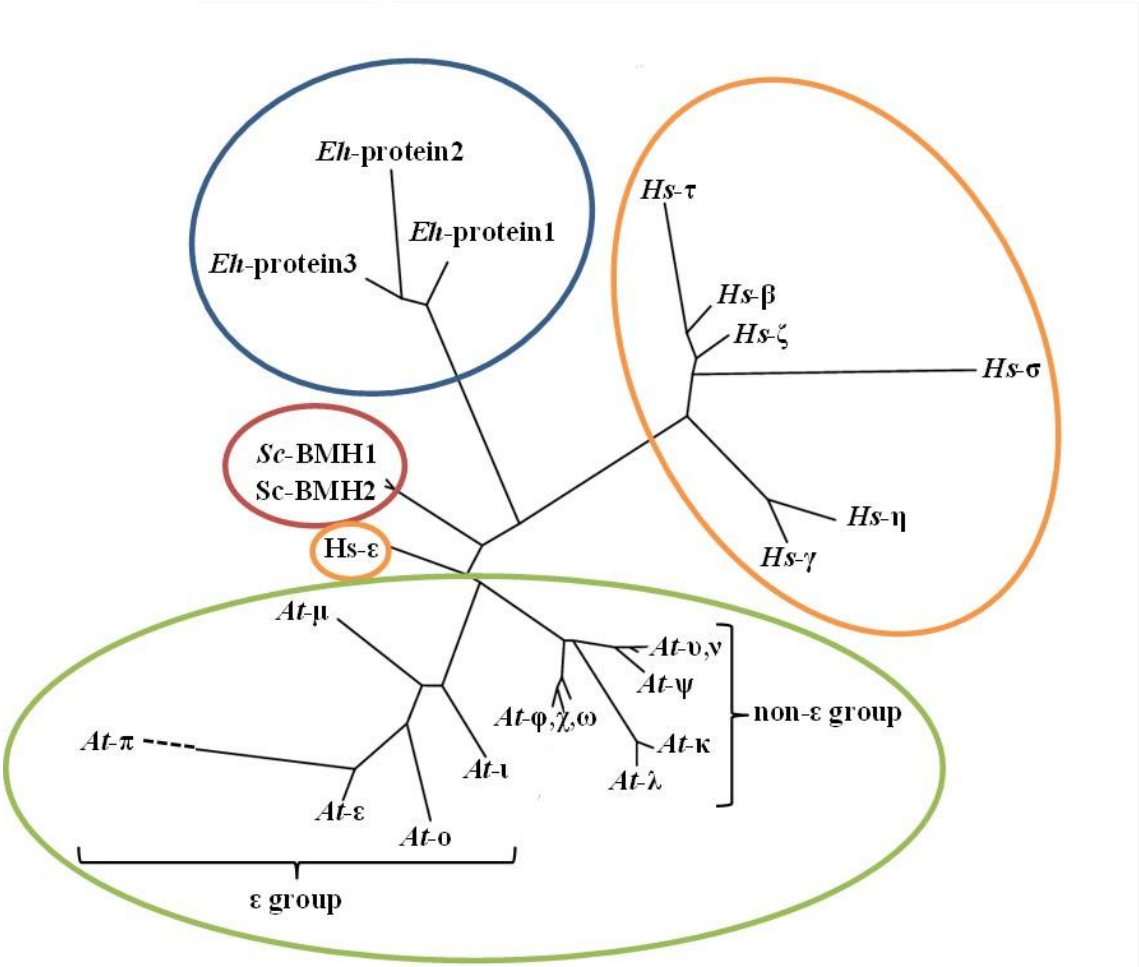

Figure 1: Phylogenetic tree of 14-3-3 paralogs from eukaryotic species. The depicted species are 1) Plantae; *Arabidopsis thaliana* (mouse-ear cress), 2) Animalia; *Homo sapiens* (human), 3) Fungi; *Saccharomyces cerevisiae* (baker's yeast), 4) Protista; *Entamoeba histolytica. Arabidopsis* 14-3-3 isoforms are divided into two distinct subgroups: epsilon (ε) and non-epsilon. The phylogenetic tree was generated with the Phylogeny.fr program (http://www.phylogeny.fr/) tree-style phylogram, using the full-length 14-3-3 protein sequences from each species.

It is also evident that 14-3-3 proteins are essential to eukaryotic function. For example, disruption of the two 14-3-3 genes (BMH1, BMH2) in yeast was reported to be lethal, but the introduction of an *Arabidopsis* 14-3-3 protein rescued this phenotype (1), suggesting a conserved functional role between plant and fungal 14-3-3 proteins.

DIMERIZATION AND PHOSPHOBINDING PARTNER RECOGNITION

All eukaryotes possess multiple 14-3-3 gene paralogs, adding functional complexity to this family of regulatory proteins. This multigenic complexity has many genomic, molecular, and biochemical characteristics, including 1) a broad range of distinct gene paralogs among eukaryotes; 2) variable spatiotemporal expression among paralogs; 3) diversity of subcellular localization; 4) variable binding partner motifs; and 5) variable 14-3-3 dimerization domains. 14-3-3 proteins interact with their binding partners through three well-defined binding motifs, which upon phosphorylation act as a target for 14-3-3 binding. These canonical 14-3-3 binding motifs include mode I - RXX(pS/pT)XP (2), mode II - RX(F/Y)X(pS)XP (2), and mode III - SW(pT)X-COOH (3). A modified mode I motif, LX(R/K)SX(pS/pT)XP, is prevalent in plants (4). In *Arabidopsis*, thirteen unique paralogs exist and can be subdivided into two distinct subgroups, epsilon and non-epsilon (Figure 1). These paralogs allow for the formation of up to 169 dimers (both homo- and heterodimers), and this variation is believed to increase their functional diversity. Mammals generally contain seven 14-3-3 paralogs, while fungi usually contain two (Figure 1). Multiple studies have assessed the

binding partner specificity of 14-3-3 gene paralogs and have found, in general, moderate changes in binding partner preference rather than an abrupt inability to interact (5), suggesting a high level of functional overlap among plant paralogs. This finding could explain how a plant 14-3-3 protein was able to rescue a lethal phenotype in yeast 14-3-3 knockout lines (1). This functional redundancy is also supported by 14-3-3 sequence conservation that exists across isoforms of many species. Variation in 14-3-3 sequence primarily occurs at the N- and C- termini, which are implicated in dimerization and binding partner entry/exit, respectively, and are thought to contribute to 14-3-3 isoform specificity (6,7).

SUBCELLULAR DYNAMICS AND FUNCTIONS OF PLANT 14-3-3 PROTEINS

Cytoplasm

Initial research suggested 14-3-3 proteins were primarily cytosolic. However, subsequent research has detected 14-3-3 proteins in nearly every other subcellular compartment, including the nucleus (8), plastid (9), cell membrane (10), and mitochondria (11). Nevertheless, binding and subsequent cytoplasmic sequestration of transcription factors is one well-characterized regulatory function of 14-3-3 proteins (Figure 2). For example, upon phosphorylation, transcription factor BZR1 and a bZIP transcriptional activator RSG are retained in the cytoplasm through binding of 14-3-3 λ, ω, and μ (12-14). Site-directed mutagenesis of the canonical 14-3-3 binding motif prevented trafficking and resulted in strong nuclear localization of these transcription factors. Functionally,

cytoplasmic sequestration of BZR1 and RSG decreased expression levels of BR-responsive and GA-biosynthesis genes, respectively (12-14).

A role for 14-3-3 proteins in the cytoplasmic environment is also evident from protein-protein interaction and cytology studies. *In vitro* pull-down assays from developing *Arabidopsis* seeds using recombinant 14-3-3 χ or ε as bait revealed that approximately 40% of identified proteins were cytoplasmic (15). Furthermore, 14-3-3 ω and φ/GFP fusion proteins were observed to be distributed throughout the cytoplasm of *Arabidopsis* trichomes and guard cells (16). A recent study demonstrated the light-dependent phosphorylation of *Arabidopsis* cytosolic invertase (CINV1) was followed by subsequent binding of 14-3-3 proteins, which enhanced the activity of invertase in root tissue (17). Collectively, these data suggest a strong role for 14-3-3 proteins in the cytoplasmic protein-protein interaction networks of plants.

Nucleus

As previously discussed, 14-3-3-mediated, transorganellar shuttling of transcription factors is a mechanism by which transcriptional activity can be repressed. Conversely, other reports have identified 14-3-3 proteins as transcriptional activators or coactivators. One of the first descriptions of enhanced transcriptional activity came from gene reporter assays in onion epithelial cells. In these assays, a 14-3-3 DNA-binding domain chimeric protein increased the transcriptional activity of a GAL4-GUS reporter gene (18). Additionally, 14-3-3 proteins can impact transcriptional activity by influencing multiprotein complex formation, as exemplified by the florigen activation complex

(FAC). Co-expression of two components of the FAC, GF14b (a rice 14-3-3 paralog) and Hd3a (a rice FLOWERING LOCUST (FT) homolog), was largely cytosolic in rice protoplasts (8). However, coexpression of a third component, OsFD1 (a bZIP transcription factor), completed the FAC, resulting in nuclear localization of all three components and increased transcript levels of OsMADS15 (an *Arabidopsis* APETALA1 homolog) (8). Despite a clear role of 14-3-3 proteins in nuclear-cytoplasmic shuttling, the mechanism by which they transition between compartments is currently debated. 14-3-3 proteins do contain a leucine-rich C-terminal helix, suggestive of a consensus nuclear export sequence that could control cytoplasmic sequestration of transcription factors (19). Other evidence suggests that internal localization signals within 14-3-3 binding partners dictate subcellular movements (20). Since evidence exists for both 14-3-3-mediated nuclear export and import, it is likely both mechanisms contribute to the localization of 14-3-3 proteins and their binding partners.

Chloroplast & mitochondria

Despite reported chloroplast and mitochondrial localization (9,11,21), the mechanisms by which 14-3-3 proteins translocate the envelope membrane is currently unknown, as plant 14-3-3 proteins do not contain canonical N-terminal plastid or mitochondrial target peptides. It is possible 14-3-3 proteins 'hitchhike' on precursor proteins during plastid or mitochondrial translocation; although, the precursor may not necessarily be the 14-3-3 binding partner *in organello*. For example, the target sequences of three tobacco chloroplast-bound precursor

proteins, the small subunit of RuBisCO, and the oxygen-evolving complex subunits OE23 and OE33 contain a modified 14-3-3 binding motif (22). Site-directed mutagenesis of this consensus motif interferes with 14-3-3 and wheat germ lysate-synthesized precursor protein associations (22). Additionally, *in vivo* isolates of the ribulose-1,5-bisphosphate carboxylase/oxygenase small subunit precursor (preSSU) revealed a large oligomeric complex (~200 kDa) between preSSU, 14-3-3 proteins, and Hsp70 (22). This multimeric complex resulted in four-fold higher plastid translocation rates when compared to monomeric preSSU, suggesting 14-3-3 proteins actively participate in the mechanisms of precursor protein import pathways (22). Whether 14-3-3 mitochondrial or chloroplast import is a consequence of a 'hitchhiking' mechanism remains unclear, but it should be considered since 14-3-3 proteins are directly involved in the import machinery of plastid precursor proteins (Figure 2).

Plasma membrane

The influence of 14-3-3 proteins extends beyond the regulation of soluble cytoplasmic proteins and into the realm of plasma membrane proteins. Proton (H^+)-ATPases and potassium (K^+) channels are two well-known plasma membrane 14-3-3 binding partners (Figure 2). Identification of the wilt-inducing phytotoxin fusicoccin receptor, a 14-3-3 protein, was a major advance in recognition of 14-3-3 associations with integral membrane proteins (23,24). This finding facilitated the discovery of 14-3-3-mediated H^+-ATPase activation, in which 14-3-3 binds to and alleviates the phosphorylated C-terminal auto-

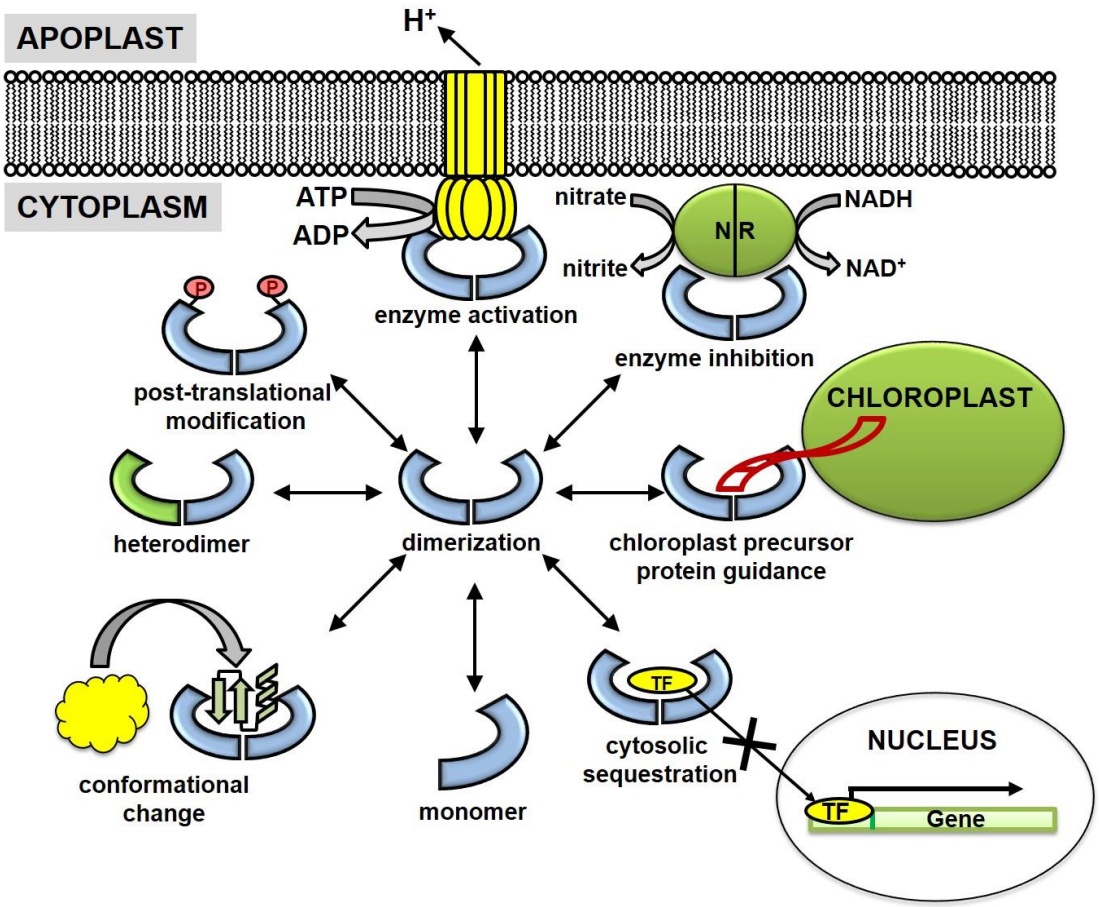

Figure 2: Cellular mechanisms of plant 14-3-3 proteins. 14-3-3 proteins are generally believed to function as dimers (hetero- and homo-dimers), although evidence also supports a functional role for 14-3-3 monomers. Several key 14-3-3 mechanisms are enzyme activation, enzyme inhibition, chloroplast precursor protein guidance, cytosolic sequestration, and conformational changes of binding partners. Post-translational modifications (PTMs) of 14-3-3 proteins (phosphorylation, acetylation, ubiquitination) have been identified but lack the functional characterization. Abbreviations: nitrate reductase (NR) and transcription factor (TF)

inhibitory domain (25,26). H^+-ATPase activation by 14-3-3 proteins also can be understood in the context of blue light-induced stomatal opening. This process is controlled through an electrochemical gradient generated by H^+ pumping and ensuing K^+ accumulation in guard cells (27). Both blue light-induced H^+-ATPase activation and 14-3-3/H^+-ATPase interactions suggest a direct role of 14-3-3

proteins in the regulation of membrane potentials (28). Indeed, 14-3-3 proteins also influence the activity of voltage-gated K^+ channels. Patch clamp assays in *Xenopus* oocytes overexpressing K^+ channel (KAT1) were conditionally activated upon injection of recombinant 14-3-3 proteins (29). Inside-out macropatch and binding assays suggest activation of KAT1 was mediated through a direct association with 14-3-3 proteins and not as a consequence of auxiliary pathways (29,30). These results provide strong evidence that 14-3-3 proteins are a positive regulator of plasma membrane-bound ion channels, but they also support a synergistic role between H^+ and K^+ transport systems, perhaps in the regulation of stomatal aperture.

Vacuolar membrane

Similar to the regulation of plasma membrane proteins, 14-3-3 proteins also influence K^+ channels in the vacuolar membrane. The vacuolar two-pore K^+ channel (TPK1) is a Ca^{2+}-activated regulator of cytoplasmic potassium levels (31,32). Similar to P-type H^+-ATPases, 14-3-3 proteins associate and activate TPK1 through a canonical 14-3-3 binding motif (32,33). In accordance with TPK1's Ca^{2+} activation, multiple Ca^{2+}-dependent protein kinases (CPKs) phosphorylate TPK1 *in vitro*, including the salt stress-activated CPK3 (33,34). Furthermore, plants treated with sodium chloride display elevated levels of TPK1 phosphorylation (33). These results suggest that, under salt-stress conditions, CPK3 phosphorylates TPK1, promoting 14-3-3-mediated activation and potassium efflux out of the vacuole. This proposed regulatory mechanism relies

on 14-3-3 proteins acting in a tripartite system to maintain ionic homeostasis within cells and suggests a functional role for 14-3-3/CPK interactions. Interestingly, preferential phosphorylation of 14-3-3 ε (Ser65) by CPK3 was previously described *in vitro* (10). Perhaps salt-stress conditions promote 14-3-3 phosphorylation by CPK3, thereby creating an additional mechanism of TPK1 regulation. Collectively, these studies support the role of 14-3-3 proteins as positive regulators of both plasma and vacuolar membrane ion homeostasis.

SPATIOTEMPORAL EXPRESSION OF 14-3-3 GENES IN ARABIDOPSIS

Seedlings

The first description of 14-3-3 expression patterns in *Arabidopsis* was performed using 14-3-3 χ promoter-driven GUS assays (35). GUS staining was primarily localized to the roots of developing seedlings but also was observed in flower buds, siliques, and the embryonic root of imbibed seeds (35). Subsequent microarray technologies allowed for a comprehensive analysis of 14-3-3 expression profiles (36,37). Not only does the amplitude of 14-3-3 expression patterns vary considerably among isoforms, but the expression trends in different tissues are variable as well (Figure 3). These data imply that 14-3-3 isoforms are constitutively expressed to maintain, or respond to, the cellular demands of plants and also can become conditionally elevated.

Examination of 14-3-3 proteins in seedlings has revealed multiple biological roles, including involvement in primary metabolism, phototropism, and cold acclimation (38-40). Of these, the role of 14-3-3 proteins in metabolism is

best described. For instance, 14-3-3 χ protein levels become elevated when supplemented with glucose, creating a delay in the transition from heterotrophic to photoautotrophic growth (40). A molecular genetic analysis of 14-3-3 isoforms (κ, χ, ψ) using both overexpression and knockout lines revealed altered levels of metabolic intermediates of glycolysis, citric acid cycle, and shikimate pathways (38). The altered metabolic intermediates in 14-3-3 overexpression lines were attributed to enzyme inhibition rather than activation; for example, phosphoenolpyruvate carboxylase (PEPCase) activity was reduced in 14-3-3 χ over-expression lines and unaltered in κ and ψ overexpression lines. A 14-3-3 χ association with PEPCase has been described in developing *Arabidopsis* seed (15). A recent study used GUS assays and qPCR analysis to demonstrate enhanced expression of 14-3-3 ψ in seedling tissue exposed to low temperatures, implicating this isoform in freezing tolerance and cold acclimation (41). However, 14-3-3 ψ knockout seedlings displayed enhanced expression of cold-induced genes, suggesting 14-3-3 ψ is a negative regulator of cold-induced gene expression in *Arabidopsis* seedling tissue.

14-3-3 proteins also have mechanistic roles in the perception of light. 14-3-3 v knockouts displayed impaired vertical hypocotyl growth, similar to phyA and phyB phytochrome mutants, suggesting that 14-3-3 v is important in red light response (42). Interestingly, 14-3-3 μ knockout lines displayed no alterations in hypocotyl growth under the same conditions (42). Furthermore, yeast two-hybrid assays revealed interaction of 14-3-3 isoforms μ and v with CONSTANS (CO), a transcriptional regulator with known involvement in the photoperiod pathway (42).

Together, these phenotypes illustrate the importance of specific 14-3-3 isoforms in the control of both primary metabolism and phototropism in seedlings.

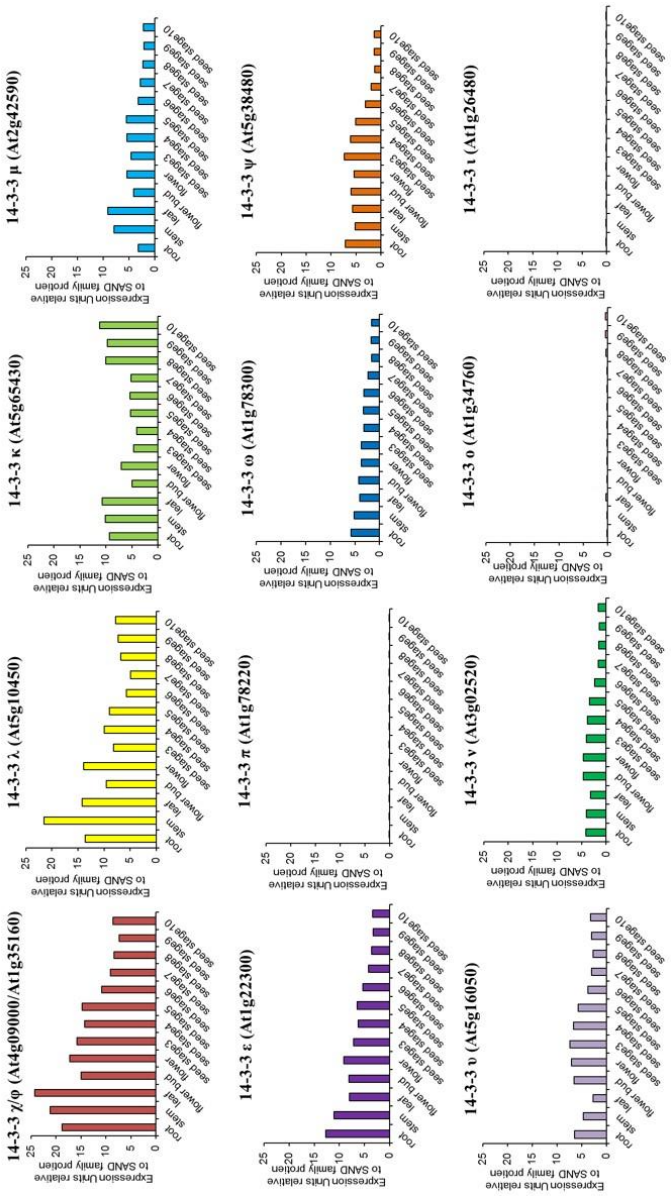

Figure 3: Organ-specific *Arabidopsis* 14-3-3 expression profiles. Gene expression data were obtained from EFP Browser. The y-axis represents raw expression units and is relative to SAND family (At2g28390) expression levels. The oligo-probe used in the microarrays cannot distinguish between 14-3-3 χ (At4g09000) and φ (At1g35160), thus the gene expression data were plotted together. The following organs were used in the analysis: root, stem, leaf, flower bud, flower, seed stage3, seed stage4, seed stage5, seed stage6, seed stage8, seed stage9, and seed stage10.

Leaves

Blue light-induced stomatal opening through phototropins (PHOT1 and PHOT2) is one mechanism by which plants regulate stomatal aperture (43). PHOT2 and 14-3-3 λ have been shown to interact through a 14-3-3 recognition motif on the kinase domain of PHOT2 (44). Furthermore, a phot1/14-3-3 λ knockout line had decreased levels of stomatal opening upon increased blue light fluence rates, while phot2/14-3-3 λ and phot1/14-3-3 κ knockout lines had no effect (45). Together, these data suggest that regulation of PHOT2-mediated stomatal opening is controlled through an isoform-specific interaction with 14-3-3 λ. Another component of blue light-induced stomatal opening is regulation of P-type H^+-ATPases (Figure 4). As described above, P-type H^+-ATPases are activated through 14-3-3 binding to the phosphorylated penultimate Thr of the autoinhibitory domain (26,28,43,46,47).

14-3-3 proteins are implicated in regulation of leaf starch accumulation through light-dependent inactivation of enzymes, such as starch synthase. Immunolocalization of *Arabidopsis* 14-3-3 proteins visualized by electron microscopy revealed 14-3-3 immunodecorated chloroplast starch granules (9). In *Arabidopsis* leaf tissues, 14-3-3 ε and μ antisense lines increased leaf starch content up to four-fold higher than wild-type plants, suggesting these isoforms (both of the ε subgroup) negatively regulate starch accumulation (Figure 4, (9)). In addition, both biotinylated recombinant 14-3-3 overlay experiments and co-immunoprecipitation assays performed with maize starch proteins revealed 14-3-3 interactions with DU1 or DU1-like members of the starch synthase III family. Interestingly, leaf starch degradation pathways were unaffected.

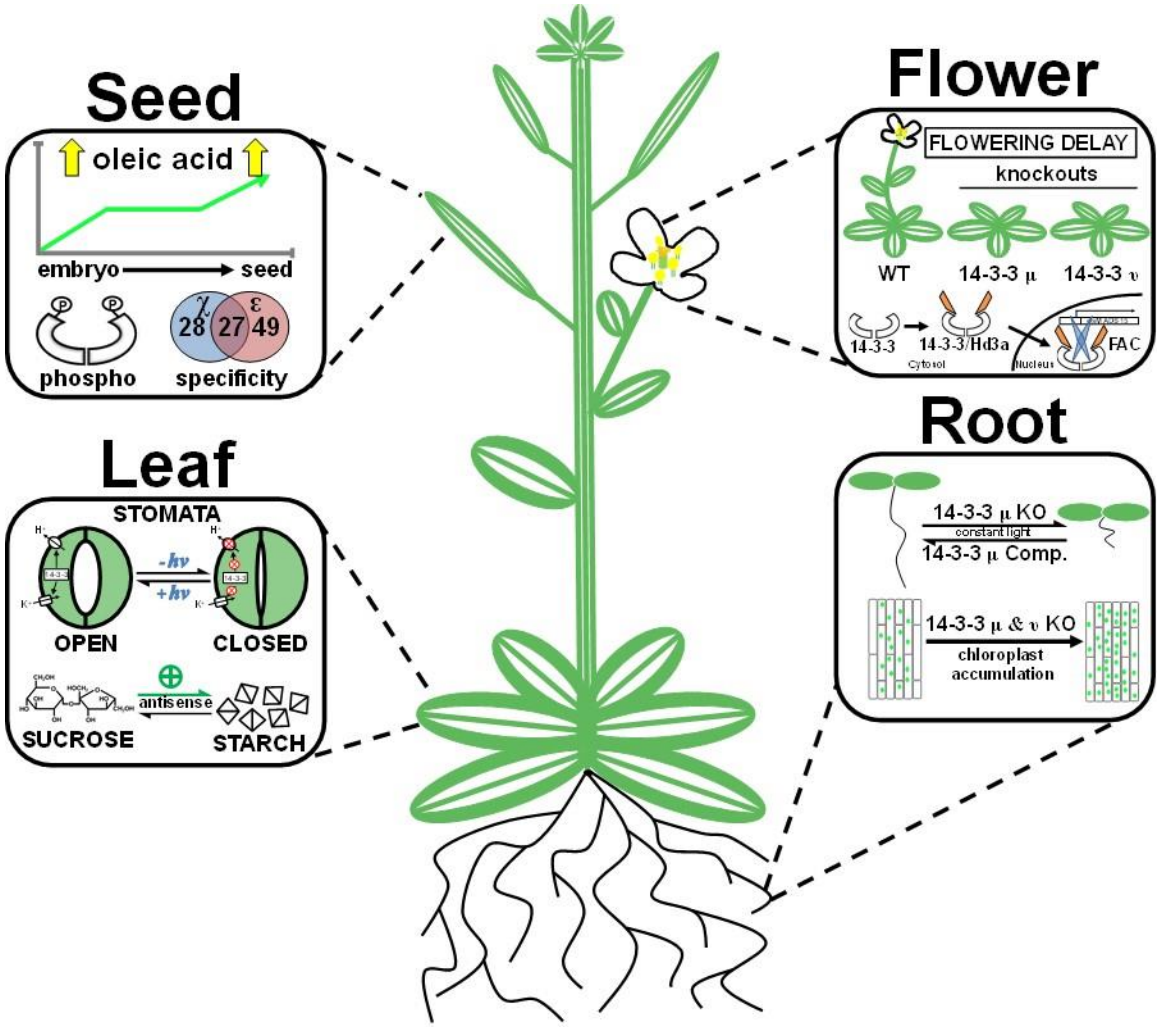

Figure 4: Organ-specific mechanisms of plant 14-3-3 proteins. The figure displays specific 14-3-3 functions across the seed, flower, leaf, and root. Seed) 14-3-3 proteins are phosphorylated, display isoform-specific interactions, and have elevated expression levels in an isogenic sunflower line bred for high oleic acid content. Flower) 14-3-3 proteins act as a positive regulator of floral development. 14-3-3 μ and υ knockouts result in a flowering delay. Additionally, rice 14-3-3 proteins create a heterohexamer florigen activation complex (FAC) with bZIP transcription factor OsFD1 and FLOWERING LOCUST (FT) homolog Hd3a, which induces expression of a gene (OsMADS15) involved in floral development. Leaf) 14-3-3 acts as a positive regulator of blue light (+*hv*) induced stomata opening by activating P-type H^+-ATPases and voltage-gated K^+ channels. 14-3-3 antisense (ε and μ) lines increase starch accumulation in leaves. Root) 14-3-3 μ knockout lines (KO) severely stunt root growth, and complementation lines (Comp.) rescue the retarded root phenotype. 14-3-3 μ and υ knockout lines increase chloroplast accumulation in roots.

The committed step of nitrogen metabolism, nitrate reductase, is controlled through a dark-dependent inactivation mechanism in mature *Spinacia oleracea* leaves, and this inhibition is strongly linked to nitrate reductase phosphorylation (48). Inactivation of nitrate reductase through phosphorylation and subsequent 14-3-3 binding is well-established in plants (5,49). Similar to seedlings, these studies reiterate the relationship between 14-3-3 proteins in phototropic responses and primary metabolism and suggest that 14-3-3 proteins negatively affect the pathways of carbon and nitrogen metabolism by preventing enzymatic activity.

Roots

The function of 14-3-3 isoforms in root development is conditional and isoform-specific. The most obvious example comes from 14-3-3 μ knockout lines, which have a ~75% reduction in root length when grown under constant light (Figure 4, (50)). Interestingly, 14-3-3 μ and ν knockout lines display increased chloroplast accumulation within roots when grown under constant white light (Figure 4, (50)). However, even this phenotype is conditional, with only the 14-3-3 μ lines displaying this phenotype under blue light conditions (50). An additional example comes from *Bradyrhizobium japonicum*-induced soybean nodulation. It was initially reported that transcript levels of soybean 14-3-3 SGF14c (the *Arabidopsis* 14-3-3 μ ortholog) become elevated in response to rhizobium-inoculation of soybeans (51). Recently, a functional role for 14-3-3 proteins in soybean nodulation has been described from RNA-mediated silencing of SGF14c and SGF14l (52). RNA interference of these two 14-3-3 paralogs impaired both

nodule development and maturation; while immature nodule formation increased by more than twenty-fold, the total number of mature nodules was reduced three-fold (52). Interestingly, this phenotype was specific, as no additional morphological changes in root anatomy were observed (52). A recent study demonstrated involvement of *Arabidopsis* 14-3-3 μ in root growth responses under mild water stress conditions (53). After treatment with polyethylene glycol, 14-3-3 μ over-expression lines displayed increased root growth and root proton extrusion as well as enhanced allocation of carbon from the shoots to the roots when compared to wild-type. Another recent study performed genetic crosses of *Arabidopsis* T-DNA lines for six different 14-3-3 genes and assessed seedling primary root lengths (54). Interestingly, the phenotypic analyses revealed decreased primary root lengths in the triple and quadruple mutants and no apparent difference in primary root lengths in single and double mutants. These results suggest involvement of multiple 14-3-3 isoforms in primary root growth and support previous reports of functional redundancy among 14-3-3 proteins. Collectively, these findings represent a growing trend of 14-3-3 paralogs in development-specific phenotypes.

Flowers

The initiation of floral development is the result of numerous biological inputs that converge to activate the reproductive phase of a plant's life cycle. Several studies have suggested 14-3-3 proteins are directly involved in floral development. Promoter-driven GUS reporter assays initially demonstrated

expression of 14-3-3 χ in multiple flower organs (i.e. petals, pistils, and stems). Later, 14-3-3 μ and v knockout lines were shown to negatively affect photoperiodic flowering under long day and short night conditions (Figure 4, (42)). However, plants grown under short day and long night conditions displayed no visual delay in floral development. A systematic phosphoproteomic screen of mature dehydrated pollen grains identified 609 phosphorylation sites (55), a significant portion of which contain 14-3-3 binding motifs, suggesting a role for 14-3-3 proteins in pollen development (55). Finally, as discussed above, 14-3-3 proteins are essential to the formation of a ternary FAC, which stimulates transcription of a floral development gene that ultimately drives floral development (8).

Developing seed

A global proteomic analysis of seed maturation identified multiple 14-3-3 isoforms in soybean (SGF14a, SGF14b, SGF14d, SGF14c), rapeseed (v, κ, ε), castor (ω, λ, v, μ, o), and *Arabidopsis* (χ, ω, λ, υ, κ, μ, ε). In *Arabidopsis*, these isoforms collectively represent as much as 1% of the entire developing seed proteome from 2D gel analyses (56). A global phosphoproteomic profiling study of *Brassica napus* seed identified two phosphorylated 14-3-3 isoforms (χ and ε), suggesting 14-3-3 phosphorylation could influence seed development (57). In a recent study performed in developing maize kernels, 77 specific binding partners were identified using affinity chromatography coupled to mass spectrometry for two 14-3-3 isoforms (58). Sixty percent of these binding partners were common

to both isoforms, and many were implicated in various cellular processes, including protein destination and storage. As further evidence of 14-3-3 proteins role in seed oil accumulation, a 2D-DIGE-based proteomic analysis of a near-isogenic sunflower line bred for high oleic acid content displayed elevated levels of 14-3-3 protein expression compared to a parental line (Figure 4, (59)). A separate study performed in developing *Arabidopsis* seed used pull-down assays with recombinant 14-3-3 χ and ε as bait to identify 104 14-3-3 binding partners, 45 of which were functionally related to metabolism (15). This comparative 14-3-3 interactome study revealed unique binding partner preferences between 14-3-3 χ and ε (Figure 4). For example, 14-3-3 χ preferentially forms heterodimers with phylogenetically similar 14-3-3 isoforms (ω, φ, ψ, ν) (15). Collectively, these studies suggest a role of 14-3-3 proteins in storage reserve deposition during seed maturation.

DISCOVERY AND FUNCTION OF 14-3-3 PHOSPHORYLATION

Since 14-3-3 proteins are phosphorylated, this post-translational modification (PTM) increases the number of protein variants in a potentially functional manner. The first description of plant 14-3-3 phosphorylation came from a systematic study of phosphoproteins in developing seed of *Brassica napus* (57). Using high-resolution 2D gels coupled to total and phosphoprotein multiplexed staining, it was discovered that 14-3-3 χ and ε are both phosphorylated (57). Later, another phosphoproteomic study comparing knockout and overexpression lines of SnRK2.8 revealed differential phosphorylation of 14-3-3 κ and χ in

Arabidopsis root tissues (60). In total, seventeen *in vivo* 14-3-3 phosphorylation sites on eight unique isoforms have been described (61-65).

Further characterization of 14-3-3 phosphorylation through *in vitro* kinase assays revealed candidate protein kinases for *in vivo* phosphorylation sites. For instance, SnRK2.8 phosphorylated 14-3-3 κ and χ at Ser93 and Ser95, respectively. Additionally, multiple sites on 14-3-3 χ (Ser72, Ser88, Ser125, Thr156) and ε (Thr18, Ser65, Thr244) were phosphorylated by CPKs (CPK1, 3, 6, 8, 24, 28), none of which overlapped with SnRK2.8 (10). Furthermore, one phosphorylation site, ε-Thr18, was unique to this isoform.

Despite *in vitro* and *in vivo* evidence of 14-3-3 phosphorylation, only recently has a functional role begun to emerge. In one study, 14-3-3 phosphorylation disrupted an association between 14-3-3 and CPK3, facilitating proteasomal degradation of CPK3 (66). Site-directed mutagenesis of a 14-3-3 phosphorylation site on 14-3-3 χ (Ser72 to Asp) prevented inhibition of nitrate reductase (10). Similarly, phosphorylation of 14-3-3 ω at Ser62 and Ser67 caused destabilization of dimer formation *in vitro* (67). Interestingly, Ser67 of 14-3-3 ω aligns with Ser72 of 14-3-3 χ, and this residue is conserved across all isoforms. Collectively, these data suggest a general mechanism of functional phosphorylation for the *Arabidopsis* 14-3-3 isoforms, specifically by reducing the affinity for binding partner interactions possibly through dimer destabilization.

Although our understanding of 14-3-3 phosphorylation is limited, evidence suggests phosphorylation of semi-conserved residues by unique kinases could

contribute to their functional diversity in plants. While additional PTMs on plant 14-3-3 proteins have been identified, including ubiquitination and Lys-acetylation, their functional significance is even less clear than phosphorylation, though speculation is centered on proteasomal degradation pathways (9,68).

CONCLUDING REMARKS

This review highlighted recent advances in the plant 14-3-3 field regarding regulation at the spatiotemporal and subcellular levels as well as post-translational modification. The large number of isoforms expressed in plants, coupled to their redundant involvement in an intricate web of interactions, reveals the complexity of plant 14-3-3 research at present. At the cellular level, 14-3-3 proteins regulate the localization and function of their binding partners by means of physical occlusion, scaffolding, or altered conformational changes. While the immediate impact of these protein associations is often clear, their downstream effects are frequently ambiguous. In tissues, isoform-specific 14-3-3 knockout and overexpression can visually affect specific developmental stages. However, these phenotypes are often conditional and subtle, which is likely a result of 14-3-3 functional redundancy. Furthermore, discovery of 14-3-3 phosphorylation presents an additional area of future focus, as several studies have identified 14-3-3 phosphorylation sites *in planta*. Currently, the known effects of 14-3-3 phosphorylation are few and include altered monomer/dimer ratios and disruption of binding partner interactions. The need for further investigation is apparent, as the effects of this modification on 14-3-3 regulation and function appear to be substantial.

CHAPTER II

ARABIDOPSIS 14-3-3 X ISOFORM DISPLAYS REGULATORY ROLES IN PHOSPHORUS STRESS THROUGH INTERACTIONS WITH PLASMA MEMBRANE H^+-ATPASES

INTRODUCTION

Phosphorus stress is of high agricultural importance, as it is one of the most limiting nutrients in the soil, largely due to its poor mobility (69,70). There are several characteristic plant responses to phosphorus stress adaptation including changes in root system architecture and altered gene and protein expression, and enzyme activity (69-71). Protein expression is altered in a tissue-specific and temporal manner to allow for phosphate recycling, reallocation, and import. For instance, phosphatases and phosphate transporters are up-regulated to help recycle internal phosphate and transfer phosphate from the soil or vegetative tissue to the root (69,71,72). Additionally, root plasma membrane H^+-ATPases (AHA) have been implicated in plant adaptation to phosphorus stress (71,73). In one study, AHA activity and root phosphate uptake were increased in AHA overexpression lines compared to wild-type when grown under phosphate-limiting conditions (73). AHA proteins help acidify the soil around the root, converting organic phosphate (P_o) in the soil to inorganic phosphate (P_i), which is the soluble form taken up by plants (69). Furthermore, AHA generates an electrochemical gradient across the plasma membrane, driving P_i transport into root cells (69,71).

The 14-3-3 proteins are phosphoprotein binding regulatory proteins, which have been implicated in a wide variety of biotic and abiotic stresses in plants. Several studies suggest 14-3-3 proteins are involved in phosphorus stress in *Arabidopsis* (74,75). One study in *Arabidopsis* seedlings demonstrated persistent starch accumulation in a 14-3-3 null mutant (grf9) compared to wild-

type (Col-0) after transfer from phosphate-limiting media to phosphate-sufficient media (74). A later report in *Solanum lycopersicum* revealed altered 14-3-3 transcript levels in plants exposed to phosphate-limiting conditions (75). In this study, expression of a 14-3-3 gene (TFT6) was down-regulated in leaves after eight days of low phosphate treatment, while expression of a different 14-3-3 gene (TFT7) was up-regulated in root tissue 24 hours after low phosphate treatment. Furthermore, *Arabidopsis* TFT7 overexpression lines displayed an increase in AHA activity and root proton extrusion under both low phosphate and phosphate-sufficient conditions (75). These results suggest 14-3-3 proteins are involved in adaptation to phosphorus stress in a spatiotemporal manner, and demonstrates phosphate-dependent activation of H^+-ATPases by 14-3-3 proteins.

Several 14-3-3 client proteins have been identified in plants including sucrose phosphate synthase, nitrate reductase, and plasma membrane H^+-ATPases (76-78). Interactions with the plasma membrane H^+-ATPase family AHA have been widely established in plants (47,79-81). Reports have demonstrated binding of 14-3-3 proteins to a phosphorylated C-terminal canonical motif (YpTV) in a regulatory manner, an interaction enhanced by the addition of fungal toxin fusicoccin (78,81-84). 14-3-3 interaction with AHA alters the conformation of the auto-inhibitory C-terminal region of AHA, thereby activating the H^+-ATPase (26,85).

The 14-3-3 proteins not only bind phosphorylated proteins, but are phosphorylated themselves. Several reports have identified 14-3-3

phosphorylation sites both *in vitro* and *in vivo*, although the functional role(s) of these modifications *in planta* are still emerging. A recent report revealed phosphorylation of 14-3-3 isoforms χ and ε by six different calcium-dependent protein kinases (CPKs) *in vitro* (10). In this study, *in vitro* activity assays demonstrated that mutation of Ser^{72} to aspartate on 14-3-3 χ, a site conserved across all isoforms and located within the dimerization domain, repressed previously-characterized 14-3-3 χ inhibition of phosphorylated nitrate reductase (pNR). Another study demonstrated phosphorylation of 14-3-3 ω at Ser^{62} and Ser^{67} resulted in destabilization of dimer formation *in vitro*. Ser^{67} of 14-3-3 ω corresponds to Ser^{72} of 14-3-3 χ (67). Furthermore, phosphorylation of Tyr^{137} on the maize 14-3-3 isoform GF14-6 reduced the affinity of an H^+-ATPase peptide *in vitro* and interactions with H^+-ATPase *in planta* (86). A host of studies have demonstrated additional phosphorylation events on 14-3-3 isoforms from *A. thaliana*, *B. napus*, and *O. sativa* (57,61-65,87). For instance, a large-scale *in vivo* phosphoproteomic study performed in developing seeds of *B. napus* identified differential phosphorylation of 14-3-3 isoforms χ and ε (57). Collectively, these results suggest the need for additional functional analysis of 14-3-3 phosphorylation sites. Several possible roles of phosphorylation include affecting dimer formation, alteration of client protein interactions, and altered client entry and exit to and from the 14-3-3 phospho-binding cleft.

Based on previous evidence that 14-3-3s are involved in phosphorus stress, we investigated a role for 14-3-3 isoform χ under this condition. The observed phenotypes in 14-3-3 χ T-DNA mutant lines such as altered primary

root growth and primary root phosphate content were used to determine the function of 14-3-3 χ phosphorylation *in vivo*. We have demonstrated a functional role for 14-3-3 χ phosphorylation at Ser^{72}, a conserved site among 14-3-3 isoforms and located within the 14-3-3 dimerization domain. Collectively, these results demonstrate 14-3-3 χ involvement in phosphate mobilization via interaction with AHA and suggest a possible general post-translational regulatory mechanism for the 14-3-3 family in plants.

MATERIALS AND METHODS

14-3-3 χ T-DNA mutant lines

Two independent mutant lines were obtained from ABRC (Arabidopsis Biological Resource Center, Ohio State University) and designated *14-3-3 χ-1* (Salk-018664) and *14-3-3 χ-2* (Salk-142285).

RT-PCR

RNA was isolated from 8 d-old *Arabidopsis* seedlings grown on ½ Murashige and Skoog (MS) agar plates under 24 h light conditions. cDNA was synthesized via M-MLV reverse transcriptase (Promega, Madison, WI) using Oligo (dT) 15 primers (Promega). Gene-specific primers were designed and synthesized by Sigma (St. Louis, MO). PCR was performed using in-house recombinantly-expressed Taq polymerase (HPLC-purified) and an annealing temperature of

55°C (35 cycles) in a thermocycler (Eppendorf, Hamburg, Germany, Model no. 5345).

Immunoblot analysis

Arabidopsis seedlings were grown for 8 days on either ½ MS agar plates or in liquid media. Seedlings (50) were ground with a plastic micropestle in 6X SDS sample buffer [0.35 M Tris-HCl pH 6.8, 0.35 M SDS, 30% (v/v) glycerol, 5% (w/v) SDS] on ice. Samples were heated for 5 min at 70°C and centrifuged at 9,000 x g in a tabletop centrifuge (Eppendorf). Protein (lysate) was quantified using the Bradford method (Bio-Rad Laboratories, Hercules, CA) using bovine gamma globulin standard as a standard. Proteins (50 µg) were resolved by SDS-PAGE (13% (w/v) acrylamide) and transferred onto a PVDF membrane (Millipore, Billerica, MA). Membranes were stained with Ponceau S and imaged before incubating in blocking buffer [5% (w/v) milk, phosphate buffered saline-Tween media (PBST) [10 mM NaH_2PO_4 pH 7.2, 150 mM NaCl, 0.3% (v/v) Tween 20,], (25°C, 1 h). Membranes were probed with a 1:10,000 dilution of primary antibody/blocking buffer at 4°C for 16 h. Membranes were washed twice with PBST and incubated in a 1/1,000 dilution of goat anti-rabbit HRP-conjugated secondary antibody (Southern Biotech, Birmingham, AL)/PBST at 25°C for 1 h. Western blot quantitation was performed using ImageQuant TL v8.1 software (GE Healthcare Life Sciences, Pittsburgh, PA).

Liquid media growth assay

Arabidopsis seeds (50) were sterilized by incubation in a solution of 50% (v/v) bleach, 1% (v/v) Triton X-100 for 10 min and washed five times with sterile water Seedlings were stored in sterile water in the dark for 3 d at 4°C. Erlenmeyer flasks (250 mL) were washed with phosphate-free detergent and autoclaved. Liquid growth media were prepared from a modified Hoagland media protocol containing no phosphate, 1 mM ammonium phosphate, or 1 mM potassium phosphate. Sterilized media (50 mL) were put into individual flasks, and seeds (50) were added to each flask sterilely. Seedlings were grown for 8 d on a C10 platform shaker (New Brunswick Scientific, Hamburg, Germany) at 130 rpm at 25°C with 24 h light.

Root phosphate quantitation

Arabidopsis roots were removed from 8 d-old seedlings grown in liquid media. Seedling fresh weight was recorded on an XS105 Dual Range analytical balance (Mettler Toledo, Columbus, OH). Roots were rinsed briefly in distilled, deionized water and dried in an incubator at 55°C for 2 d. A standard curve of potassium phosphate was prepared in triplicate. A 1:6 reaction mixture of Reagent 1 [10% (w/v) ascorbic acid]: Reagent 2 [0.42% (w/v) ammonium molybdate·tetrahydrate in 1 N H_2SO_4] was added to dried roots and potassium phosphate standards. Reactions were incubated at 37°C for 1 h. Spectroscopy was performed in a 96 well plate using a plate reader at 720 nm absorbance (BioTek, Winooski, VT).

Recombinant protein expression

The 14-3-3 χ coding sequence was PCR amplified in-frame from *Arabidopsis* cDNA and subcloned into expression vectors via the Gateway cloning system (Invitrogen, Carlsbad, CA). Recombinant constructs were transformed into *E.coli* strain BL21 cells. Proteins were expressed and purified as previously described using Ni-NTA affinity chromatography (15). Protein was quantified using a modified Bradford assay with a bovine gamma globulin standard (Bio-Rad Laboratories).

Blue Native Gel Electrophoresis

Blue native (BN) gel electrophoresis was accomplished using a gradient of 3.2-8% (w/v) acrylamide. Gradient was produced by a Miniplus 2 peristaltic pump (Gilson Inc., Middleton, WI). The BN separating gel mixtures contained 50 mM BN buffer [150 mM Tris-HCl pH 7.0, 200 mM ε-aminocaproic acid] in the presence of 3.2 or 8% (w/v) acrylamide. Protein samples (5 µg) were added to 30 µL of 1X non-denaturing sample buffer and kept on ice. Gels were run at constant amperage (10 mA, 4°C, 2 h).

Complementation of 14-3-3 χ T-DNA mutant lines

Cloning for complementation was performed using *Arabidopsis* Col-0 genomic DNA (gDNA) from 8 d-old seedlings as a template for amplification. The 14-3-3 χ gene was amplified in frame with its native promoter and 3' UTR using sense

primer 5’-CACCAACATTTTTGCTCTCT-3’ and anti-sense primer 5’-GGACAAGAATTAGACTGCC-3’. The Gateway cloning system (88) was utilized by directional cloning of the PCR product into a pENTR/D-TOPO vector (Life Technologies, Carlsbad, CA). The product was then subcloned into a pEarleyGate 301 vector (89) using the LR clonase reaction (Life Technologies). All site-directed mutagenesis was performed prior to the LR clonase reaction via a QuikChange II mutagenesis kit (Agilent Technologies, Santa Clara, CA). Site-directed mutagenesis of 14-3-3 χ Ser^{72} to Asp^{72} was accomplished using sense primer 5'-AGCTCGTCGTGCTTCGTGGAGAATCATTGATTCGATCGAACAAAAG-3' and anti-sense primer 5'-CTTTTGTTCGATCGAATCAATGATTCTCCACGAAGCACGACGAGCT-3'. The subcloned destination vector was transformed into *Agrobacterium tumefaciens* GV3101 strains. Floral dipping was performed in the *Arabidopsis 14-3-3 χ-1* background as previously described (90). Transformed plants were selected with Basta spray, and T_4 generation lines were used for phenotypic analyses.

Antibody production

Polyclonal antibodies for 14-3-3 isoforms χ and ε were produced in New Zealand white rabbits using purified recombinant proteins (Cocalico Biologicals, Reamstown, PA). Polyclonal antibody against AHA proteins was obtained from Agrisera Antibodies (Vännäs, Sweden).

14-3-3 χ co-immunoprecipitation assays

Protein A beads (10 µL) (Sigma Aldrich, St. Louis, MO) were added to a 1.5 mL polypropylene tube. Beads were washed three times with immunoprecipitation buffer (50 mM HEPES-KOH pH 8.0, 2 mM EDTA, 2 mM dithiothreitol (DTT), 10% (v/v) glycerol) (1 mL). Immunoprecipitation buffer (150 µL) was added to beads. Anti-rabbit 14-3-3 χ primary antibody (1 µL) was added to half of tubes and incubated at RT for 1 h. Beads were washed three times in immunoprecipitation buffer (200 µL). Plant tissue was homogenized with a ceramic mortar and pestle in 4 mL immunoprecipitation buffer on ice. Lysate was centrifuged at 2000 xg at 4°C for 5 mins. Plant lysate (1 mL) was added to each tube. One tube per treatment contained only plant lysate (no beads or antibody) to be used as a protein input. Tubes were incubated for 3 hours on rotary agitator at 4°C. Lysate was removed from beads, and beads were washed three times with immunoprecipitation buffer (1 mL). Protein was eluted from beads with 6X SDS sample buffer (0.35 M Tris-HCl pH 6.8, 0.35 M SDS, 30% (v/v) glycerol, 5% (w/v) SDS). Lysate (30 µL) was added to 30 uL 6X SDS sample buffer. Samples were heated at 60°C for 5 min prior to gel electrophoresis. Immunoblot analysis was performed using 14-3-3 χ and AHA primary antibodies.

14-3-3 pull-down assays

Recombinantly-purified His-tagged protein (10 µg) was added to a Ni-NTA column and incubated for 1 h at 4°C. *Arabidopsis 14-3-3 χ-2* seedlings were

grown for 8 d on ½ strength Murashige and Skoog (MS) plates. Seedlings were homogenized in immunoprecipitation buffer (1 mL). Samples were centrifuged in tabletop centrifuge (4°C, 10 min, 2,000 xg). Lysate was added to beads and incubated on a rotary agitator (4°C, 3 h). Beads were washed 3 times with immunopreciptation buffer (1 mL). Protein was eluted with imidazole (200 mM). Samples were heated at 60°C for 5 min prior to gel electrophoresis. Immunoblot analysis was performed using 14-3-3 χ and AHA primary antibodies.

RESULTS

Characterization of 14-3-3 χ T-DNA mutant lines

Two independent *Arabidopsis* T-DNA mutant lines were obtained from ABRC and designated *14-3-3 χ-1* (Salk-018664) and *14-3-3 χ-2* (Salk-142285). These lines differ in the location of the T-DNA insertion in the 14-3-3 χ gene, as *14-3-3 χ-1* has an insertion within the third exon, while *14-3-3 χ-2* has an insertion within the first exon (Figure 5A). To ensure that 14-3-3 χ protein abundance was reduced or absent in the T-DNA lines, immunoblot analysis was performed using a 14-3-3 χ-specific polyclonal antibody (Figure 5B). Immunoblot analysis of *Arabidopsis* seedlings revealed substantially reduced 14-3-3 χ abundance in the mutant lines compared to wild-type (Col-0). Abundance of 14-3-3 isoform ε was unaltered in the mutant lines compared to wild-type. It is uncertain which portion of the 14-3-3 χ protein the antibody recognizes, therefore, RT-PCR was performed to determine if partial 14-3-3 χ transcript was present in mutant lines, which could lead to variable phenotypes. This experiment was also necessary

due to the fact that the T-DNA insertions reside in different locations for each line. RT-PCR analysis revealed partial 14-3-3 χ transcript (up to 549 bp) in the *14-3-3 χ-1* line, while no transcript accumulation was detected in the *14-3-3 χ-2* line (Figure 5C).

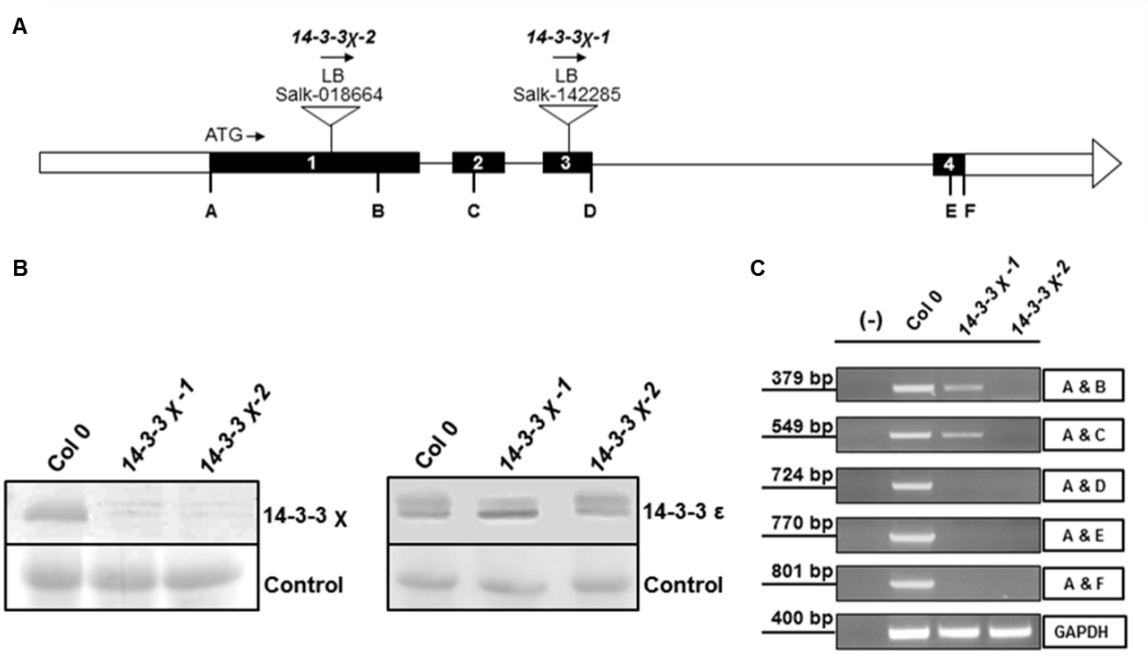

Figure 5: Characterization of 14-3-3 χ T-DNA mutant lines. **A)** 14-3-3 χ gene map showing the location of T-DNA insertions for mutant lines. **B)**Immunoblot analysis of 8 day old seedlings using a 14-3-3 χ antibody. Ponceau S staining was used as a loading control. **C)** RT-PCR analysis of 14-3-3 χ transcript levels using primers designed along different regions of the 14-3-3 χ gene (A-F). RNA was extracted from 8 day-old Col-0 and T-DNA mutant seedlings. GAPDH was used as a control to assess cDNA quality. White boxes represent primer pairs used during RT-PCR analysis, which correspond to regions in the 14-3-3 χ gene labeled in (A).

Primary root length is altered in 14-3-3 χ T-DNA mutant lines under varying phosphate levels

To determine if 14-3-3 χ has a phosphate response phenotype in roots, primary root lengths were measured after growing *Arabidopsis* seedlings in liquid media absent of phosphate or supplemented with a phosphate source, including ammonium phosphate and potassium phosphate (Figure 6). The primary root lengths of the T-DNA lines were significantly increased compared to wild-type (Col-0) when grown in phosphate-limiting media. In contrast, mutant seedlings grown in media supplemented with ammonium phosphate displayed significantly shorter primary roots compared to wild-type. The primary root lengths of *14-3-3 χ-2* seedlings grown in media supplemented with potassium phosphate remained relatively unaffected, however, *14-3-3 χ-1* primary root lengths were significantly shorter compared to wild-type. Overall, primary root length quantitation reveals 14-3-3 χ is involved in primary root growth during adaptation to phosphorus stress.

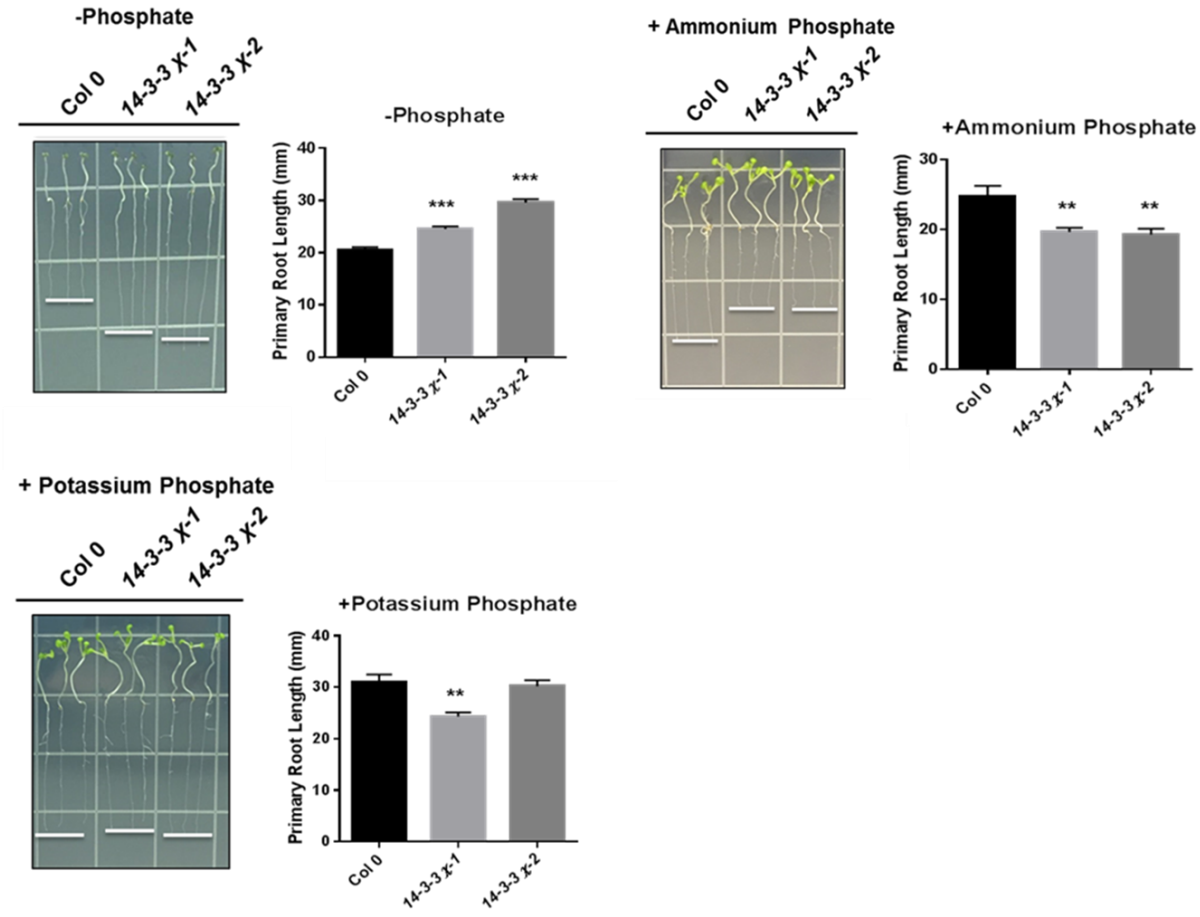

Figure 6. Primary root length is altered in 14-3-3 χ T-DNA mutant lines under phosphate-sufficient and phosphate-deficient conditions. *Arabidopsis* seedlings were grown for 8 d in phosphate deficient (-Phosphate) and phosphate-sufficient (Potassium phosphate, Ammonium phosphate) liquid media. White bars indicate seedling primary root tips. Primary root lengths were measured using ImageJ software. Statistical significance was determined using a paired, two-tailed student's t-test. p-values: **≤0.01 ***≤0.005

AHA expression is increased in 14-3-3 χ T-DNA mutant lines

With previous evidence that 14-3-3 proteins interact with AHA and 14-3-3 χ mediates the enhancement of AHA activity *in vitro*, AHA transcript levels were observed using seedlings grown under phosphate-sufficient (ammonium phosphate) and phosphate-limiting conditions (Figure 7A). RT-PCR analysis

revealed increased transcript levels for both AHA1 and AHA2 isoforms in the 14-3-3 χ T-DNA mutant lines compared to wild-type (Col-0) under phosphate-sufficient conditions, while little change in transcript levels was detected under phosphate-limiting conditions. AHA protein abundance was investigated by immunoblot analysis with seedlings grown under phosphate-limiting and phosphate-sufficient conditions using an antibody recognizing all AHA isoforms (Figure 7B). Immunoblot analysis revealed increased AHA protein expression in the 14-3-3 χ T-DNA mutant lines compared to Col-0. However, immunoblot quantitation revealed that this increased AHA protein abundance was only statistically significant when *14-3-3 χ-2* seedlings were grown in media supplemented with potassium phosphate. Collectively, these data indicate that the absence of 14-3-3 χ affects the expression of AHA isoforms.

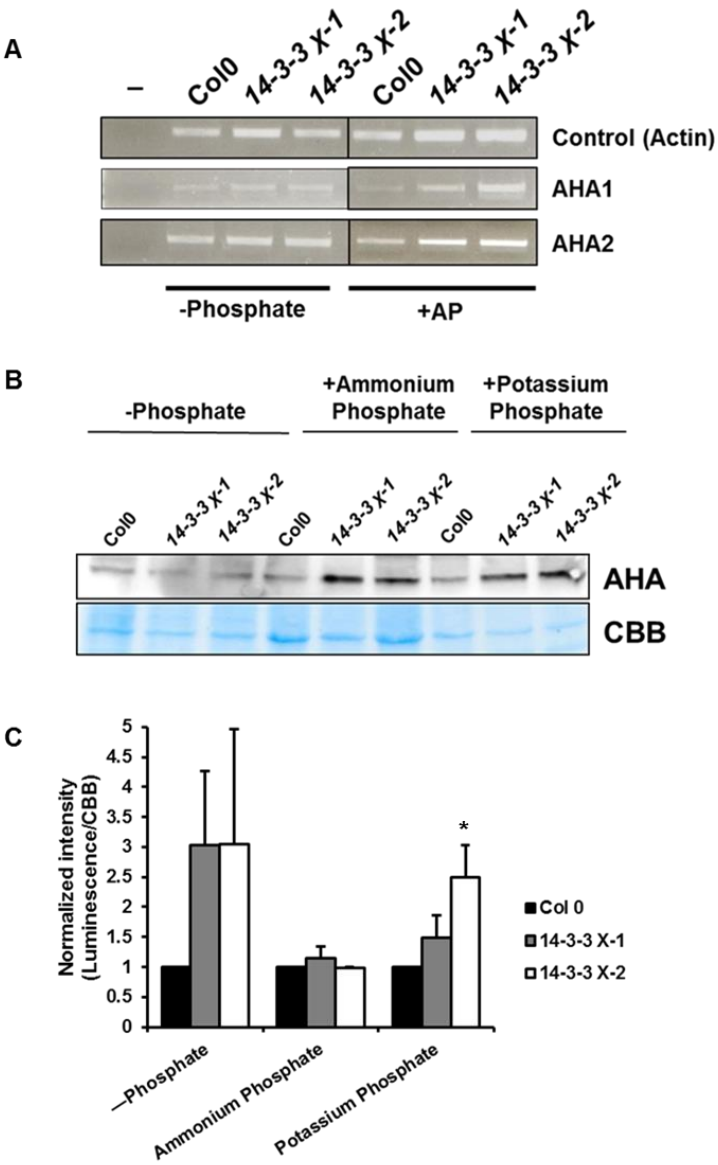

Figure 7: AHA is up-regulated in 14-3-3 χ T-DNA mutant lines A) RT-PCR analysis of AHA1 and AHA2 transcript levels in wild-type (Col-0), 14-3-3 χ-1, and 14-3-3 χ-2 *Arabidopsis* seedlings. Analysis was performed on 8-d old seedlings grown liquid media without phosphate (-Phosphate) and with 1 mM ammonium phosphate (+AP). Primers specific to actin were used as a control. B) Immunoblot analysis was performed with an AHA-specific antibody on 8-d old *Arabidopsis* seedlings grown in liquid media containing no phosphate (-Phosphate), 1 mM ammonium phosphate (+Ammonium phosphate), and 1 mM potassium phosphate (+Potassium phosphate). C) Immunoblot quantitation was performed using ImageQuant software to determine the ratio of immunoblot luminescence to loading control coomassie brilliant blue (CBB) intensities. Immunoblot was performed in biological triplicate. p-value: *≤0.05

14-3-3 χ directly interacts with AHA under varying phosphate conditions

To determine if the increase in AHA expression in the absence of 14-3-3 χ is due to direct 14-3-3 χ interactions with AHA, co-immunoprecipitation (Co-IP) assays were performed with Col-0 seedlings grown in liquid media using a 14-3-3 χ-specific antibody (Figure 8). Negative controls with no antibody bound to the Protein A beads were performed to assess non-specific binding. The total cell lysate was also analyzed to compare abundance of both AHA and 14-3-3 χ. No AHA protein was detected in the equal protein loadings of cell lysate, while a significant amount of AHA protein was detected in the Co-IP eluates. A low amount of 14-3-3 χ protein was detected in the negative controls in all three treatments, indicating 14-3-3 signal in the immunoprecipitated samples was not a result of non-specific binding. The lysate displayed no 14-3-3 χ protein in the samples grown in phosphate-limiting media, while protein was detected in the lysate from seedlings grown under phosphate-sufficient conditions. 14-3-3 χ protein abundance was significantly increased in the Co-IPs with antibody conjugated to the Protein A beads. Results from these data demonstrate that 14-3-3 χ and AHA co-immunoprecipitate and that this interaction is isoform specific.

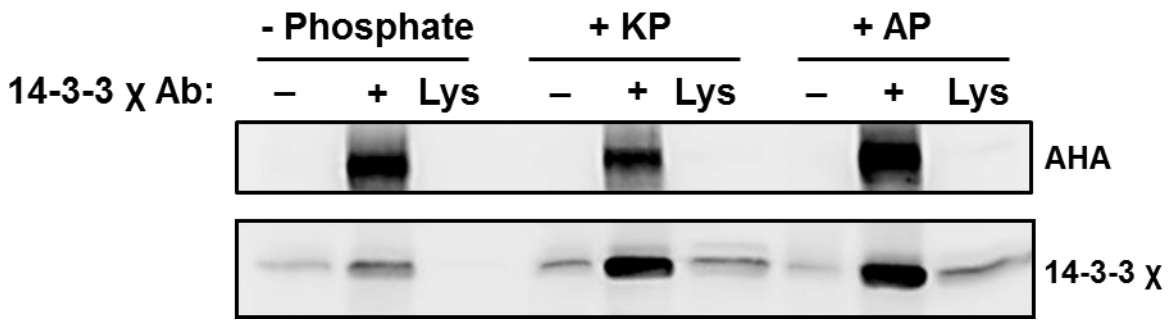

Figure 8: Immunoblot analysis of co-immunoprecipitation (Co-IP) assays display a 14-3-3χ interactions with AHA under phosphate-sufficient and phosphate-deficient conditions. Wild-type (Col-0) *Arabidopsis* seedlings were grown hydroponically for 8 d in phosphate deficient (-Phosphate) and phosphate-sufficient [Potassium phosphate (+KP), Ammonium phosphate (+AP)] liquid media. Negative controls (-) were performed without antibody bound to Protein A beads as a control for non-specific binding. Co-IP assays (+) were performed with antibody bound to Protein A beads. Lysate (Lys) was isolated before Co-IPs to show changes in protein expression between treatments. Immunoblot analysis was performed with both AHA- and 14-3-3 χ-specific primary antibodies. Co-IPs were performed in biological triplicate.

Primary root phosphate content is elevated in 14-3-3 χ T-DNA mutant lines

Since it is known that H^+-ATPases are involved in phosphate import into the roots, primary root phosphate was quantified from seedlings grown in phosphate-limiting and phosphate-sufficient conditions (Figure 9). In all growth media, the fold change in primary root phosphate content was higher in the 14-3-3 χ T-DNA mutant lines compared to Col-0. This increase in root phosphate was statistically significant when seedlings were grown in media supplemented with ammonium phosphate. Interestingly, root phosphate levels correlate with AHA expression analysis, suggesting up-regulation of AHA affects phosphate import into the root.

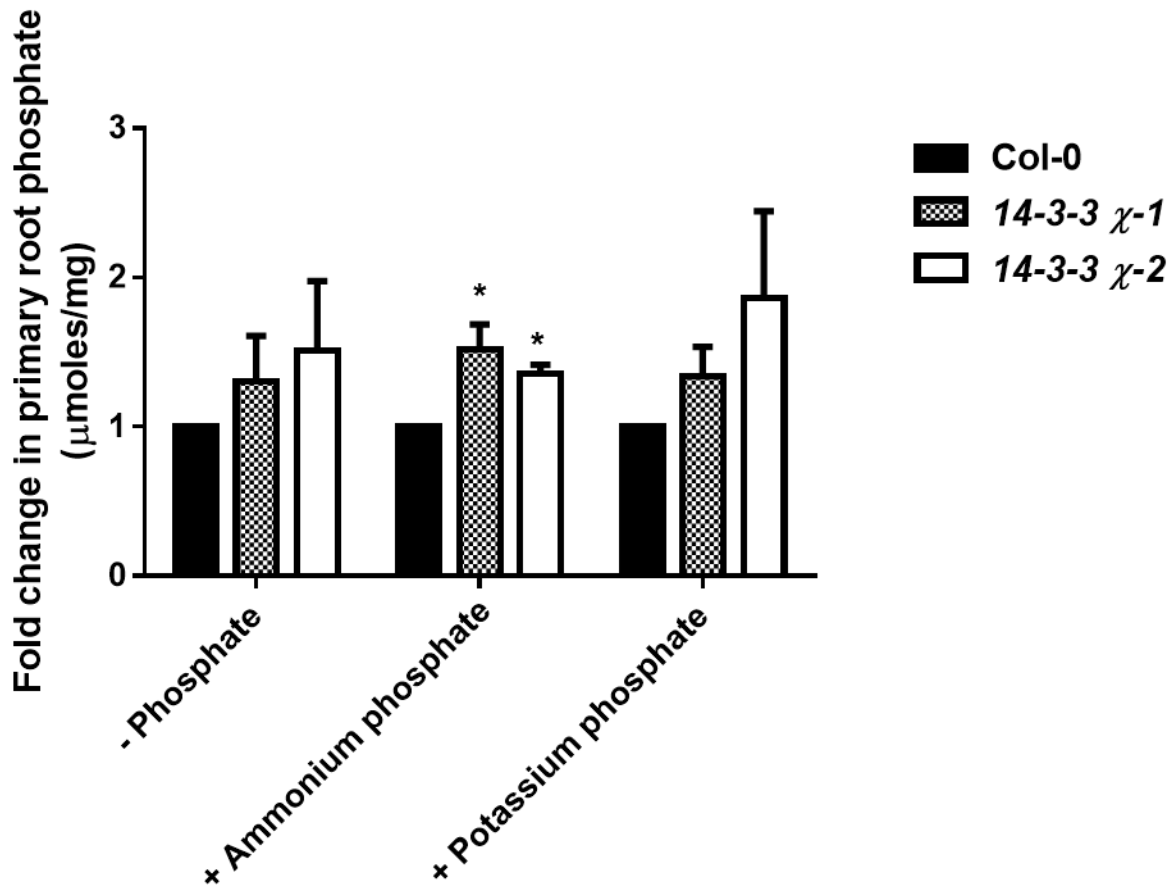

Figure 9: Primary root phosphate content is increased in 14-3-3 χ T-DNA mutant lines compared to Col-0 under phosphate-sufficient and phosphate-deficient conditions. *Arabidopsis* seedlings were grown hydroponically for 8 d in phosphate-deficient (-Phosphate) and phosphate-sufficient (+Potassium phosphate, +Ammonium phosphate) conditions. Root phosphate was quantified using a colorimetric assay at an absorbance of 720 nm. This graph is representative of three independent growth assays performed with 50 seedlings pooled per biological replicate in each growth media. p-value: *≤0.05

The 14-3-3 χ^{S72D} phosphomimic lacks the ability to complement phosphate-dependent phenotypes

To confirm that the observed phenotypes were due to the absence of 14-3-3 χ expression in the T-DNA mutant lines, stable transformation of *14-3-3 χ-1* with the wild-type form of 14-3-3 χ was performed, which complemented both the

primary root length and phosphate phenotypes under all growth conditions assayed (Figure 10A-B). Immunoblot analysis revealed 14-3-3 χ protein expression in the transgenic line was at comparable levels to Col-0 (Figure 10C). These results suggest that the absence of 14-3-3 χ is responsible for the observed phosphate-dependent phenotypes and implicates its role in phosphorus stress.

To determine the phosphate-dependent, functional effects of 14-3-3 χ phosphorylation on a potential regulatory site *in vivo*, we complemented the 14-3-3 χ-1 mutant line with the phosphomimetic form of 14-3-3 χ at the Ser^{72} residue. The 14-3-3 χ phosphomimic was constructed by site-directed mutagenesis of Ser^{72} to aspartate, mimicking constitutive phosphorylation. Phenotypic characterization was performed on T_4 generation lines to determine the effect(s) of 14-3-3 phosphorylation *in vivo* (Figure 10). Under phosphate-limiting conditions, primary root length of the 14-3-3 χ phosphomimic was significantly increased compared to Col 0, while this increase was not different than the native complemented line (Figure 10A). Interestingly, the primary root length phenotype was complemented by the phosphomimetic form of 14-3-3 χ under phosphate-sufficient conditions. The primary root phosphate levels were significantly increased in the 14-3-3 χ phosphomimic line when grown in media supplemented with ammonium phosphate, although this increase was not different than the native 14-3-3 χ complemented line (Figure 10B). Furthermore, there was significant reduction in root phosphate levels when the phosphomimic line was grown in potassium phosphate-supplemented media, however, this reduction

was not statistically significant compared to the native 14-3-3 χ complemented line.

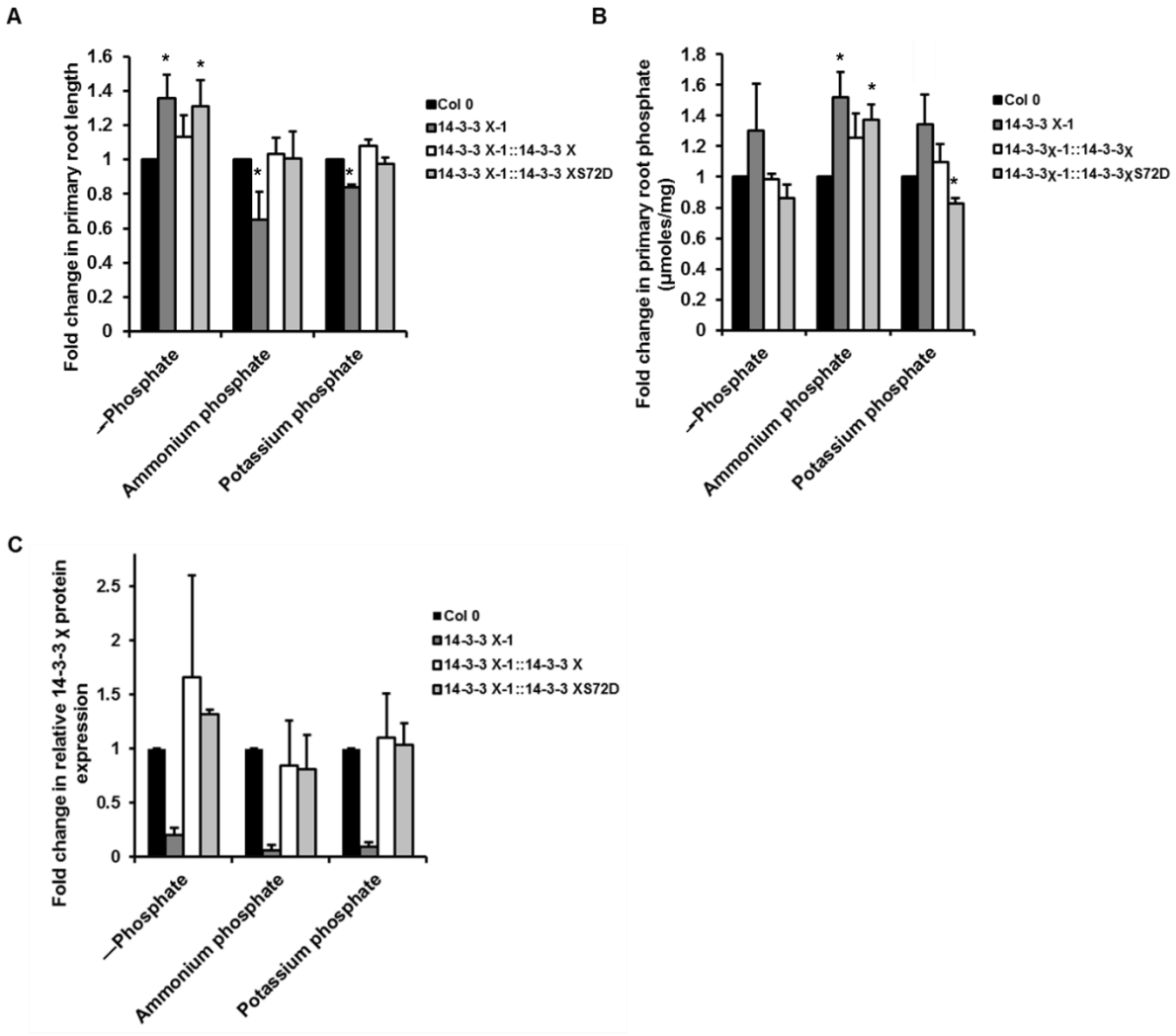

Figure 10. Phenotypic characterization of phosphomimetic 14-3-3 χ complementation. A) Primary root length quantitation of Col 0 and 14-3-3 χ complementation lines. B) Primary root phosphate quantitation of Col 0 and 14-3-3 χ complementation lines. C) Immunoblot quantitation of Col 0 and 14-3-3 χ complementation lines. Immunoblots were quantified using ImageQuant software. Seedlings were grown hydroponically for 8 days in media supplemented with no phosphate, 1 mM ammonium phosphate, or 1 mM potassium phosphate. Graphs are representative of 3 independent growth assays performed with 50 pooled biological replicates per line in each assay. Quantified values for complementation lines are normalized to Col 0. Statistical significance was performed using a paired, two-tailed, student's t-test compared to Col 0. p-value: *≤0.05.

The 14-3-3 χ^{S72D} phosphomimic displays altered dimer formation compared to the native form

To determine if the inability of 14-3-3 χ^{S72D} to complement phenotypes was due to altered dimer formation, the phosphomimetic protein and its non-mutated form were subjected to gel electrophoresis under non-denaturing conditions. Immunoblot analysis revealed the majority of 14-3-3 χ protein formed dimers, while the phosphomimetic form displayed a 12-fold higher monomer-to-dimer ratio than the non-mutated form (Figure 11A). This suggests that mutation of this residue may destabilize dimer formation. However, this destabilization is only fractional, as some dimer formation is still apparent in the phosphomimic 14-3-3 χ protein. Nevertheless, the difference in monomer/dimer formation is notable and could impact the ability of 14-3-3 χ^{S72D} to complement some of the mutant phenotypes.

The 14-3-3 χ^{S72D} phosphomimic displays an altered ability to interact with AHA

To determine if dimer destabilization of 14-3-3 χ^{S72D} has an effect on interactions with AHA, 14-3-3 pull-down assays were performed with *Arabidopsis* seedling tissue. In these assays, the *14-3-3 χ-2* T-DNA mutant line was used to prevent interference with endogenous 14-3-3 χ. The constitutively non-phosphorylated 14-3-3 χ^{S72A} and phosphomimetic 14-3-3 χ^{S72D} recombinant proteins were separately bound to Ni-NTA columns and incubated with *Arabidopsis 14-3-3 χ-2* seedling lysate. The eluate was subjected to immunoblot analysis, which

revealed altered ratios of AHA/14-3-3 intensity as a result of 14-3-3 χ phosphomimetic mutation.

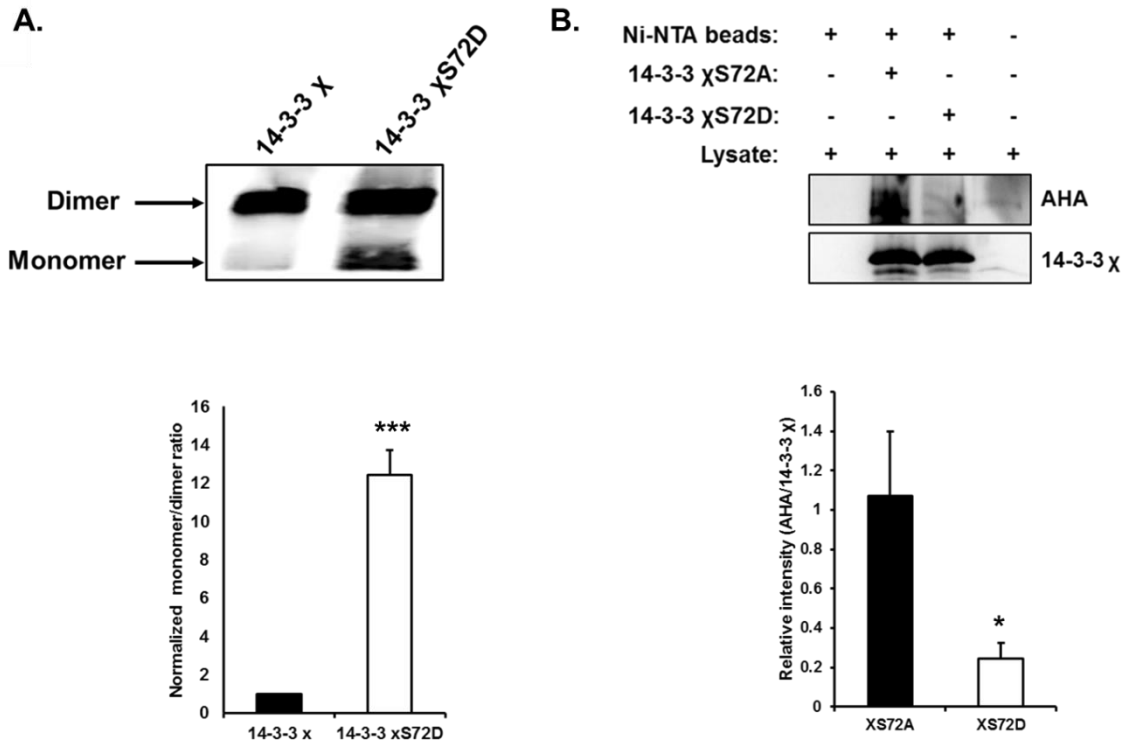

Figure 11. Phosphomimetic mutation of 14-3-3 χ alters dimer formation and interactions with AHA. A) Immunoblot analysis of Blue Native PAGE reveals altered monomer/dimer ratios of 14-3-3 χ. Recombinantly purified 14-3-3 χ and phosphomimetic 14-3-3 χS72D protein (5 µg) was subjected to gel electrophoresis under non-denaturing conditions, and immunoblot analysis was performed using a 14-3-3χ-specific primary antibody. Arrows indicate molecular weight shifts between dimeric and monomeric forms of 14-3-3 χ. Ratios were quantified using ImageQuant software. This immunoblot is representative of 3 biological triplicates performed. B) Pull-down assays revealed altered interactions with AHA protein. Recombinantly-purified 14-3-3 χS72A and phosphomimetic 14-3-3 χS72D protein (10 µg) were bound to a Ni-NTA nickel column. *Arabidopsis 14-3-3 χ-2* seedling lysate was added to column, and protein was eluted with imidazole (200 mM). Eluate was subjected to gel electrophoresis followed by immunoblot analysis. Immunoblots were probed with AHA and 14-3-3 χ antibodies, and luminescence intensities were quantified using ImageQuant software. Immunoblot is representative of 3 biological replicate experiments. Statistical significance was determined using a student's t-test. p-value: *≤0.05, ***≤0.005

The pull-down assays performed with 14-3-3 χ^{S72D} displayed a 77% reduction in the ratio of AHA/14-3-3 when compared to pull-down assays performed with the 14-3-3 χ^{S72A} (Figure 11B). Collectively, these results suggest that phosphorylation of 14-3-3 χ at Ser^{72} destabilizes dimer formation and affects 14-3-3 χ interactions with AHA protein.

DISCUSSION

Previous studies have demonstrated 14-3-3 proteins interact with AHA and are involved in phosphorus stress (4,5,30). Our study has expanded upon these findings by investigating the function of 14-3-3 isoform χ *in planta* under varying phosphate conditions. Not only were 14-3-3 χ-specific interactions with AHA proteins observed, but phosphate-dependent phenotypes including altered primary root length and root phosphate content were identified in two independent 14-3-3 χ T-DNA mutant lines. The primary root phenotypic results suggest that phosphate import or re-allocation is misregulated in the absence of 14-3-3 χ.

In addition to root phenotypes, AHA expression levels were elevated in mutant lines compared to wild-type, suggesting that 14-3-3 χ could be one of the primary 14-3-3 isoforms responsible for AHA activation under these growth conditions. These data are in agreement with a previous report which monitored AHA activity after independent addition of seven *Arabidopsis* 14-3-3 isoforms using *in vitro* activity assays (7). Of these isoforms, 14-3-3 χ had the greatest positive effect on AHA activity. Furthermore, these results demonstrate 14-3-3

isoform-specific interactions with AHA, supporting a previous study which used surface plasmon resonance to monitor binding affinities of 14-3-3 isoforms to an immobilized peptide corresponding to the C-terminal region of AHA (91). In this study, 14-3-3 χ displayed the second-highest binding affinity to the AHA peptide of the nine isoforms tested. Swatek et al.(10) displayed 14-3-3 χ localization to the plasma membrane when transiently expressed in *N. benthamiana* leaves, making 14-3-3 χ interactions with AHA plausible.

Under the assumption that 14-3-3 χ is a primary regulator of AHA, the absence of 14-3-3 χ could thereby reduce the activity of AHA, resulting in its up-regulation to compensate for this activity loss. This supports our observations and could also provide an explanation for the increased root phosphate levels displayed in the mutant lines under these growth conditions. A previous study observed similar elevated root phosphate levels in AHA overexpression lines grown under phosphate-limiting conditions (3). Although it cannot definitively be stated that the altered primary root phosphate content is due to 14-3-3 χ interaction with AHA, it is likely that this is a potential source of misregulation as indicated by AHA expression analyses and co-immunoprecipitation assays. While several studies have identified 14-3-3 interactions with AHA both *in vitro* and *in vivo*, the role of this association in the context of phosphorus stress has not yet been established. Overall, these results provide novel evidence of 14-3-3 χ involvement in phosphorus stress and implicate 14-3-3 χ as a regulator of root phosphate import through interactions with AHA.

Arabidopsis 14-3-3 proteins have been widely-studied, however, it remains difficult to identify isoform-specific phenotypes due to high sequence conservation and similar expression patterns among the thirteen expressed isoforms. In addition, as 14-3-3 proteins are general phospho-binding modulators, it is particularly challenging to isolate specific targets and pathways with which 14-3-3 proteins are involved. Although previous studies have identified several candidates for 14-3-3 interactions along with effects of 14-3-3 binding such as inhibition of nitrate reductase or activation of plasma membrane H^+-ATPases (5,77,78), these interactions remain largely redundant among 14-3-3 isoforms. This study not only provides evidence of an isoform-specific phenotype, but also identifies a possible source of this phenotype due to misregulation.

Phosphorylation of 14-3-3 proteins has been previously identified in plants, however, little is known about the functional effects of these modifications *in vivo*. To expand upon previous functional evidence of 14-3-3 χ Ser^{72} phosphorylation *in vitro*, our study sought to investigate an *in vivo* function for this 14-3-3 χ phosphorylation site by stable expression of a phosphomimetic form of 14-3-3 χ (Ser^{72}→Asp) in the *14-3-3 χ-1 Arabidopsis* null mutant background. Phosphate growth assays were performed to determine the effects of this modification *in vivo*. Phenotypes of the phosphomimic complemented line were compared to wild-type (Col 0) to determine statistical significance.

Under low phosphate growth, primary root lengths of both the phosphomimic line and the 14-3-3 χ knockout line were significantly increased

compared to Col 0, suggesting that the phosphomimic was unable to complement the primary root length phenotype. However, it is notable that the primary root length of the phosphomimic was not significantly increased compared to the line transformed with the native 14-3-3 χ. Conversely, the phosphomimic line complemented primary root length phenotypes when grown under phosphate-sufficient conditions. Quantitation of primary root phosphate revealed no significant difference in the phosphomimic line compared to Col 0 under low phosphate conditions. Interestingly, the phosphomimic line displayed significantly increased root phosphate levels compared to Col 0 when grown in media supplemented with ammonium phosphate. However, again this increase was not statistically significant compared to the 14-3-3 χ-transformed line. An opposite effect was observed for phosphomimic lines grown in media supplemented with potassium phosphate. These results indicated a significant decrease in primary root phosphate levels of the phosphomimic line compared to Col 0 but not the 14-3-3 χ-transformed line.

Perhaps, 14-3-3 χ is phosphorylated at Ser^{72} in the wild-type and native complemented lines under these specific growth conditions as well, which would explain why complementation of root phenotypes in the phosphomimic lines occurs under phosphate-sufficient, but not phosphate-deficient conditions. Furthermore, the 14-3-3 χ phosphomimic could be displaying dominant negative effects. In this case, the mutation could still enable 14-3-3 χ interactions with AHA, however, this interaction would result in reduced activation of AHA due to altered dimer stability and would ultimately prevent binding of other 14-3-3

isoforms. Lastly, it is possible that mutation of only one amino acid is not sufficient to have a significant phenotypic effect *in vivo*. Nevertheless, these data do reveal slight phenotypic changes as a result of phosphomimetic mutation of 14-3-3 χ at Ser^{72}, possibly due to destabilization of dimer formation and/or altered interactions with AHA.

The dimer stability of 14-3-3χ^{S72D} was investigated, which revealed altered dimer formation compared to the non-mutated form. This result is similar to a previous study, which demonstrated dimer destabilization after phosphorylation of 14-3-3 ω at Ser^{67} (67). This residue aligns with Ser^{72} of 14-3-3 χ, and these residues are conserved across all *Arabidopsis* isoforms as well as 14-3-3 isoforms of other plant species. In addition, pull-down assays revealed a 77% reduction in AHA interactions with phosphomimetic 14-3-3 χ^{S72D} compared to the non-phosphorylated 14-3-3 χ^{S72A}. Collectively, these data suggest that phosphorylation of 14-3-3 χ has a negative effect on the function of this isoform, through destabilization of dimer formation, and affects interactions with AHA. These data also support the phenotypes observed in the phosphomimic transgenic lines, as interactions with AHA could be affected *in vivo* as a result of this mutation. Furthermore, these results support the possibility of a general post-translational regulatory mechanism for 14-3-3 isoforms.

CONCLUDING REMARKS

The biochemical data obtained in this study provided evidence for 14-3-3 χ involvement in phosphorus stress in *Arabidopsis*, through phosphate-dependent phenotypes and increased expression of AHA in 14-3-3 χ T-DNA mutant lines. 14-3-3 χ-specific interactions with AHA were also established in both phosphate-deficient and phosphate-sufficient media. This result, coupled to the increased AHA expression and root phosphate levels, indicates this 14-3-3 χ could be a primary regulator of AHA activity and root phosphate import. Furthermore, we have elucidated the effects of 14-3-3 χ phosphorylation on both dimer stability and protein interactions *in vitro* and also observed reduced 14-3-3 χ function upon phosphorylation *in vivo*, which has potential regulatory implications for all 14-3-3 isoforms.

CHAPTER III

DEVELOPMENT AND VALIDATION OF AN ASSAY FOR ABSOLUTE QUANTITATION OF HETEROMERIC ACCASE AND BADC PROTEINS IN ARABIDOPSIS THALIANA

Introduction

Multiple reaction monitoring (MRM) is a tandem mass spectrometry-based approach for accurate quantitation of selected proteins in a complex sample. This method of quantitation is usually performed on a triple quadrupole (QqQ) mass spectrometer and enables multiplexed monitoring of transition ions within a single, liquid chromatography-tandem mass spectrometry (LC-MS/MS) analysis. The low resolution capabilities of the triple quadrupole instrument require assessment of retention time in addition to precursor, and product ion information for accurate peptide quantification. Typically, at least three fragment ions, or transitions, are monitored for each precursor peptide targeted (92).

For absolute quantitation during an MRM assay, AQUA (Absolute QUAntitation) peptides can be used as internal standards, which are heavy isotope labeled, high purity peptides designed against a target peptide of interest (93,94). The heavy label ($^{13}C^{15}N$) is positioned at the C-terminal lysine or arginine of the tryptic AQUA peptide, which does not affect the chemical characteristics of the peptide. Therefore, the AQUA and native peptides co-elute during liquid chromatography separation and also display identical fragmentation patterns. The mass shift of the AQUA peptide allows quantitation of the native peptide in the biological sample.

There are several advantages of using the AQUA-MRM method over other quantitative biochemical techniques. AQUA-MRM is more sensitive than immunoblot analysis, and in some instances, peptides can be quantified at attomolar levels, enabling detection of low abundant proteins (93). Furthermore,

AQUA-MRM displays a higher specificity for the protein of interest compared to immunoblot analysis (92,95,96). While antibodies can be produced for protein detection, they are often costly, and specificity is not guaranteed. By targeting a specific peptide, this method allows for quantitative differentiation of isoforms with high sequence similarity (97,98). Finally, the multiplex capability of this assay allows simultaneous monitoring of multiple peptides in a single analysis, resulting in high throughput and reproducibility among biological replicates, while also controlling for spray stability between LC-MS/MS analyses.

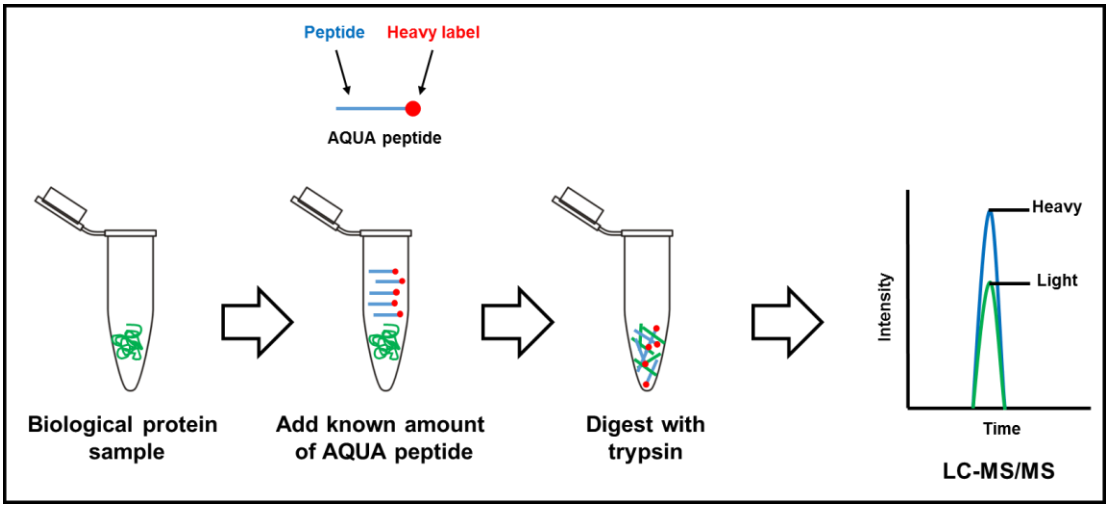

Figure 12. Experimental workflow of AQUA-MRM analysis. 1) Protein is extracted from biological sample. 2) A known amount of heavy-labeled AQUA peptide is added to the biological sample. 3) The sample is digested with trypsin. 4) AQUA and native peptides are monitored simultaneously using MRM mass spectrometry analysis.

Although the AQUA-MRM method offers several advantages, the synthesis of AQUA peptides can be costly, ranging from hundreds to thousands of dollars. Therefore, careful consideration of ideal peptides for MRM quantitation is required, using a general criteria for peptide selection (92): 1) Peptides must be unique to the proteome(s) of interest, as quantitation could be affected by interfering ions, 2) Peptides must contain no modifiable amino acids and cannot be flanked by lysines or arginines within three amino acids upstream or downstream of the tryptic cleavage site, as both could result in missed cleavage events, 3) Peptides must be detectable in the biological sample of the species being analyzed. Peptides which pass the criteria are then subjected to custom AQUA synthesis.

The AQUA-MRM method can be used for absolute protein quantitation in a variety of biological applications including identification of post-translational modifications, biomarker discovery, and metabolic engineering strategies (96,99-101). For instance, heterologous expression of proteins can be challenging, as protein abundance levels can vary depending on the host organism and the promoter used for gene expression (102,103). Absolute quantitation of protein abundance can be achieved through AQUA-MRM analysis, and these levels can be compared to those of the native organism to evaluate the headspace potential for increasing flux through a specific pathway. Furthermore, protein complexes such as heteromeric ACCase are often points of regulatory control. By identifying rate-limiting subunits of the complexes or conditional changes in

subunit stoichiometry, engineering strategies can be employed for modulation of enzyme activity.

We have developed a quantitative AQUA-MRM assay for quantitation of heteromeric acetyl-CoA carboxylase (ACCase) and BADC inhibitory proteins in *Arabidopsis thaliana*. ACCase is a protein complex that catalyzes the committed step of *de novo* fatty acid biosynthesis in plastids and consists of four subunits: α-carboxyl transferase (α-CT), β-carboxyl transferase (β-CT), biotin carboxylase (BC), and two isoforms of biotin carboxyl carrier protein (BCCP1 and BCCP2). The inhibitory proteins consist of three different isoforms that are designated BADC1, BADC2, and BADC3. Previous results have demonstrated BADC inhibition of the ACCase complex through protein-protein interactions (Salie et al., unpublished). This assay aims to investigate BADC inhibition of ACCase under inducible experimental conditions in *Arabidopsis thaliana* by quantifying changes in subunit stoichiometry of the complex. Prior to performing the assay, careful assessment and validation went into the design and method development to ensure successful quantitation of ACCase subunits and BADC proteins. Here, we discuss the AQUA peptide design, synthesis, and optimization of a novel multiplexed assay, which will be used to determine the stoichiometry of ACCase subunits *in vivo* and specifically compare BADC:BCCP protein ratios under conditions of FAS stimulation and inhibition.

EXPERIMENTAL PROCEDURES

AQUA peptide design and synthesis

Arabidopsis heteromeric ACCase and BADC proteins (TAIR accession numbers AT2G38040, ATCG00500, AT5G35360, AT5G16390, AT5G15530, AT3G56130, AT1G52670, and AT3G15690) were digested with trypsin *in silico* to generate a list of possible tryptic peptides for mass spectrometry analysis. Peptides containing flanking arginines and lysines or internal modifiable cysteine and methionine residues were excluded from the list. Peptides were also BLAST searched against the TAIR 10 *Arabidopsis* proteome, and unique peptides were selected. The list of peptides was then monitored in an unscheduled multiple reaction monitoring method using tryptic digest matrices of recombinant protein and *Arabidopsis* seed and leaf protein extracts. Peptides that produced an adequate signal (Normalized level (NL) > 10^3) were selected for AQUA peptide synthesis.

AQUA peptide synthesis

Selected peptides were used as a template for custom AQUA^{TM} synthesis from Sigma Life Science Custom Products (The Woodlands, TX). Two peptides were synthesized per ACCase subunit and one peptide was synthesized per BADC isoform (Table 1) at a purity ≥ 95%. AQUA peptides were shipped in 0.5 nmol lyophilized aliquots.

Plant growth and protein extraction

Arabidopsis ecotype Columbia-0 plants were grown under constant light at 24°C. Silique and leaf tissue was collected and stored at -80°C. Protein was extracted from tissue as previously described (103). Plant tissue (100 mg) was homogenized in an extraction buffer (0.9 M sucrose, 100 mM Tris-HCl pH 8.0, 10 mM EDTA, 0.4% ß-mercaptoethanol (v/v)). One volume of Tris-buffered phenol was added to the homogenate and incubated with agitation at 4°C for 1 h. Samples were centrifuged at 17000 x g at 4°C for 5 minutes, and the phenol phase was transferred into a clean polypropylene tube. The samples were back-extracted with one volume of extraction buffer and incubated with agitation for 5 minutes. Centrifugation was repeated as described above, and the phenol phase was transferred to five volumes of ice-cold precipitation solution (100mM ammonium acetate in 100% methanol) to precipitate protein. Samples were vortexed, and protein was precipitated overnight at -80°C. Samples were centrifuged at 4,000 xg at 4°C for 10 minutes before each wash step. Protein was washed twice with precipitation solution, twice with 80% (v/v) acetone in water, and once with 70% (v/v) ethanol in water. Protein was stored at -80°C in 70% ethanol prior to sample preparation.

Preparation of samples for AQUA-MRM

Protein was dissolved in urea buffer (8 M urea, 50 mM Tris-HCl, pH 8.0) and quantified using the Bradford method with bovine gamma globulin (BGG) as a

protein standard (BioRad Laboratories, Hercules, CA). Protein was portioned into 20 µg aliquots and reduced with DTT at a final concentration of 10 mM. Samples were incubated for 1 h at 37°C. Samples were alkylated with iodoacetamide (IAA) at a final concentration of 50 mM and incubated at room temperature in the dark for 1 hour. Urea was diluted with 3 volumes of a solution of 10 mM ammonium bicarbonate and 10 mM DTT. Trypsin was added at a 1:50 ratio (trypsin:protein) and incubated at 37°C for 16 h. Tryptic peptides were lyophilized via centrifugal evaporator and stored at -80°C prior to mass spectrometry analysis.

MRM method development

AQUA peptides were resuspended in 0.1% formic acid to a final concentration of 5 pmol/µL. Initial assessment of peptides was performed to acquire peptide retention times and select the top eight most intense transition ions from each precursor peptide based on peak area intensity. A scheduled collision energy method was used to optimize transition ion collision energies for each precursor ion by varying the collision energy and monitoring the resulting transition ion peak area intensity response. Optimized collision energy values were imported into a final optimized MRM method.

AQUA peptide dilution series

A six-point, 10-fold AQUA peptide dilution series was performed in *Arabidopsis* seed tryptic peptide matrix and subjected to multiplexed LC-MS/MS analysis. The dilution series was run sequentially in biological quadruplicate from 0.01-1000 fmol AQUA peptide/injection. Analytical standards were doped into 1 µg of the seed peptide matrix.

Recombinant protein expression and SDS PAGE

Genes were PCR amplified from *Arabidopsis* cDNA and subcloned into a pET28a 6XHis-Tag expression vector (Novagen, Darmstadt, Germany). Recombinant constructs were transformed into *E.coli* strain BL21 cells. Protein was expressed and purified as previously described using Ni-NTA affinity chromatography under native conditions (15). Purified protein was quantified using the Bradford method with bovine gamma globulin (BGG) as a protein standard (BioRad Laboratories, Hercules, CA), subjected to SDS PAGE (12 % (w/v) acrylamide) and stained with Coomassie Brilliant Blue (CBB) to confirm protein expression (Figure 5). The band volume from densitometry scanning of CBB-stained gels was quantified using ImageQuant TL software v. 8.1 (GE Healthcare Life Sciences, Pittsburgh, PA) to assess protein purity.

AQUA-MRM analysis of recombinant protein linear response

Recombinant peptides were resuspended in 0.1% (v/v) formic acid in water to a final concentration of 0.4 µg/µL. A six-point, two-fold recombinant protein dilution series was performed in 1 µg *Ricinus communis* seed tryptic peptide matrix. The dilution series was run sequentially in biological quadruplicate ranging from 31.25-1000 ng recombinant protein/injection. The AQUA peptide corresponding to the protein analyzed was loaded at 100 fmol/injection with the exception of BADC3, which was loaded at 1000 fmol/injection.

Mass spectrometry analysis

Targeted mass spectrometry was performed on a TSQ Vantage EMR triple quadrupole instrument (Thermo Scientific, San Jose, CA) interfaced with a nanoLC 1-D plus liquid chromatography system (Ekisgent, Framingham, MA). Autosampling, chromatography, and mass spectrometry were performed as previously described (104). Peptides were bound on a C8 Cap Trap (Michrom Bioresources, Inc., Auburn, CA) and eluted over a 12.5 min gradient of 2-60% solvent B (0.1% (v/v) formic acid in acetonitrile). The total method time was 25 min at a flow rate of 500 nL/min. All analysis was performed with 1 µg of protein digest on column and a 5 µL injection volume. The AQUA peptides were injected within the linear range of detection, and all analysis performed was multiplexed. Data analysis was performed using Skyline software v. 2.6.0.7176 (MacCoss Lab, Department of Genome Sciences, University of Washington).

RESULTS AND DISCUSSION

AQUA peptide design and synthesis

Each ACCase protein was digested *in silico* with trypsin to generate a list of possible peptides for the AQUA-MRM assay. Peptides smaller than eight amino acids and/or containing modifiable cysteine and methionine residues were excluded from the list. Peptides with C- and N-terminal flanking arginines or lysines within three residues from the cleavage site were also excluded, as these residues could result in miscleavage events. The ACCase subunits analyzed here are all nuclear-encoded but chloroplast-localized, therefore, peptides within the predicted transit peptide of each protein were also excluded. Previous spectra from high-resolution Orbitrap analysis of *Arabidopsis* seedling protein were assessed to determine if peptides had previously been identified using mass spectrometry (Table 1). Of the selected peptides, only DIVELELK (BCCP2) and

LNAQLVPKPSEVEALVTEICDSSSIAEFELK (BADC3) were not previously identified on the Orbitrap. Selected peptide sequences were also BLAST searched against the *Arabidopsis* proteome to ensure that the peptide was unique to the proteome. Recombinant protein as well as *Arabidopsis* seed and leaf protein extracts were analyzed in a targeted unscheduled MRM method to confirm a signal in the native proteome. All of the selected peptides produced a signal in the recombinant protein analysis. All peptides with the exception of SASSAPSPSQAKPSSEK (BADC1) and LNAQLVPKPSEVEALVTEICDSSSIAEFELK (BADC3) peptides produced a

signal in the leaf protein extract, and LNAQLVPKPSEVEALVTEICDSSSIAEFELK (BADC3) was the only peptide that also lacked a signal in the seed protein extract (Table 1). Although the BADC1 and BADC3 peptides were not detected in both of the protein matrices, these peptides were still selected for peptide synthesis due to the lack of alternative peptides available within the deduced primary sequences.

Table 1. List of peptides selected for AQUA peptide synthesis*

Mass $[M+H]^+$	Peptide sequence	Unique in Arabidopsis Proteome	Flanking	Orbitrap	Recombinant protein	Seed	Leaf
αCT: AT2G38040							
1600.7925	SEELGQGEAIANNLR	Y	YADLK.SEELGQGEAIANNLR.TMFGL	Y	Y	Y	Y
1356.727	DLYTHLTPIQR	Y	RQALK.DLYTHLTPIQR.VNIAR	Y	Y	Y	Y
β-CT: ATCG00500							
1052.4717	AMDSFAPGEK	Y	GELSK.AMDSFAPGEK.TTISQ	Y	Y	Y	Y
1360.6532	NFISDDTFFVR	Y	SKDIR.NFISDDTFFVR.DSNKN	Y	Y	Y	Y
BC: AT5G35360							
1393.7474	ITSYLPSGGPFVR	Y	PGPGR.ITSYLPSGGPFVR.MDSHV	Y	Y	Y	Y
1161.5799	FGNVVHFGER	Y	VLADK.FGNVVHFGER.DCSIQ	Y	Y	Y	Y
BCCP1: AT5G16390							
1139.6095	SPAPGEPPFIK	Y	GTFYR.SPAPGEPPFIK.VGDKV	Y	Y	Y	Y
957.5615	DIVELQLK	Y	LVDSR.DIVELQLK.QLDCE	Y	Y	Y	Y
BCCP2: AT5G15530							
1111.5782	SPGPGEPPFVK	Y	GTFYR.SPGPGEPPFVK.VGDKV	Y	Y	Y	Y
958.5455	DIVELELK	Y	LVDSK.DIVELELK.QLDCE	N	Y	Y	Y
BADC1: AT3G56130							
1645.8027	SASSAPSPSQAKPSSEK	Y	EPMNK.SASSAPSPSQAKPSSEK.VSPFK	Y	Y	Y	N
BADC2: AT1G52670							
1562.7769	TSSSSADRPQTLANK	Y	LAITK.TSSSSADRPQTLANK.AADQG	Y	Y	Y	Y
BADC3: AT3G15690							
3359.729	LNAQLVPKPSEVEALVTEICDSSSIAEFELK	Y	YLSLK.TTFGSVK.AVQVS	N	Y	N	N

*Peptides were initially assessed after *in silico* tryptic digestion. The peptide mass, sequence, uniqueness to the *Arabidopsis* proteome, and the peptide N- and C-terminal flanking residues are listed. Previous identification on the Orbitrap, recombinant protein, and *Arabidopsis* seed and leaf protein extract is indicated.

AQUA peptides were synthesized for each selected sequence with a C-terminal arginine or lysine labeled with stable isotopes ($^{13}C^{15}N$). Two peptides were selected for each ACCase subunit (α-CT: SEELGQGEAIANNLR,

DLYTHLTPIQR; β-CT: AMDSFAPGEK, NFISDDTFFVR; BC: FGNVVHFGER, ITSYLPSGGPFVR; BCCP1: SPAPGEPPFIK, DIVELQLK; BCCP2: SPGPGEPPFVK, DIVELELK). One peptide was chosen for each BADC protein (BADC1: SASSAPSPSQAKPSSEK, BADC2: TSSSSADRPQTLANK, BADC3: LNAQLVPKPSEVEALVTEICDSSSIAEFELK), due to the limited number of optimal peptides available in the protein sequences. The protein sequences of each ACCase subunit, with selected AQUA quantitation peptides highlighted, are shown in Figure 13.

Notably, all of the chosen BADC peptides contain internal lysines or arginines in their sequences: SASSAPSPSQA**K**PSSEK, TSSSSAD**R**PQTLANK, LNAQLVP**K**PSEVEALVTEICDSSSIAEFELK. This is acceptable, however, because these tryptic cleavage sites are located on the N-terminal side of proline residues. Established protease rules indicate that tryptic cleavage is suppressed when prolines are C-terminal to a lysine or arginine cleavage site (95,105). Recombinant protein was analyzed using AQUA-MRM to ensure that peptides produced from theoretical cleavage at these sites did not produce a signal. Therefore, we can expect that proteolysis will not occur at these cleavage sites and the chosen peptides will be suitable for this assay.

BCCP1 Protein Sequence

MASSSFSVTSPAAAASVYAVTQTSSHFPIQNRSRRVSFRLSAKPKLRFLSKPSRSSYPVVKAQSNKVSTGASSNAAKVDGPSSAEG
KEKNSLKESSASSPELATEESISEFLTQVTTLVKLVDSRDIVELQLKQLDCELVIRKKEALPQPQAPASYVMMQQPNQPSYAQQMAP
PAAPAAAAPAPSTPASLPPPSPPTPAKSSLPTVKSPMAGTFYRSPAPGEPPFIKVGDKVQKGQVLCIVEAMKLMNEIESDHTGTVVDI
VAEDGKPVSLDTPLFVVQP

BCCP2 Protein Sequence

MASLSVPCVKICALNRRVGSLPGISTQRWQPQPNGISFPSDVSQNHSAFWRLRATTNEVVSNSTPMTNGGYMNGKAKTNVPEPAE
LSEFMAKVSGLLKLVDSKDIVELELKQLDCEIVIRKKEALQQAVPPAPVYHSMPPVMADFSMPPAQPVALPPSPTPTSTPATAKPTSA
PSSSHPPLKSPMAGTFYRSPGPGEPPFVKVGDKVQKGQIVCIIEAMKLMNEIEAEKSGTIMELLAEDGKPVSVDTPLFVIAP

BADC1 Protein Sequence

MASSAALGSLHQTLGSAINSQSEVHSLSGNWSASGNSCVPRWRLSNRNSNYRLVLRAKAAKSSTTTISDGSSDASVSDGKKTVRRI
TFPKEVEALVHEMCDETEVAVLQLKVGDFEMNLKRKIGAATNPIPVADISPTVAPPIPSEPMNKSASSAPSPSQAKPSSEKVSPFKNT
SYGKPAKLAALEASGSTNYVLVTSPAVGKFQRSRTVKGKKQSPSCKEGDAIKEGQVIGYLHQLGTELPVTSDVAGEVLKLLSDDGD
SVGYGDPLVAVLPSFHDINIQ

BADC2 Protein Sequence

MNSCSLGAPKVRIFATNFSRLRCGNLLIPNNQRLFVDQSPMKYLSLRTTLRSVKAIQLSTVPPAETEAIADVKDSDETKSTVVNTHLM
PKSSEVEALISEITDSSSIAEFELKLGGFRLYVARKLTDESSPPPQQIQPVVAASATPEGVHTNGSATSSSLAITKTSSSSADRPQTLA
NKAADQGLVILQSPTVGYFRRSKTIKGKRTPTICKEKDIVKEGQVLCYIEQLGGQIPVESDVSGEIVKILREDGEPVGYNDALITVLPSF
PGIKKLQ

BADC3 Protein Sequence

MASCSLGVPKIKISAVDLSRVRSGSLLIPYNQRSLLRQRPVKYLSLKTTFGSVKAVQVSTVPTAETSATIEVKDSKEIKSSRLNAQLVP
KPSEVEALVTEICDSSSIAEFELKLGGFRLYVARNIADNSSLQPPPTPAVTASNATTESPESNGSASSTSLAISKPASSAADQGLMILQ
SPKVGFFRRSKTIKGKRLPSSCKEKDQVKEGQILCYIEQLGGQFPIESDVTGEVVKILREDGEPVGYNDALISILPSFPGIKKLQ

α-CT Protein Sequence

MASISHSSLALGGASSASASDYLRSSSNGVNGVPLKTLGRAVFTTIRRKDLAVTSRLKKGKKFEHPWPANPDPNVKGGVLSYLAEF
KPLGDTQKPVTLDFEKPLVELEKKIVDVRKMANETGLDFTEQIITLENKYRQALKDLYTHLTPIQRVNIARHPNRPTFLDHIHNITDKFM
ELHGDRAGYDDPAIVTGIGTIDGKRYMFIGHQKGRNTKENIMRNFGMPTPHGYRKALRMMYYADHHGFPIVTFIDTPGAYADLKSEEL
GQGEAIANNLRTMFGLKVPILSIVIGEGGSGGALAIGCANKMLMLENAVFYVASPEACAAILWKTSKAAPEAAEKLRITSKELVKLNV
ADGIIPEPLGGAHADPSWTSQQIKIAINENMNEFGKMSGEELLKHRMAKYRKIGVFIEGEPIEPSRKINMKKREAVFSDSRKLQGEVD
KLKEQILKAKETSTEAEPSSEVLNEMIEKLKSEIDDEYTEAAIAVGLEERLTAMREEFSKASSEEHLMHPVLIEKIEKLKEEFNTRLTDA
PNYESLKSKLNMLRDFSRAKAASEATSLKKEINKRFQEAVDRPEIREKVEAIKAEVASSGASSFDELPDALKEKVLKTKGEVEAEMA
GVLKSMGLELDAVKQNQKDTAEQIYAANENLQEKLEKLNQEITSKIEEVVRTPEIKSMVELLKVETAKASKTPGVTEAYQKIEALEQQI
KQKIAEALNTSGLQEKQDELEKELAAARELAAEESDGSVKEDDDDDEDSSESGKSEMVNPSFA

B-CT Protein Sequence

MEKSWFNFMFSKGELEYRGELSKAMDSFAPGEKTTISQDRFIYDMDKNFYGWDERSSYSSSYSNNVDLLVSSKDIRNFISDDTFFVR
DSNKNSYSIFFDKKKKIFEIDNDFSDLEKFFYSYCSSSYLNNRSKGDNDLHYDPYIKDTKYNCTNHINSCIDSYFRSYICIDNNFLIDSNN
FNESYIYNFICSESGKIRESKNYKIRTNRNRSNLISSKDFDITQNYNQLWIQCDNCYGLMYKKVKMNVCEQCGHYLKMSSSERIELSID
PGTWNPMDEDMVSADPIKFHSKEEPYKNRIDSAQKTTGLTDAVQTGTGQLNGIPVALGVMDFRFMGGSMGSVVGEKITRLIEYATN
QCLPLILVCSSGGARMQEGSLSLMQMAKISSVLCDYQSSKKLFYISILTSPTTGGVTASFGMLGDIIIAEPYAYIAFAGKRVIEQTLKKA
VPEGSQAAESLLRKGLLDAIVPRNLLKGVLSELFQLHAFFPLNTN

BC Protein Sequence

MDASMITNSKSITSPPSLALGKSGGGGVIRSSLCNLMMPSKVNFPRQRTQTLKVSQKKLKRATSGGLGVTCSGGDKILVANRGEIAV
RVIRTAHEMGIPCVAVYSTIDKDALHVKLADEAVCIGEAPSNQSYLVIPNVLSAAISRGCTMLHPGYGFLSENALFVEMCRDHGINFIG
PNPDSIRVMGDKATARETMKNAGVPTVPGSDGLLQSTEEAVRVANEIGFPVMIKATAGGGGRGMRLAKEPGEFVKLLQQAKSEAA
AAFGNDGCYLEKFVQNPRHIEFQVLADKFGNVVHFGERDCSIQRRNQKLLEEAPSPALTAELRKAMGDAAVAAAASIGYIGVGTVEF
LLDERGSFYFMEMNTRIQVEHPVTEMIYSVDLIEEQIRVAMGEKLRYKQEDIVLRGHSIECRINAEDPFKGFRPGPGRITSYLPSGGPF
VRMDSHVYSDYVVPPSYDSLLGKLIVWAPTREKAIERMKRALNDTIITGVPTTINYHKLILDVEDFKNGKVDTAFIVKHEEELAEPQEIV
AVKDLTNATV

Figure 13. ACCase and BADC protein sequences. Peptides selected for AQUA peptide synthesis are highlighted in blue. Two peptides were selected for each ACCase subunit, and one peptide was selected for each BADC protein.

Determination of AQUA peptide retention times, fragmentation patterns, and collision energy optimization

The AQUA peptides were initially analyzed in an unscheduled MRM method to determine retention times and the most abundant fragment ions for each peptide. The top eight most abundant fragment ions (transitions) were selected for each AQUA peptide, and diagnostic fragmentation patterns produced from the calculated peak area of each transition ion were determined, resulting in a rank assignment for each transition ion (Table 2). A scheduled MRM method was then created to target each AQUA peptide and its selected transition ions, limiting a two minute retention time window for each peptide, as listed in Table 3.

Table 2. List of transition ions of selected peptides for AQUA-MRM analysis*

α-CT				
Peptide: SEELGQGEAIANNLR				
	Heavy: 805.904 (+2)	**Light: 800.8999 (+2)**		
Transition Ion	**m/z**	**m/z**	**Rank**	**Charge state**
G (y11)	1152.5995	1142.5913	3	(+1)
G (y9)	967.5195	957.5112	2	(+1)
A (y7)	781.4554	771.4472	4	(+1)
I (y6)	710.4183	700.41	7	(+1)
A (y5)	597.3343	587.326	1	(+1)
N (y4)	526.2971	516.2889	8	(+1)
E (b2)	217.0819	217.0819	6	(+1)
E (b3)	346.1245	346.1245	5	(+1)

α-CT				
Peptide: DLYTHLTPIQR				
	Heavy: 456.2499 (+3)	**Light: 452.9139 (+3)**		
Transition Ion	**m/z**	**m/z**	**Rank**	**Charge state**
L (y6)	737.4544	727.4461	3	(+1)
T (y5)	624.3703	614.362	2	(+1)
P (y4)	523.3226	513.3144	1	(+1)
Q (y2)	313.1858	303.1775	8	(+1)
Y (y9)	569.8158	564.8116	4	(+2)
T (y8)	488.2841	483.28	6	(+2)
H (y7)	437.7603	432.7561	5	(+2)
I (b9)	352.1904	352.1904	7	(+3)

β-CT				
Peptide: NFISDDTFFVR				
	Heavy: 685.8344 (+2)	**Light: 680.8302 (+2)**		
Transition Ion	**m/z**	**m/z**	**Rank**	**Charge state**
I (y9)	1109.5501	1099.5419	2	(+1)
S (y8)	996.4661	986.4578	5	(+1)
D (y7)	909.434	899.4258	6	(+1)
D (y6)	794.4071	784.3988	7	(+1)
T (y5)	679.3801	669.3719	4	(+1)
F (y3)	431.264	421.2558	3	(+1)
F (b2)	262.1186	262.1186	8	(+1)
I (b3)	375.2027	375.2027	1	(+1)

Table 2. Continued

β-CT				
Peptide: AMDSFAPGEK				
	Heavy: 530.7466 (+2)	Light: 526.7395 (+2)		
Transition Ion	m/z	m/z	Rank	Charge state
D (y8)	858.4083	850.3941	1	(+1)
S (y7)	743.3814	735.3672	5	(+1)
F (y6)	656.3494	648.3352	7	(+1)
A (y5)	509.2809	501.2667	3	(+1)
P (y4)	438.2438	430.2296	2	(+1)
M (b2)	203.0849	203.0849	4	(+1)
D (b3)	318.1118	318.1118	8	(+1)
S (b4)	203.0756	203.0756	6	(+2)

BC				
Peptide: ITSYLPSGGPFVR				
	Heavy: 702.3815 (+2)	Light: 697.3774 (+2)		
Transition Ion	m/z	m/z	Rank	Charge state
S (y11)	1189.624	1179.6157	5	(+1)
L (y9)	939.5286	929.5203	4	(+1)
P (y8)	826.4445	816.4363	1	(+1)
V (y2)	284.1956	274.1874	8	(+1)
P (y8)	413.7259	408.7218	7	(+2)
T (b2)	215.139	215.139	6	(+1)
Y (b4)	465.2344	465.2344	2	(+1)
L (b5)	578.3184	578.3184	3	(+1)

BC				
Peptide: FGNVVHFGER				
	Heavy: 391.2009 (+3)	Light: 387.8648 (+3)		
Transition Ion	m/z	m/z	Rank	Charge state
V (y6)	754.387	744.3787	5	(+1)
H (y5)	655.3186	645.3103	3	(+1)
F (y4)	518.2597	508.2514	2	(+1)
G (y3)	371.1913	361.183	1	(+1)
G (y9)	512.7635	507.7594	7	(+2)
V (y6)	377.6971	372.693	8	(+2)
H (y5)	328.1629	323.1588	4	(+2)
H (b6)	327.6715	327.6715	6	(+2)

Table 2. Continued

BCCP1				
Peptide: SPAPGEPPFIK				
	Heavy: 574.3155 (+2)	Light: 570.3084 (+2)		
Transition Ion	m/z	m/z	Rank	Charge state
A (y9)	963.5389	955.5247	6	(+1)
P (y8)	892.5018	884.4876	3	(+1)
G (y7)	795.4491	787.4349	7	(+1)
P (y5)	609.385	601.3708	2	(+1)
A (y9)	482.2731	478.266	8	(+2)
P (y8)	446.7546	442.7475	5	(+2)
P (b2)	185.0921	185.0921	1	(+1)
A (b3)	256.1292	256.1292	4	(+1)

BCCP1				
Peptide: DIVELQLK				
	Heavy: 483.2915 (+2)	Light: 479.2844 (+2)		
Transition Ion	m/z	m/z	Rank	Charge state
V (y6)	737.4647	729.4505	1	(+1)
E (y5)	638.3963	630.3821	2	(+1)
L (y4)	509.3537	501.3395	5	(+1)
Q (y3)	396.2696	388.2554	6	(+1)
L (y2)	268.2111	260.1969	8	(+1)
I (b2)	229.1183	229.1183	7	(+1)
V (b3)	328.1867	328.1867	4	(+1)
E (b4)	229.1183	229.1183	3	(+1)

BCCP2				
Peptide: SPGPGEPPFVK				
	Heavy: 560.2999 (+2)	Light: 556.2928 (+2)		
Transition Ion	m/z	m/z	Rank	Charge state
G (y9)	935.5076	927.4934	6	(+1)
P (y8)	878.4862	870.472	3	(+1)
G (y7)	781.4334	773.4192	8	(+1)
P (y5)	595.3694	587.3552	1	(+1)
P (y10)	516.7838	512.7767	7	(+2)
G (y9)	468.2575	464.2504	4	(+2)
P (y8)	439.7467	435.7396	5	(+2)
P (b2)	185.0921	185.0921	2	(+1)

Table 2. Continued

BCCP2				
Peptide: DIVELELK				
	Heavy: 483.7835 (+2)	Light: 479.7764 (+2)		
Transition Ion	m/z	m/z	Rank	Charge state
V (y6)	738.4487	730.4345	4	(+1)
E (y5)	639.3803	631.3661	1	(+1)
L (y4)	510.3377	502.3235	5	(+1)
E (y3)	397.2537	389.2395	6	(+1)
L (y2)	268.2111	260.1969	7	(+1)
I (b2)	229.1183	229.1183	2	(+1)
E (b6)	699.3559	699.3559	8	(+1)
E (b4)	229.1183	229.1183	3	(+2)
BADC1				
Peptide: SASSAPSPSQAKPSSEK				
	Heavy: 551.9438 (+3)	Light: 549.2724 (+3)		
Transition Ion	m/z	m/z	Rank	Charge state
P (y10)	1066.5619	1058.5477	5	(+1)
A (y7)	754.4185	746.4043	7	(+1)
P (y5)	555.2864	547.2722	2	(+1)
A (y13)	661.3455	657.3384	6	(+2)
P (y12)	625.827	621.8199	1	(+2)
S (y11)	577.3006	573.2935	8	(+2)
P (y10)	533.7846	529.7775	3	(+2)
A (b2)	159.0764	159.0764	4	(+1)
BADC2				
Peptide: TSSSSADRPQTLANK				
	Heavy: 524.2685 (+3)	Light: 521.5971 (+3)		
Transition Ion	m/z	m/z	Rank	Charge state
A (y3)	340.207	332.1928	7	(+1)
N (y2)	269.1699	261.1557	5	(+1)
S (y13)	691.8593	687.8522	1	(+2)
S (y12)	648.3433	644.3362	2	(+2)
S (y11)	604.8273	600.8202	3	(+2)
A (y10)	561.3113	557.3042	6	(+2)
R (y8)	468.2793	464.2722	8	(+2)
S (b2)	189.087	189.087	4	(+1)

Table 2. Continued

BADC3				
Peptide: LNAQLVPKPSEVEALVTEICDSSSIAEFELK				
	Heavy: 1123.2526 (+3)	Light: 1120.5812 (+3)		
Transition Ion	m/z	m/z	Rank	Charge state
A (y6)	744.4018	736.3876	5	(+1)
F (y4)	544.3221	536.3079	7	(+1)
L (y2)	268.2111	260.1969	6	(+1)
N (b2)	228.1343	228.1343	3	(+1)
A (b3)	299.1714	299.1714	1	(+1)
Q (b4)	427.23	427.23	4	(+1)
L (b5)	540.314	540.314	8	(+1)
V (b6)	639.3824	639.3824	7	(+1)

*The top eight most abundant transition ions were selected for each AQUA peptide based on peak area intensity. The ion type, heavy and light mass-to-charge ratio (m/z), peak area intensity rank, and monitored charge states of each transition ion are listed for each peptide and its corresponding protein. The heavy and light precursor m/z and charge states (+N) are listed for each set of transition ions.

AQUA peptide linear response

To determine the lower limit of quantitation (LLOQ) for each AQUA peptide and ultimately, the optimal amount of peptide to add to each sample that is both within the linear range of detection and quantitatively reproducible, a six-point, ten-fold dilution series was performed. Matrix effects often cause changes in AQUA peptide responses after addition to the biological sample (100), therefore, the AQUA peptide dilution series was performed in an *Arabidopsis* seed peptide matrix to account for any matrix effects that could interfere with quantitative analysis of the linear range of detection for each peptide. In each LC-MS/MS analysis, 1 µg seed peptide matrix was injected, with the AQUA

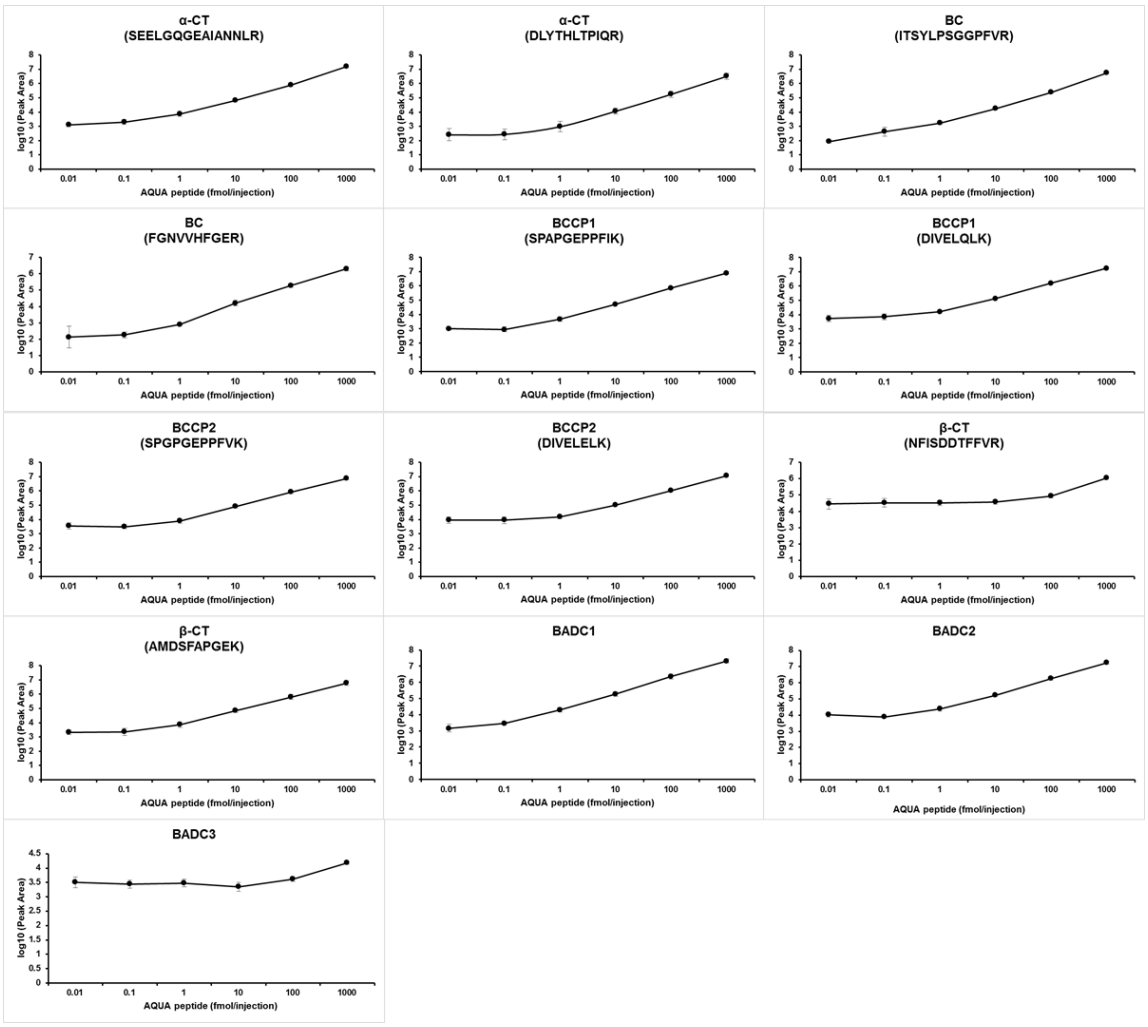

Figure 14. Analysis of AQUA peptide linear response. A six-point, ten-fold dilution series of AQUA peptides was performed ranging from 0.01-1000 fmol/injection in 1 µg *Arabidopsis* seed tryptic peptide matrix. Peptide responses were monitored in a multiplexed AQUA-MRM assay. The linear peak area responses for each peptide were log base 10 transformed and plotted as a function of fmol AQUA peptide/injection.

peptide dilution injections ranging from 0.01- 1000 fmol. The resulting peak areas for each peptide were log base 10 transformed and plotted as a function of fmol AQUA peptide/injection (Figure 14). For each peptide, the retention time, R^2 value, line equation, and lower limit of quantitation (LLOQ) was determined

(Table 3). Assay were performed with four biological replicates, providing standard deviations for statistical analysis. The relative standard deviations for each peptide were calculated by dividing the standard deviation by the average peak area for each dilution point. For all peptides, the relative standard deviation (RSD) was below 8% within the linear range of detection. The line slope ranged from 0.96-1.18 for all peptides with the exception of β-CT peptide NFISDDTFFVR with a slope of 0.74 and BADC3 peptide LNAQLVPKPSEVEALVTEICDSSSIAEFELK with a slope of 0.41. The LLOQ for all peptides was 1 fmol/injection with the exception of the BADC3 peptide and β-CT peptides which both had a LLOQ of 100 fmol/injection.

Table 3. Results from MRM analysis of AQUA peptide dilution series*

Protein target	AQUA Peptides	TAIR Accession	m/z	RT (min)	R^2	Line equation	LLOQ (fmol/injection)
α-Carboxyltransferase	SEELGQGEAIANNLR	AT2G38040	805.9	12.4-14.4	0.995	y = 1.108x + 3.772	1
	DLYTHLTPIQR		456.2	12.6-13.6	0.999	y = 1.179x + 2.930	1
β-Carboxyltransferase	AMDSFAPGEK	ATCG00500	530.7	9.6-11.6	1.000	y = 0.970x + 3.865	1
	NFISDDTFFVR		685.8	16.1-18.1	0.920	y = 0.736x + 3.715	100
Biotin carboxylase	FGNVVHFGER	AT5G35360	391.2	12.2-14.2	0.996	y = 1.128x + 2.984	1
	ITSYLPSGGPFVR		702.4	14.6-16.6	0.981	y = 1.038x + 3.405	1
BCCP1	SPAPGEPPFIK	AT5G16390	574.3	12.7-13.7	0.995	y = 1.01x + 3.814	1
	DIVELQLK		483.3	14.1-16.1	0.999	y = 1.014x + 4.179	1
BCCP2	SPGPGEPPFVK	AT5G15530	560.3	12.4-14.4	1	y = 0.986x + 3.918	1
	DIVELELK		483.8	14.1-16.1	0.997	y = 0.967x + 4.119	1
BADC1	SASSAPSPSQAKPSSEK	AT3G56130	551.9	7.4-9.4	0.998	y = 0.98x + 4.367	1
BADC2	TSSSSADRPQTLANK	AT1G52670	524.3	8.4-10.4	0.999	y = 0.962x + 4.337	1
BADC3	LNAQLVPKPSEVEALVTEICDSSSIAEFELK	AT3G15690	1123.3	17.2-19.2	0.960	y = 0.412x + 2.888	100

*The protein target name, Arabidopsis TAIR accession number, peptide sequence, monitored mass-to-charge ratio (m/z), chromatographic retention time (RT), R^2 value, line equation, and lower limit of quantitation (LLOQ) are listed for each peptide.

In this analysis, we also simultaneously monitored the native peptide response in the *Arabidopsis* seed matrix. As the seed matrix injected per run

was at a fixed concentration in each sample, this enabled the use of the native peptide response as a normalizer, which could then be used to calculate the response ratio of the AQUA/native peptides. Calculating response ratios controlled for ionization and chromatographic variations inherent to LC-MS/MS. These response ratios were then log base 10 transformed and plotted as a function of AQUA peptide/injection (Figure 15).

Unfortunately, not all native peptides for the ACCase subunits produced a signal in the *Arabidopsis* seed samples (α-CT: DLYTHLTPIQR, β-CT: AMDSFAPGEK, BC: FGNVVHFGER, BCCP1: DIVELQLK, and BCCP2: DIVELELK). A reason for this could be a result of poor digestion efficiencies due to the chemical nature of the peptides and/or flanking residues on the N- or C-termini of the peptide. For instance, the α-CT peptide DLYTHLTPIQR and BCCP peptides DIVELQLK and DIVELELK possess an N-terminal acidic residue (Asp), which is known to cause tryptic miscleavage events (16). Similarly, the BC peptide FGNVVHFGER has a flanking aspartate residue in the +1 position to its C-terminal arginine and -2 position to its N-terminal residue, which could also be a source of tryptic miscleavage. The β-CT peptide AMDSFAPGEK could also experience miscleavage events due to the aspartate located in the third amino acid position. To control for accuracy, it is ideal to have two different AQUA peptides per protein in any AQUA-MRM assay. However, one quantifiable peptide will be sufficient if further controls are performed.

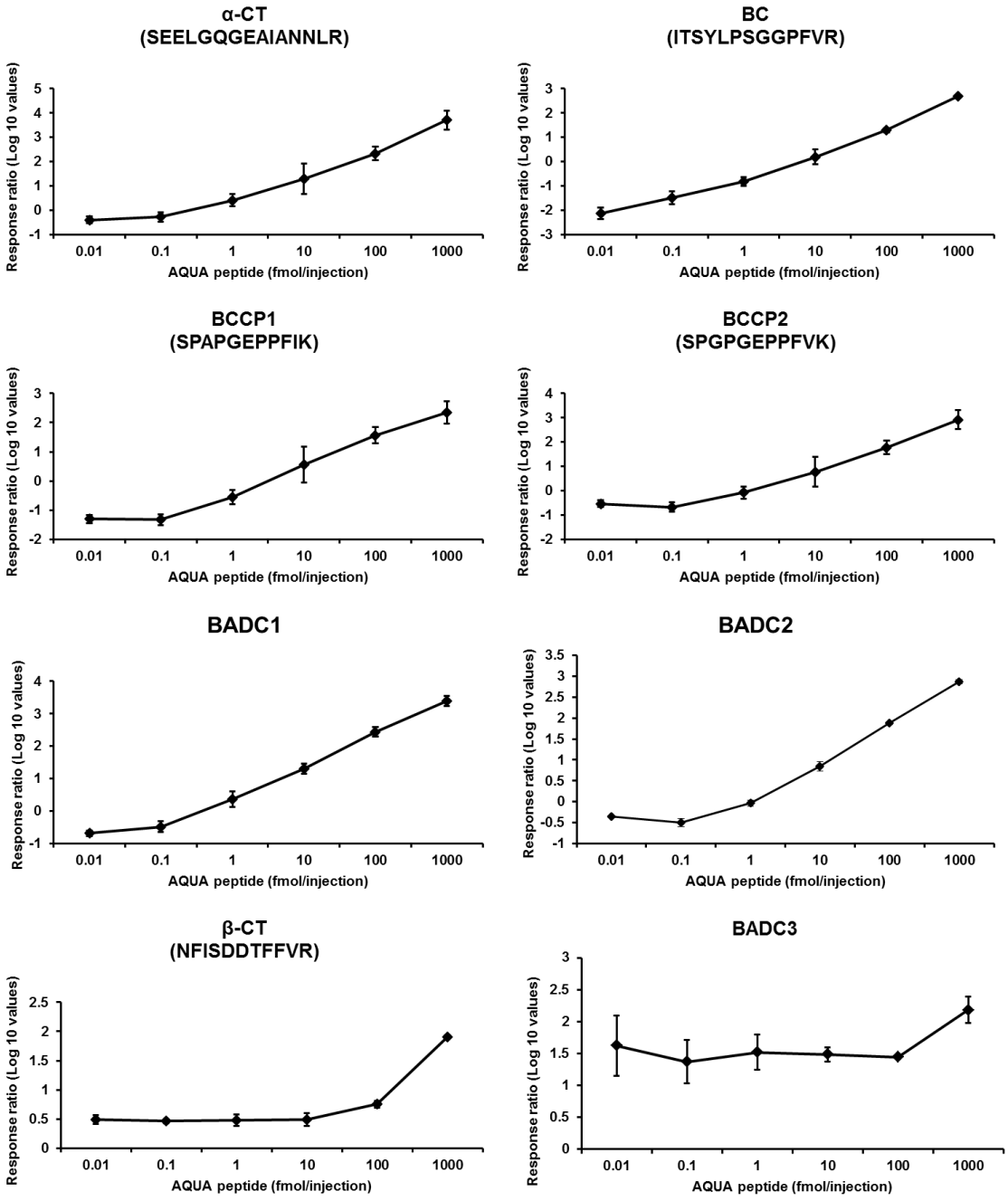

Figure 15. Analysis of AQUA peptide linear response with native peptide normalizer. A six-point, ten-fold dilution series of AQUA peptides was performed ranging from 0.01-1000 fmol/injection in 1 µg *Arabidopsis* seed tryptic peptide matrix. Peptide responses were monitored in a multiplexed AQUA-MRM assay. The AQUA/native response ratios were log base 10 transformed and plotted as a function of fmol AQUA peptide/injection.

Recombinant protein accuracy evaluation

To determine whether the peptides lacking signal in the biological sample digest poorly, an accuracy evaluation was performed using AQUA-MRM analysis of purified recombinant protein to each of the ACCase subunits. Recombinant protein was purified by affinity chromatography, and protein purity was quantified by scanning densitometry of CBB-stained SDS-PAGE gels using ImageQuant v. 8.1 software (Figure 16). The gel images were scanned as 8-bit, colored JPEG files and converted to greyscale TIFF files before uploading into the software. Unfortunately, β-CT did not successfully purify after several attempts and was therefore, excluded from this analysis. A six-point, two-fold dilution series of recombinant protein was performed ranging from 31.25-1000 ng/injection. AQUA peptides were spiked into the samples at 100 fmol/injection with the exception of the BADC3 peptide, of which 1000 fmol was injected. Recombinant protein injected was corrected based on protein purity. Corrections were performed by multiplying the recombinant protein injected onto the mass spectrometer by the percent purity of the protein. For example, if 1000 ng of a 90% pure recombinant protein was injected, then this value would be corrected to 900 ng. To account for matrix effects but prevent incidental analysis of native *Arabidopsis* peptides, the recombinant protein dilution series was performed in a *Ricinus communis* background matrix. To verify that no background native or AQUA signal was present, the *R. communis* matrix was first analyzed in the AQUA-MRM method without addition of AQUA peptide or recombinant protein. The recombinant protein linear response was quantified from AQUA-MRM

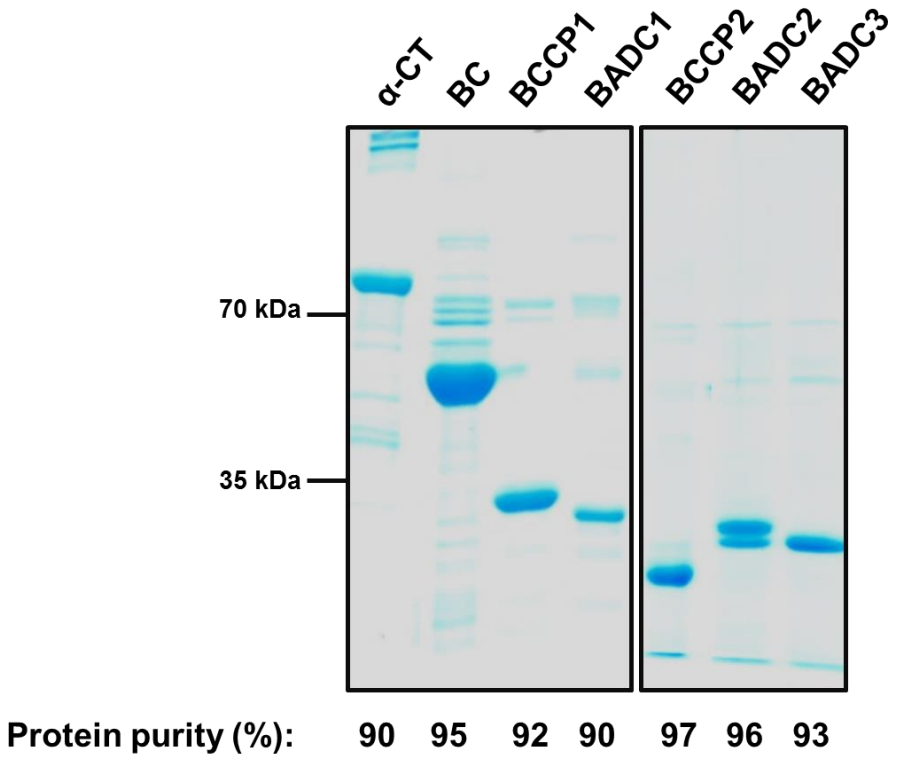

Figure 16. Assessment of ACCase recombinant protein purity. Proteins were purified by affinity chromatography and subjected to gel electrophoresis under denaturing conditions. The SDS-PAGE gel (13% (w/v) acrylamide) was stained with Coomassie Brilliant Blue (CBB). Protein purities were quantified using ImageQuant TL software v. 8.1 (GE Healthcare Life Sciences) by scanning densitometry of CBB stained gels to obtain the band volume for each ACCase protein and contaminating proteins.

analysis using the following calculations: 1) Response ratio (Light peak area/Heavy peak area) x fmol AQUA peptide = fmol recombinant peptide, 2) fmol recombinant peptide x recombinant protein molecular weight (g/mol) = g recombinant protein, and 3) g recombinant protein x (1e9 ng) = ng recombinant protein. The calculated values were plotted in ng on a logarithmic base 2 scale as a function of recombinant protein injected (Figure 17). The results from this analysis are listed in Table 4.

To achieve an ideal linear accuracy of 100%, the slope of the peptide response within the linear range of detection should be equal to 1. However, the linear responses for all of the peptides analyzed, with the exception of BCCP peptides DIVELQLK and DIVELELK, displayed slopes below 1, indicating the accuracy is below the theoretical expectation. For instance, the BC peptides ITSYLPSGGPFVR and FGNVVHFGER display slopes of 0.384 and 0.103, respectively. Therefore, the linear response of peptide ITSYLPSGGPFVR is 38.4% accurate, while the linear response of peptide FGNVVHFGER is 10.3% accurate. Similarly, the α-CT peptide SEELGQGEAIANNLR displayed a slope of 0.216, while peptide DLYTHLTPIQR displayed slope of 0.095. These data could provide an explanation for the lack of signal observed previously in the *Arabidopsis* biological sample for peptides FGNVVHFGER and DLYTHLTPIQR. BCCP peptides SPAPGEPPFIK and SPGPGEPPFVK displayed higher linear

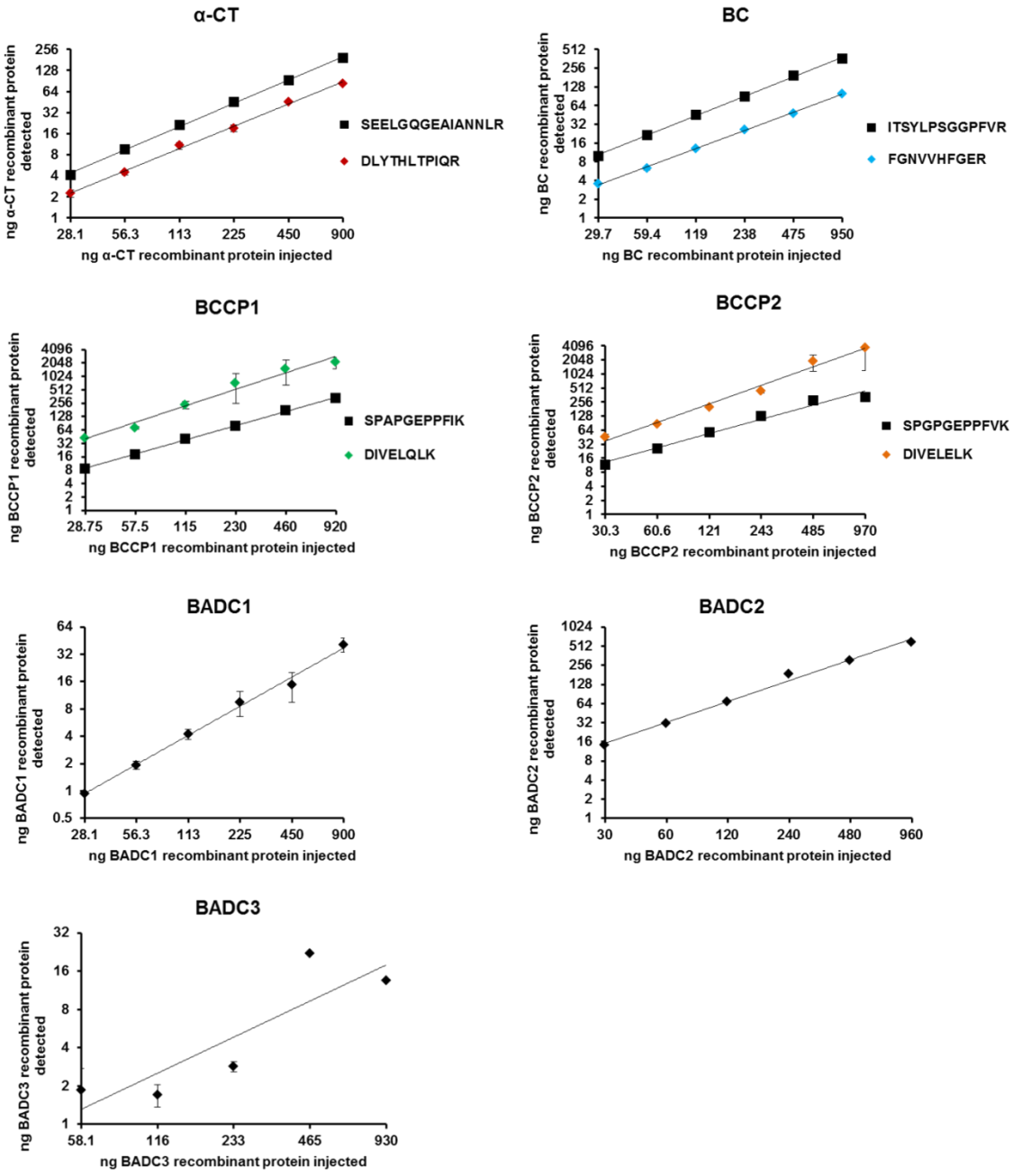

Figure 17. Linear response of ACCase recombinant protein in AQUA-MRM analysis. A six-point, two-fold recombinant protein dilution series was performed ranging from 31.25-1000 ng/injection. Recombinant protein injected values were corrected based on protein purity using the quantified band volume obtained from ImageQuant software. Values are plotted in ng on a logarithmic base 2 scale as a function of recombinant protein injected. The colored peptides lack signal in *Arabidopsis* biological seed sample.

accuracies, with slopes of 0.363 and 0.578, respectively. The BADC2 peptide displayed the highest accuracy under 100% with a slope of 0.622, which suggests that the low accuracies observed for the other peptides are not an artifact of the digestion method used. It is likely that these peptides experience poor digestion efficiency, possibly due to the chemical nature of the peptide sequence and/or surrounding amino acids, as discussed above. The BADC3 peptide displayed the lowest linear accuracy, with a slope of 0.017 and an R^2 value of 0.45. The poor response of this peptide could be partially attributed to its length (31 amino acids), which is not ideal for chromatographic elution and ionization in mass spectrometry (106,107).

Table 4. Results from recombinant protein AQUA-MRM accuracy evaluation*

Protein target	AQUA Peptides	Line equation	R^2	LLOQ (ng/injection)
α-Carboxyltransferase	SEELGQGEAIANNLR	y = 0.216x - 2.877	1	<28.1
	DLYTHLTPIQR	y = 0.095x - 0.265	0.997	<28.1
Biotin carboxylase	FGNVVHFGER	y = 0.103x + 0.622	0.999	<28.1
	ITSYLPSGGPFVR	y = 0.384x + 0.319	0.999	<28.1
BCCP1	SPAPGEPPFIK	y = 0.363x - 0.959	0.998	<28.8
	DIVELQLK	y = 3.662x - 153.14	0.999	<28.8
BCCP2	SPGPGEPPFVK	y = 0.578x - 8.940	1	<30.3
	DIVELELK	y = 1.868x - 19.749	0.998	<30.3
BADC1	SASSAPSPSQAKPSSEK	y = 0.045x - 1.153	0.981	56.3
BADC2	TSSSSADRPQTLANK	y = 0.622x + 3.941	0.994	<30.0
BADC3	LNAQLVPKPSEVEALVTEICDSSSIAEFELK	y = 0.017x + 2.17	0.454	223

*Protein target name, corresponding AQUA peptide sequence, line equation, R^2 value, and lower limit of quantitation (LLOQ) are listed. The line equations listed will be used as a correction factor for protein abundance in subsequent biological analyses.

Conversely, the BCCP peptides DIVELQLK and DIVELELK displayed slopes of 3.662 and 1.868, respectively, far exceeding the accuracy limitations. It is curious that we observe overestimations for these peptides, as they both have

similar sequences and were not detected previously in the *Arabidopsis* biological sample, which suggests that digestion efficiency is not the source of accuracy issues for these peptides.

This is not the first instance of observed accuracy issues for AQUA peptides in MRM analysis (108-110). One study compared the accuracy of the AQUA peptide strategy to protein standard absolute quantification (PSAQ) by quantifying a dilution series of staphylococcal enterotoxin proteins, SEA and TSST-1 added to a urine protein matrix (108). PSAQ is similar to the AQUA peptide strategy, however, it employs heavy-labeled recombinant protein as an internal standard to control for digestion efficiency (17). In this study, AQUA analysis revealed a 21% accuracy in the response of an SEA peptide, while PSAQ revealed a much higher accuracy of 105%. Similarly, quantitation of a peptide designed against TSST-1 using AQUA peptide standards and PSAQ displayed accuracies of 4% and 108%, respectively. These results indicate that the low accuracies observed in the AQUA-MRM analysis are likely a result of digestion efficiency. Interestingly, this study also reported a 37% overestimation of SEA protein with a second AQUA peptide, which they attributed to either inefficient solubilization of the AQUA peptides or adsorption of the AQUA peptides to the polypropylene tube. This could be a possible explanation for the overestimation we observe in the recombinant protein responses of BCCP peptides DIVELQLK and DIVELELK, as their chemical characteristics are similar. A recent study also used PSAQ for absolute quantitation of proteins in the fatty acid biosynthetic pathway in *E. coli* (99). This study claimed PSAQ is more

accurate and precise than AQUA-MRM, because it uses heavy labeled protein standards to overcome issues with digestion efficiency. Other reviews acknowledge that peptide digestion efficiencies are a disadvantage of the AQUA-MRM technique and suggest using recombinant protein standards as a solution to combat this issue (111,112). Although AQUA peptide standards display lower accuracy than other quantitative mass spectrometry techniques, they are far more cost-effective and perform better than PSAQ in stoichiometric quantitation (110), which is the ultimate goal of the ACCase AQUA-MRM assay.

As earlier mentioned, it is ideal to have two different peptides per protein for validation, however, one peptide can be acceptable if proper controls are in place. Determination of the recombinant protein linear response not only revealed information regarding peptide accuracy, but also provided a line equation that can be used as a correction factor for quantitation of protein in biological samples (Table 4). By using a recombinant protein correction factor, we can circumvent digestion efficiency issues that would otherwise not be accounted for. This also enables the use of one peptide per protein for quantitation of the ACCase subunits and BADC proteins in our future analyses.

Concluding remarks

Quantitative AQUA-MRM mass spectrometry is a useful technique which has many biological applications, however, a series of method development and validation procedures are required for optimal use of this assay. Using these

procedures, we were able to determine the lower limits of quantitation for each peptide as well as assess matrix effects for optimization of the ACCase AQUA-MRM assay. The linear accuracy of each peptide was evaluated by monitoring the response of a recombinant protein standard curve for each ACCase subunit, which in most cases revealed underestimates in quantitation, likely attributed to digestion efficiencies. From this assessment, we obtained correction factors, that can be used to overcome accuracy issues and enables the use of one peptide per protein for quantitative analysis. Collectively, the method development and validation of the ACCase AQUA-MRM assay allowed us to confidently move forward with biological experiments to quantitatively investigate BADC inhibition of the *Arabidopsis* heteromeric ACCase complex.

CHAPTER IV

TARGETED QUANTITATION OF HETEROMERIC ACETYL-COA CARBOXYLASE SUBUNITS IN VIVO USING AQUA-MRM

INTRODUCTION

The committed step of *de novo* fatty acid synthesis (FAS) in plants is catalyzed by the plastid acetyl-CoA carboxylase (ACCase). In nature, ACCase exists as both a homomeric and heteromeric form. The heteromeric form of ACCase is found in prokaryotes, algae, mosses, gymnosperms, dicot and non-graminaceous monocot plants, while all other organisms harbor a homomeric form of ACCase for *de novo* FAS (113,114). Heteromeric ACCase is comprised of four subunits including α–carboxyltransferase (α-CT), β-carboxyltransferase (β-CT), biotin carboxylase (BC), and biotin carboxyl carrier protein (BCCP). *Arabidopsis thaliana* contains two isoforms of BCCP, which are designated BCCP1 and BCCP2. These subunits form a complex to catalyze the carboxylation of acetyl-CoA to malonyl-CoA, the carbon source for *de novo* FAS. The reaction mechanism for ACCase is catalyzed in two steps for which active site coupling is facilitated by the BCCP subunit. First, a biotin cofactor covalently attached to BCCP is carboxylated by BC in a reaction requiring ATP and bicarbonate. The biotinyl-carboxyl group is then transferred to acetyl-CoA by the carboxyltransferase subunits, producing malonyl-CoA.

Multiple regulatory mechanisms have been identified for ACCase. Light-dependent regulatory phosphorylation has been demonstrated for the β-CT subunit of pea ACCase (112). In this study, β-CT phosphorylation activated ACCase, and this effect was reversible upon addition of a phosphatase. Feedback inhibition has also been established for bacterial and plant ACCase by substrates including free fatty acids as well as acyl-ACP and acyl-CoA (112,115-

119). For instance, one study reported reversible feedback inhibition of plastid ACCase after addition of oleic acid (18:1) Tween esters in *Brassica napus* suspension cells (115). This was demonstrated using ^{14}C-actetate labeling assays to monitor the rate of ^{14}C incorporation into total lipids over a time course after Tween addition. The rate of incorporation was reduced 40% three hours after addition of 10 mM Tween 80, which was ultimately attributed to inhibition of heteromeric ACCase activity. A similar study using tobacco suspension cells observed a three- to five-fold reduction of ^{14}C incorporation into fatty acids as well as limiting levels of malonyl-CoA after addition of Tween 80, again suggesting ACCase is a target of feedback inhibition (120).

Recently, we identified a family of proteins that interact with multiple subunits of *Arabidopsis* heteromeric ACCase, which we have designated BADC (Salie, et al., unpublished). BADC proteins are annotated in TAIR as biotin/lipoyl attachment domain-containing proteins, and three isoforms are expressed in *Arabidopsis* (BADC1, BADC2, and BADC3). These proteins were initially identified by mass spectrometry analysis of co-immunoprecipitation assays performed with ACCase subunit-specific antibodies. Further analysis revealed all three BADC isoforms interact with both BCCP isoforms in yeast two-hybrid assays. These proteins resemble BCCPs in size, sequence, and structure, however, they are not biotinylated (Salie et al., unpublished). Collectively, BADC interactions with ACCase and their similarity to BCCPs suggest a regulatory function for this family of proteins. BADCs could be acting as inhibitory proteins of ACCase through competitive incorporation into the complex. BADC

incorporation would reduce the number of biotinylation sites, ultimately leading to the inhibition of heteromeric ACCase. According to this model, BADCs could affect catalytic turnover. However, this model is predicated on BADC incorporation into the complex by replacing holo-BCCP subunits, which is presently unclear.

This study aims to determine the *in vivo* levels of ACCase subunits including BADCs in an absolute quantitative manner to begin making predictions about subunit stoichiometry. To accomplish this, we used a targeted mass spectrometry method, termed multiple reaction monitoring (MRM), which enables simultaneous monitoring of multiple peptide transition ions within a single tandem mass spectrometry (LC-MS/MS) analysis (92). Custom synthesized, heavy-labeled AQUA peptide standards (93) designed against the ACCase subunits were coupled with the MRM assay to provide absolute protein abundance values. Protein abundance levels were used to compare stoichiometric changes in both catalytic and putative regulatory subunits (BADC) to ACCase. Using this method, absolute changes in ACCase protein abundance were quantified in *Arabidopsis* suspension cells after exogenous addition of oleic acid Tween esters as well as changes during *Arabidopsis* silique development. Quantitative RT-PCR analysis was also performed to compare absolute changes in mRNA expression to protein abundance levels.

Our results revealed contrasting stoichiometric changes in the abundance of BCCPs and BADCs, which supports the model of BADC inhibition of ACCase. In addition, the α-CT subunit of ACCase displayed 75-90% lower abundance

levels relative to the other subunits in siliques, however, since its partner protein β-CT was not quantified it is difficult to determine the meaning of this observation.

MATERIALS AND METHODS

Arabidopsis seed samples

Arabidopsis thaliana (ecotype-Columbia) plants were grown under 24 h light conditions at 25°C. Flowers were tagged right before anthesis, and siliques harvested 7, 9, 11, and 13 days after flowering (DAF). Upon collection, siliques (20 pooled per biological replicate) were put immediately on ice and stored at -80°C until protein extraction.

Arabidopsis suspension cells

An *Arabidopsis thaliana* T87 suspension cell stock was obtained from the Arabidopsis Biological Resource Center (ABRC) (Ohio State University, Columbus, OH). Suspension cells were grown in NT-1 medium (MS salt mixture, 3% (w/v) sucrose, 1 mM potassium phosphate, 0.001% (w/v) thiamine, 0.0004% (w/v) 2,4 – D, 0.5 mM myoinositol). Cells were subcultured by transferring 7 day-old culture into fresh NT-1 media (1:10 (v/v)). The suspension cultures were maintained on a rotary shaker at 130 rpm under constant light. *Arabidopsis* suspension cells (500 µL) were collected and pelleted in a tabletop centrifuge. After removal of the media, the cells were frozen immediately in liquid nitrogen and stored at -80°C until protein extraction.

Arabidopsis suspension cell growth curves

Suspension cell growth was monitored daily over eight days, by measuring the optical density at 600 nm (OD_{600}) of 500 µL of cells using a Shimadzu UV-1650 PC (Kyoto, Japan) dual beam spectrophotometer. This method of measuring cell growth of *Arabidopsis* T87 cells has previously been reported (121). The OD_{600} was also measured in a time course after addition of 10 mM Tween 80.

Tween feeding assays

Arabidopsis suspension cells were grown for three days after subculturing, then spiked with Tween 80. A 100 mM Tween 80 (enzyme grade, lot no. 043458, product no. BP338, approximately 75% 18:1, ThermoFisher Scientific, Waltham, MA) stock was prepared in sterile NT-1 media. The Tween 80 stock was added to the suspension cells at a final concentration of 10 mM. As a negative control, a mock treatment was also performed with an equal volume of media without Tween 80. Suspension cells (500 µL) were collected in biological triplicate at 0, 30, 60, 120, and 180 min after 10 mM Tween addition and 180 min after 0 mM Tween addition (negative control, NC). Medium was removed via centrifugation, frozen in liquid nitrogen, and stored at -80°C until protein extraction.

Protein extraction

Plant material was homogenized in an extraction buffer (0.9 M sucrose, 100 mM Tris-HCl pH 8.0, 10 mM EDTA, 0.4% (v/v) ß-mercaptoethanol). One volume of

Tris-buffered phenol was added to the homogenate and incubated with agitation at 4°C for 1 h. Samples were centrifuged at 17000 x g at 4°C for 5 min, and the phenol phase was transferred into a new polypropylene tube. The samples were back-extracted with one volume of extraction buffer and incubated with agitation for 5 min. Centrifugation was repeated as described above, and the phenol phase was transferred to five volumes of ice-cold precipitation solution (100 mM ammonium acetate in 100% methanol) to precipitate protein. Samples were vortexed, and protein was precipitated overnight at -80°C. Samples were centrifuged at 4,000 xg at 4°C for 10 minutes before each wash step. Protein was washed twice with precipitation solution, twice with 80% (v/v) acetone in water, and once with 70% (v/v) ethanol in water. Protein was stored at -80°C in 70% ethanol prior to sample preparation.

Sample preparation for AQUA-MRM

Extracted protein was resuspended in a urea buffer (8 M urea, 50 mM Tris-HCl, pH 8.0). Protein was quantified using the Bradford method using bovine gamma globulin (BGG) as a protein standard (BioRad Laboratories, Hercules, CA). Protein was digested with trypsin as previously described (103). Protein was portioned into 20 µg aliquots and reduced with DTT at a final concentration of 10 mM. Samples were incubated for 1 h at 37°C. Samples were alkylated with iodoacetamide (IAA) at a final concentration of 50 mM and incubated at room temperature in the dark for 1 h. Urea was diluted with 3 volumes of a solution of 10 mM ammonium bicarbonate and 10 mM DTT. Trypsin was added at a 1:50

ratio (trypsin:protein) and incubated at 37°C for 16 h. Tryptic peptides were lyophilized via centrifugal evaporator and stored at -80°C prior to mass spectrometry analysis.

Targeted mass spectrometry

Targeted mass spectrometry was performed on a TSQ Vantage EMR triple quadrupole instrument (Thermo Scientific, San Jose, CA) interfaced with a nanoLC 1-D plus liquid chromatography system (Ekisgent, Framingham, MA). Autosampling, chromatography, and mass spectrometry were performed as previously described (104). Peptides were bound on a C8 Cap Trap (Michrom Bioresources, Inc., Auburn, CA) and eluted over a 12.5 min gradient of 2-60% solvent B (0.1% (v/v) formic acid in acetonitrile). The total method time was 25 min at a flow rate of 500 nL/min. All analysis was performed with 1 µg of protein digest on column and a 5 µL injection volume. The AQUA peptides were injected within the linear range of detection, and all analysis performed was multiplexed. Data analysis was performed using Skyline software v. 2.6.0.7176 (MacCoss Lab, Department of Genome Sciences, University of Washington).

RNA extraction

Arabidopsis suspension cells were collected in four biological replicates. Media was extracted, and cells were frozen immediately in liquid nitrogen and stored at – 80°C until RNA extraction. RNA for all qPCR experiments was extracted using

RNeasy Plant Mini Kit (Qiagen, Hilden, Germany). RNA was eluted in 50 µL RNase-free water.

cDNA synthesis

cDNA was synthesized from 500 ng of RNA, 2 µL of oligo (dT) 15 nucleotide primer, and molecular grade water was added in the final volume 16 µl. Reaction mix was incubated for 5 min 70°C. 5 µL of M-MLV reverse transcriptase buffer (Promega, Madison, WI), 50 µM dNTPs, 1 µL RNase inhibitor (Applied Biosystems, Foster City, CA), 1 µL M-MLV reverse transcriptase (Promega) were added. Reaction mixture was incubated 2 h 37°C and 10 min at 70°C. cDNA was diluted with 50 µL of molecular grade water.

Quantitative RT-PCR analysis

Absolute quantitation was performed using a PCR product calibration curve. The standard curve was generated by performing a serial dilution of PCR products of known concentrations. All qPCR assays were performed on an ABI 7500 system (Applied Biosystems). The reaction volumes were 20 µL and contained SYBR® Green PCR Master Mix (Applied Biosystems), 350 nM forward and reverse primers, and molecular grade water. SYBR® Green PCR Master Mix contains SYBR® Green I dye, AmpliTaq Gold® DNA Polymerase, dNTPs with dUTP, Passive Reference 1, and optimized buffer components. Templates in four biological replicates were added in 2 µL volumes per reaction. Triplicates of zero

template controls, containing molecular grade water, were included in each run. Thermal cycle parameters were the following: 50°C for 2 min, 95°C for 10 min (Taq polymerase activation), 95°C for 10 sec (denaturation), 60°C for 1 min (primer annealing and elongation). Melting curve analysis was performed after each qPCR run to verify the presence of the desired amplicon. The Applied Biosystems software determined the fluorescence threshold for all samples after each run.

Results

Arabidopsis suspension cell growth curve

To determine the optimal stage of cell growth for our experimental analyses, we performed a growth curve analysis by measuring the optical cell density (OD_{600}) over the course of eight days (Figure 18). This method provided a rapid estimate of cell density, which has previously been demonstrated with *Arabidopsis* T87 cells (121). The results indicated that the observed time of log phase growth was between one and four days after subculturing. Three days after subculturing was selected as the optimal time point for all further experimental analyses.

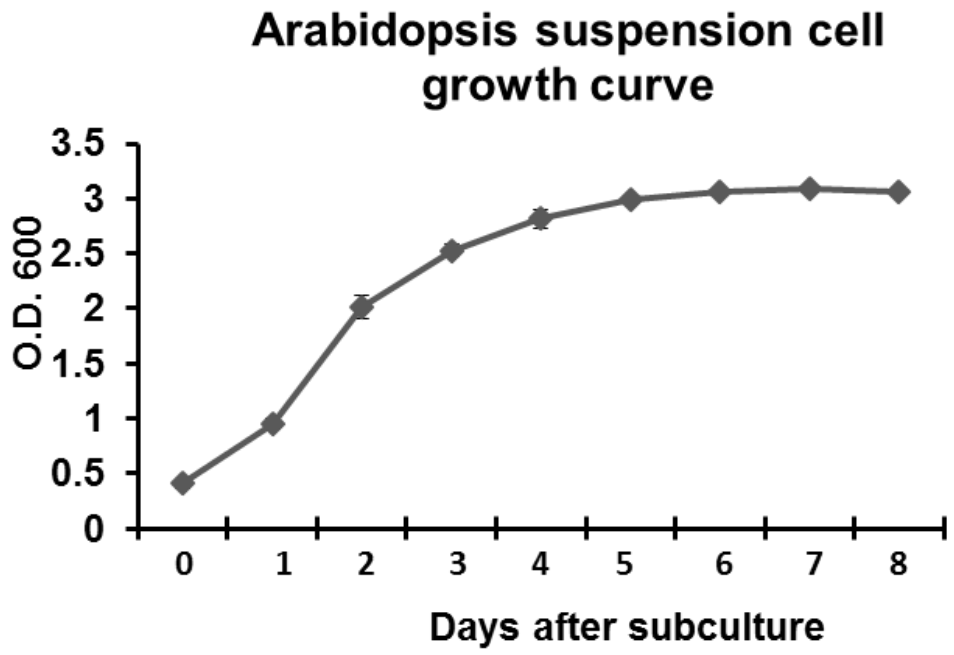

Figure 18. *Arabidopsis* suspension cell growth curve. Optical density (OD_{600}) measurements were taken daily in biological triplicate for eight days.

Effects of fatty acid replete media on Arabidopsis suspension cell growth

To assess the effects of 10 mM Tween 80 addition on *Arabidopsis* suspension cell growth, we performed a time course in which we monitored the optical cell density at several time points for 24 hours after Tween addition. The OD_{600} measurements were taken one, three, six and 24 hours after addition of 10 mM Tween (Figure 19). During this time, the cells displayed constant growth from one to six hours, with the growth increasing slightly at 24 hours. This indicated that addition of 10 mM Tween did not affect the growth of the cells up to 24 hours after Tween 80 supplementation. Therefore, this concentration was used for subsequent analyses.

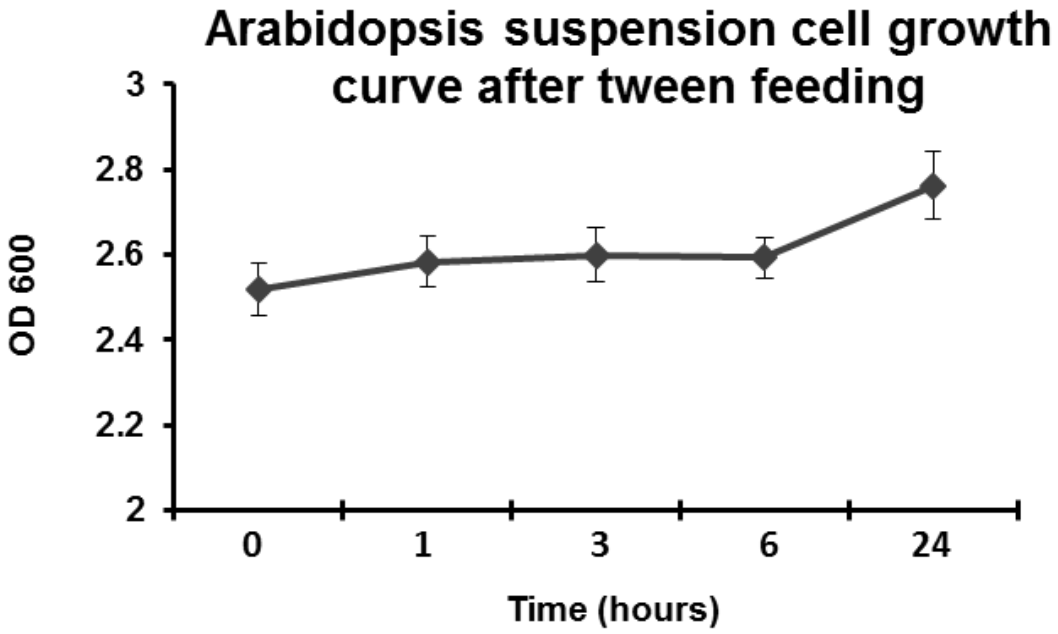

Figure 19. *Arabidopsis* suspension cell growth curve after Tween feeding. Cells were fed with 10 mM Tween 80, and optical density (OD_{600}) was monitored in biological triplicate for 24 hours. OD_{600} was measured at 0, 1, 3, 6, and 24 hours after Tween feeding.

Effects of fatty acid replete media on ACCase and BADC transcript levels

To determine the absolute changes in heteromeric ACCase and BADC transcript expression in response to Tween feeding, *Arabidopsis* suspension cells were supplied with 10 mM Tween 80 and collected over a time course of three hours (0, 30, 60, 120, and 180 minutes after Tween feeding). A mock treatment was also performed with addition of growth media without Tween 80 to determine whether observed changes in expression were not an artifact of media supplementation. Primers specific to ACCase and BADC genes were used in this analysis, and oligo-dT primers were used for cDNA synthesis. As β-CT is encoded in the chloroplast genome, transcript polyadenylation does not occur

and was therefore, excluded from qPCR analysis. These data revealed drastic changes in the transcript levels of the ACCase and BADC genes in response to Tween 80 feeding (Figure 20). The α-CT, BC, and BCCP1 subunits all displayed a ten-fold decrease in transcript levels three hours after Tween 80 feeding, while BCCP2 transcript increased five-fold three hours after Tween 80 feeding. Furthermore, absolute transcript levels for all three of the BADC genes increased eight-fold three hours after Tween 80 feeding.

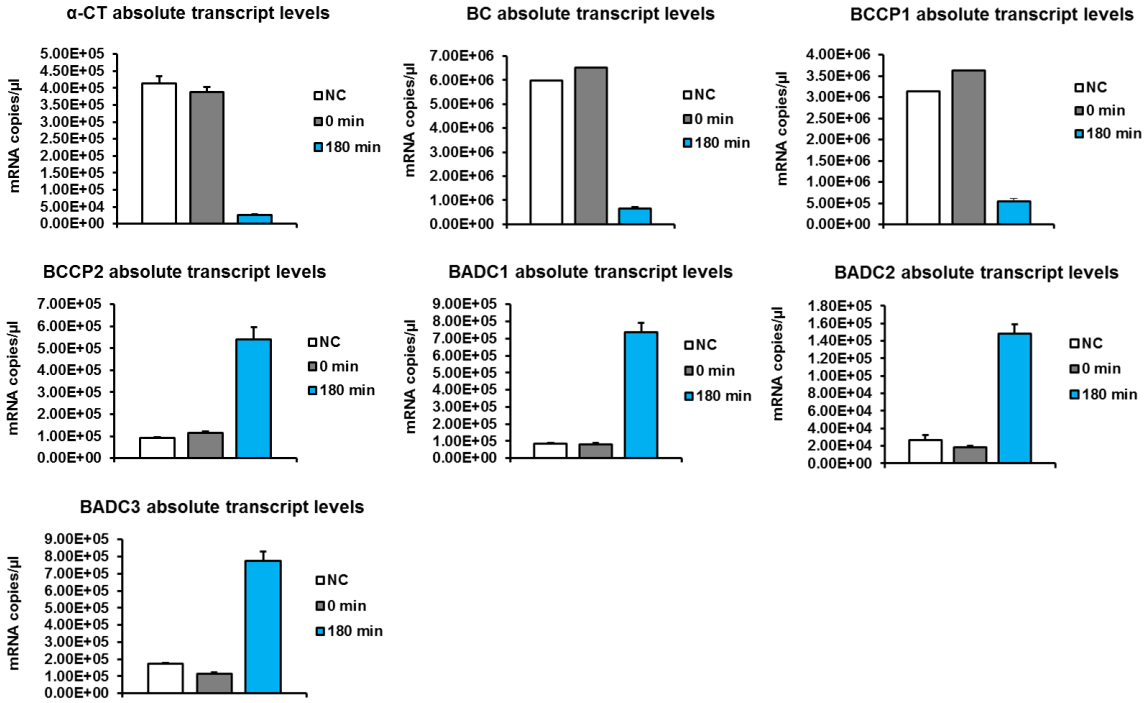

Figure 20. Absolute transcript expression profiles of individual ACCase and BADC genes in response to Tween feeding. qPCR analysis was performed with *Arabidopsis* suspension cells grown for three days after subculture before addition of 10 mM Tween. Values for negative control 180 min after 0 mM Tween feeding (NC), 0 min, and 180 min after 10 mM Tween feeding are displayed. Four biological replicates were collected and analyzed per time point.

Effects of fatty acid replete media on ACCase and BADC protein abundance

To compare the absolute changes in ACCase and BADC transcript expression to protein abundance, AQUA-MRM was performed in parallel with protein extracted from the same suspension cells as the qPCR analysis. The protein abundance profiles of each ACCase subunit and BADC protein, with the exception of β-CT and BADC3, which were below the detection limit of the assay, were plotted for each time point and negative control (Figure 21). Protein abundance was calculated using the line equations listed in Table 4 of Chapter 3, which were determined from the recombinant protein standard curve. The abundance values obtained from LC-MS/MS analysis were used as the y-variable (ng protein detected) to solve for the x-variable (ng protein injected). For instance, the line equation for the BADC2 standard curve is y=0.622x+3.941. If 50 ng of BADC2 were detected, then the corrected value would be 74 ng injected. The correction factors (line equations) were applied to the corresponding ACCase protein analyzed at each time point.

The results revealed significant, but gradual changes in ACCase and BADC protein abundance compared to transcript expression over time in response to Tween feeding. Since this is a kinetic assay, we plotted the initial (0 min) and final (three h after Tween feeding) protein abundance values along with the 0 mM Tween negative control for each subunit (Figure 22). The negative control displayed no significant difference in protein abundance compared to the 0 minute time point, with the exception of BC, which increased, indicating that changes observed were not a result of media addition. Collectively, α-CT, BC,

and BCCP1 protein abundance significantly decreased (p-values of 0.04*, 0.02*, and 0.006**, respectively) in response to Tween feeding after three hours, suggesting ACCase activity is reduced. Absolute abundance of BCCP2 was slightly reduced in response to Tween feeding after 180 min, however, this reduction was not statistically significant. Furthermore, BCCP2 was 20 times less abundant than BCCP1, suggesting its involvement in *de novo* fatty acid biosynthesis in *Arabidopsis* suspension cells is minimal. BADC1 and BADC2 protein abundance was not significantly affected in response to Tween feeding, and BADC1 was approximately ten times more abundant than BADC2.

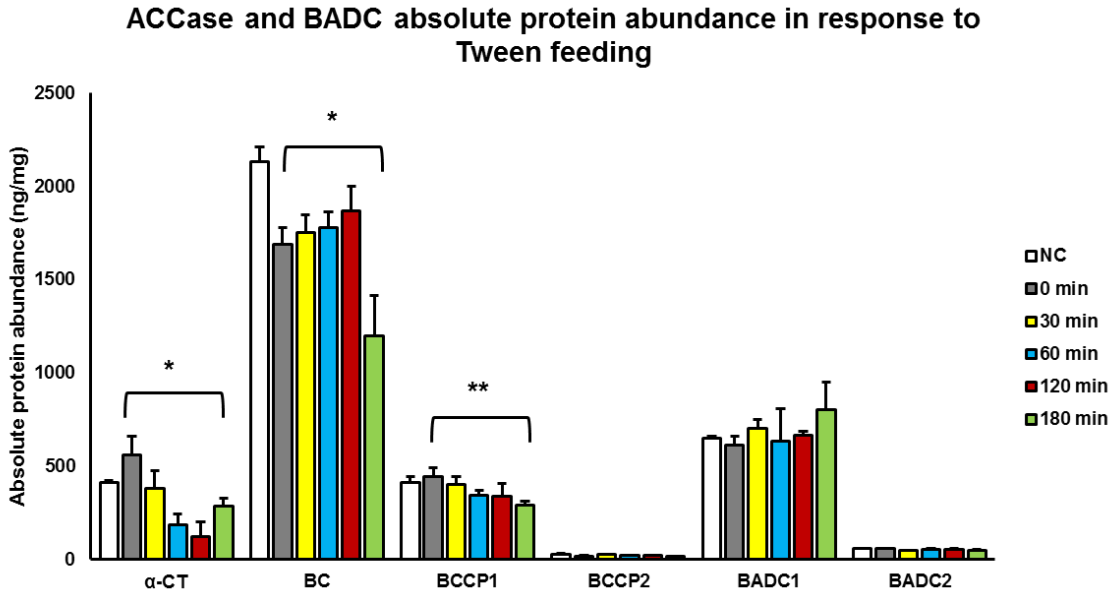

Figure 21. Protein abundance profiles of ACCase and BADC in response to Tween feeding. *Arabidopsis* suspension cells were fed with 10 mM Tween and collected after 0, 30, 60, 120, and 180 min. A negative control (NC) is included in which media containing 0 mM Tween was added and cells were collected 180 min after addition. Statistical significance was determined using a paired, two-tailed, student's t-test between the 0 and 180 minute time points. * indicates p-value ≤ 0.05. ** indicates p-value ≤ 0.01.

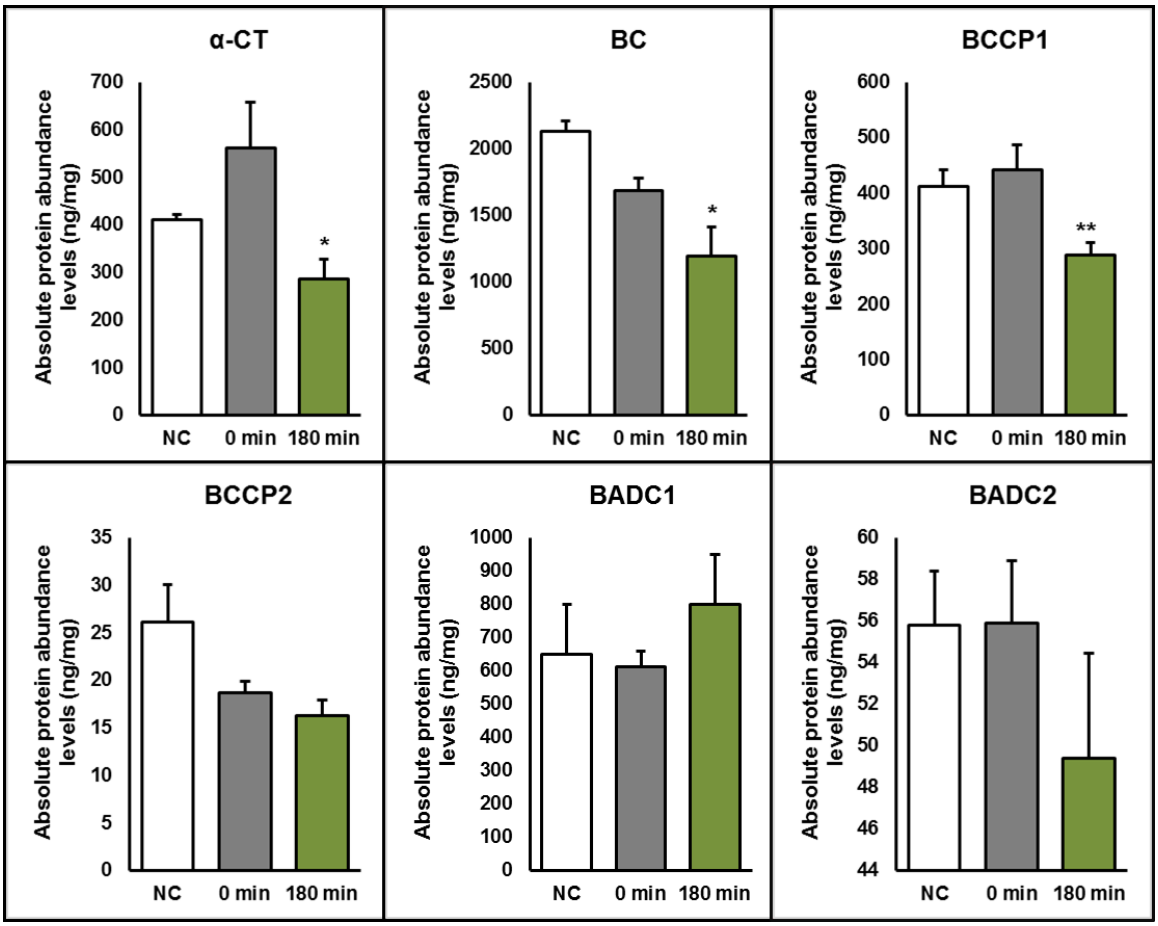

Figure 22. Individual protein abundance profiles for ACCase and BADC in response to Tween feeding. Protein abundance values are plotted for 0 mM Tween negative control at 180 min (NC), 0 min, and 180 min time points after 10 mM Tween feeding. Four biological replicates were analyzed per time point. Statistical significance was determined using a paired, two-tailed, student's t-test. * indicates p-value ≤ 0.05. ** indicates p-value ≤ 0.01.

Comparison of BCCP and BADC protein abundance in response to fatty acid replete media

One of the goals of this study was to quantitatively monitor stoichiometric changes in BCCP and BADC protein abundance to gain information regarding the potential for BADC and BCCP to have opposing regulation. Therefore, the

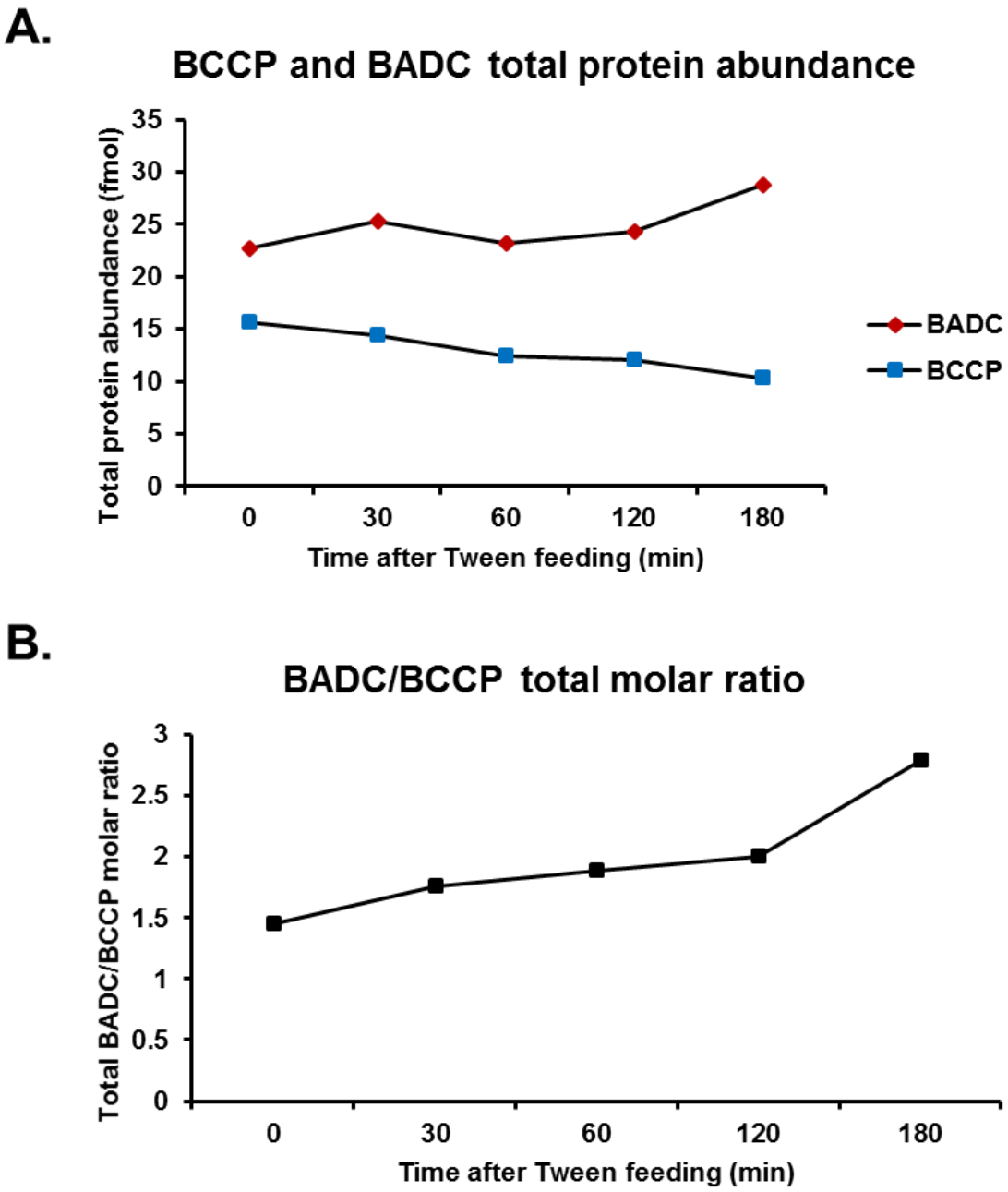

Figure 23. Comparison of BCCP and BADC total absolute protein abundance levels in response to Tween feeding. A) Total protein expression levels of BCCP and BADC over a time course (0, 30, 60, 120, 180 min) after 10 mM Tween feeding. B) Stoichiometric ratio of BADC abundance relative to BCCP abundance in response to 10 mM Tween feeding.

total BCCP and BADC abundance levels were quantified temporally in response to Tween feeding (Figure 23). This analysis revealed that while total BCCP protein abundance decreased over time after Tween feeding, total BADC protein abundance remained constant, or possibly increased slightly at 3 h (Figure 23A). When the ratios of BADC/BCCP total protein abundance were calculated, this ratio increased slightly two hours after Tween feeding and ultimately increased two-fold three hours after Tween feeding compared to the initial (0 min) time point and negative control (Figure 23B). These results indicate that BCCP protein abundance is down regulated in response to Tween feeding, while BADC abundance is unaltered or slightly enhanced.

ACCase and BADC protein abundance during Arabidopsis silique development

Protein was extracted from *Arabidopsis* developing siliques seven, nine, eleven, and thirteen days after flowering (DAF) and subjected to AQUA-MRM analysis. Recombinant protein correction factors were applied to the raw values to obtain the accurate absolute abundance of each protein using the line equation in Table 4 of Chapter 3 as described above. The absolute protein abundance of each ACCase subunit and BADC protein, with the exception of β-CT and BADC3, which were below the limit of detection, was plotted for each time point (Figure 24).

Absolute protein quantitation of ACCase subunits indicated a significant increase in both BCCP2 (p-value: 0.03*) and BC (p-value: 0.02*) protein

abundance in the eleven DAF siliques relative to seven DAF siliques (Figure 24). In general, α-CT, BCCP1, and BCCP2 protein abundance profiles resembled bell-shaped curves along the stages of development, while BC abundance increased linearly. Interestingly, α-CT was up to 75% and 90% less abundant than the total BCCP and BC subunits, respectively. Protein abundance of BADC1 and BADC2 was stable during silique development.

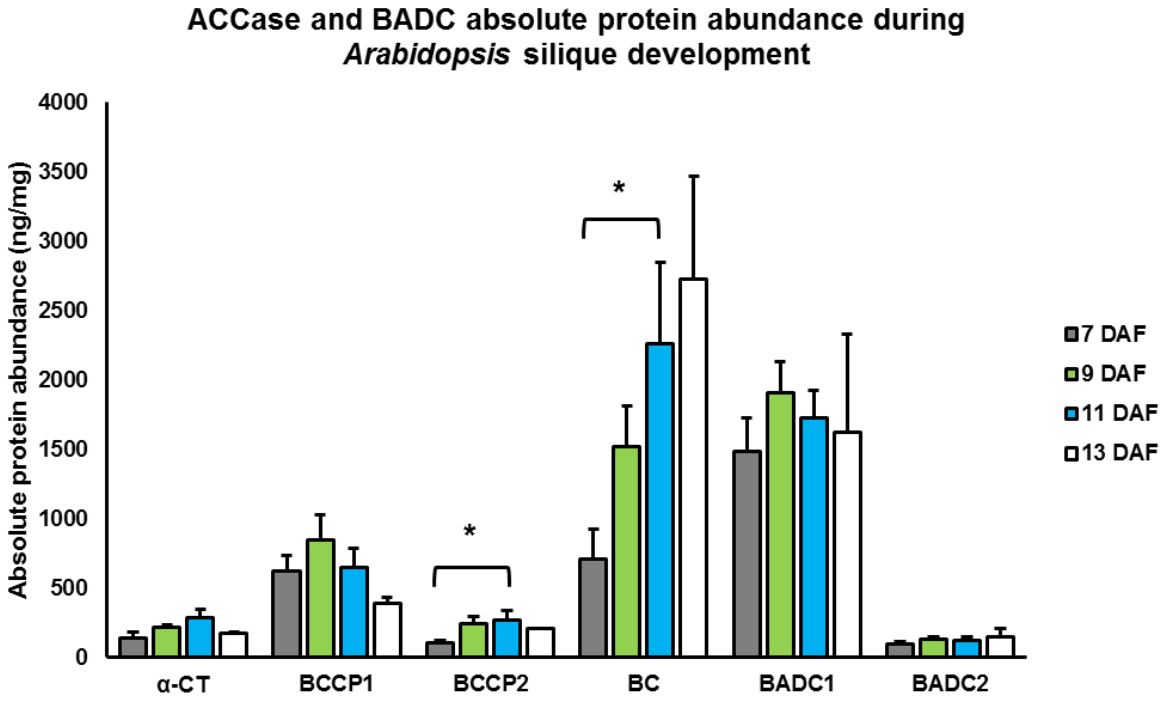

Figure 24. Protein abundance profiles for ACCase and BADC during *Arabidopsis* silique development. Values are plotted for stages of silique development 7, 9, 11, and 13 days after flowering (DAF). The graph is representative of three biological replicates. Statistical significance was determined using a paired, two-tailed, student's t-test. * indicates p-value ≤ 0.05.

Stoichiometric changes in BCCP and BADC protein abundance

To investigate the relationship between BADC and BCCP protein abundance during seed development, BCCP and BADC isoforms were quantified. BCCP1 abundance was six-fold higher than that of BCCP2 at early stages of development, and only two-fold higher at later stages of development. This result suggests that BCCP1 is the primary isoform for ACCase activity at early stages of development, while BCCP2 takes on a greater role at later stages of development. Comparison of BADC1 and BADC2 protein abundance revealed BADC1 was ten times more abundant than BADC2 during all stages of development. The transcript levels for BADC3, however, suggest this isoform is even more abundant than BADC1, however, the protein was not quantified.

The total protein abundance of BADC and BCCP isoforms during silique development revealed BADC was relatively constant with slightly higher values at nine DAF, while BCCP abundance was highest around nine DAF and decreased two-fold at thirteen DAF (Figure 25A). The ratios of BADC to BCCP revealed BADC protein abundance was two times higher than that of BCCP at seven DAF and three times higher at thirteen DAF (Figure 25B). This suggests that the stoichiometry of BADC and BCCP isoforms is altered during silique development, which could have regulatory implications for the ACCase complex. It is necessary to collect BADC3 data, however, to fully characterize this possibility.

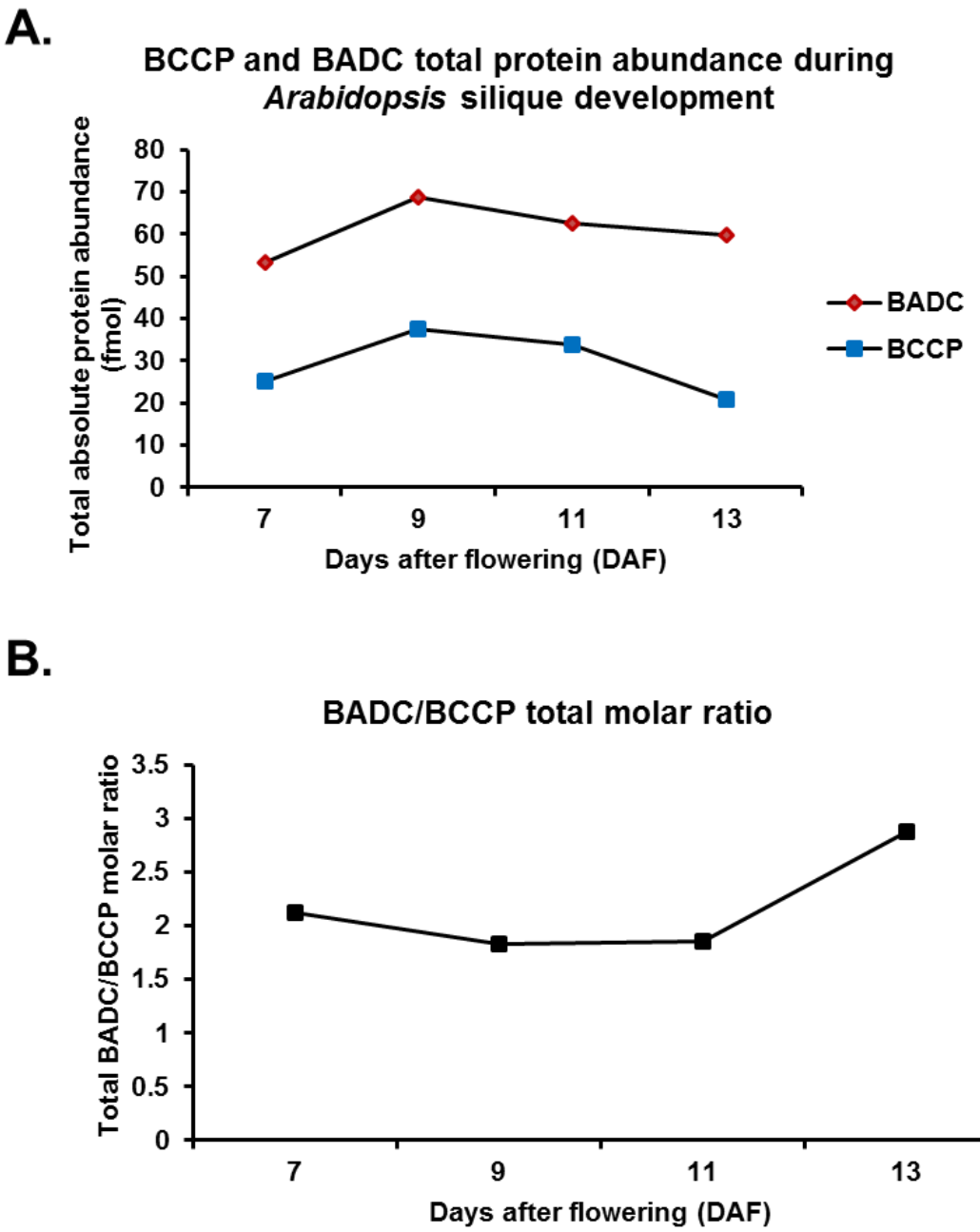

Figure 25. Comparison of total BCCP and BADC absolute protein abundance levels during *Arabidopsis* silique development. A) Total protein abundance of BCCP and BADC during silique development. B) Stoichiometric ratio of BADC abundance relative to BCCP abundance during silique development. Values are plotted for silique stages of development 7, 9, 11, and 13 days after flowering (DAF).

Comparison of protein abundance and transcript expression during Arabidopsis silique development

To determine the relationship between protein abundance and transcript expression during *Arabidopsis* silique development, comparisons were performed using qPCR analysis performed in parallel at even-day stages of development (6, 8, 10, 12, and 14 DAF) and previously published microarray data, which analyzed seeds at odd-day stages of development identical to the proteomics data (56). The normalized transcript expression from the microarray and qPCR analysis was overlaid with absolute protein abundance. The protein abundance and microarray expression were plotted as values relative to the seven DAF stage of development, while the qPCR expression was plotted as values relative to the six DAF stage of development (Figure 26).

Results from this comparison revealed that BCCP1 was the only subunit for which protein and microarray expression correlated at all stages of development, both peaking at nine DAF. However, the qPCR expression for BCCP1 increased at eight DAF and remained relatively constant. The discrepancy between the microarray and qPCR data could be due to the fact that qPCR monitored siliques while microarrays assayed dissected seed. BCCP2 microarray and qPCR expression correlated and displayed a similar trend to the protein abundance, however, both the microarray and qPCR expression decreased at earlier stages of development than protein abundance. Furthermore, BC protein abundance and microarray expression correlated from seven to nine DAF, before transcript decreased while protein expression

continued to increase linearly at later stages of development. In general, qPCR analysis of BC expression did not display significant changes during development. The α-CT transcript expression peaked at nine and ten DAF in the microarray and qPCR analysis, respectively, while the protein abundance peaked at eleven DAF. These results suggest that α-CT could experience a lag in translation during silique development and higher rates of protein turnover at later stages of development. BADC1 microarray and protein abundance correlated until the last stage of development, in which transcript levels decreased rapidly compared to protein. BADC1 transcript expression from the qPCR analysis, however, increased linearly after the eight DAF stage and decreased at the thirteen DAF stage. BADC2 protein weakly correlated with microarray analysis, however, protein abundance and qPCR expression did correlate but remained relatively unchanged during development. The transcript expression from the qPCR and microarray analyses did not correlate at all stages of development for many of the genes. However, it is notable that the qPCR analysis was performed with developing siliques, while the microarray analysis was performed with developing seed, which could be one cause of the observed variation in expression.

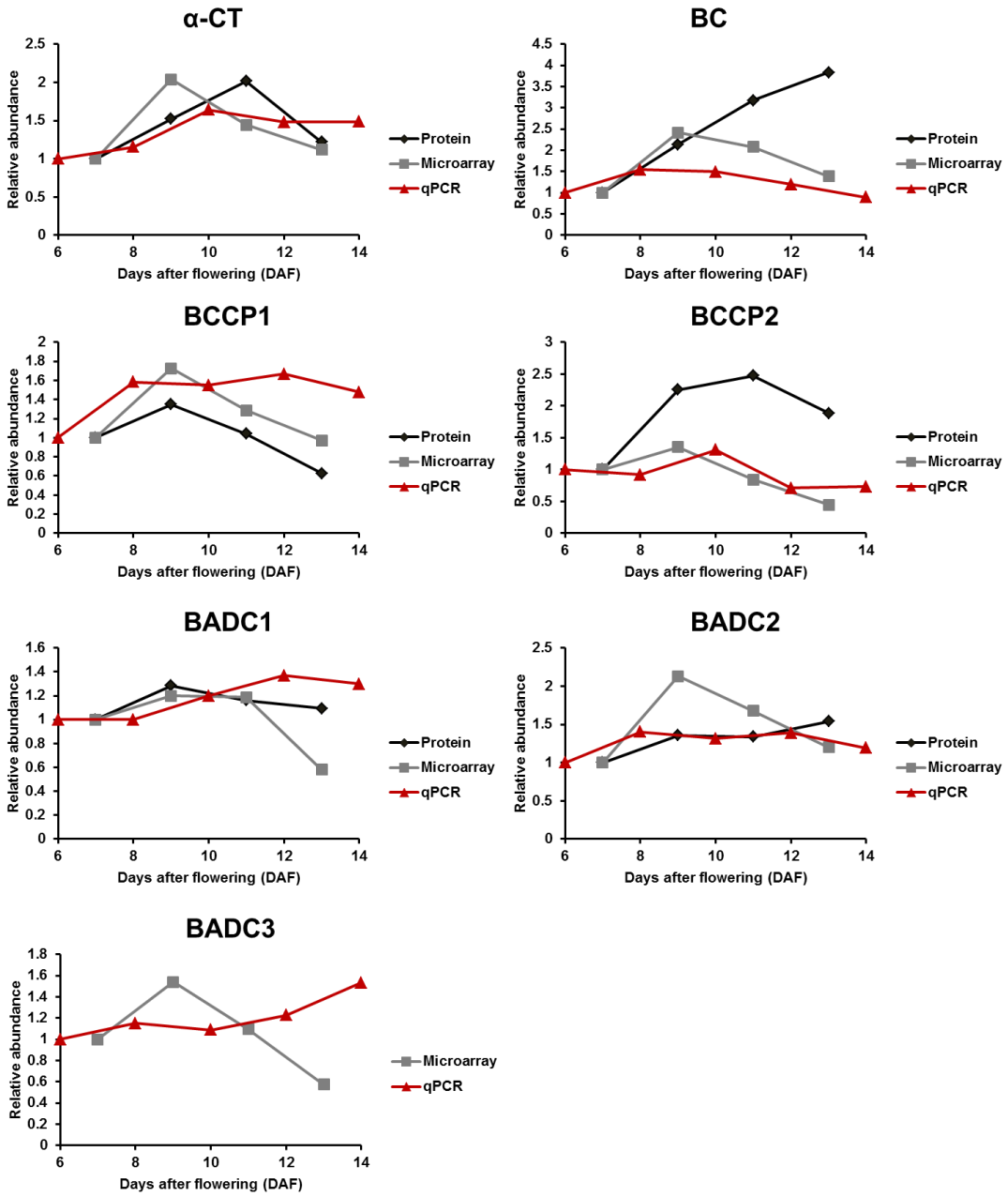

Figure 26. Comparison of relative protein abundance with transcript expression during *Arabidopsis* silique and seed development. Protein (7, 9, 11, and 13 DAF), microarray (7, 9, 11, and 13 DAF), and qPCR (6, 8, 10, 12, and 14 DAF) are plotted as values relative to the 6 and 7 DAF stages of development. Protein quantitation and qPCR were performed in developing *Arabidopsis* siliques. Microarray analysis was performed previously with developing *Arabidopsis* seed (Hajduch et al., 2010).

Discussion

Previous studies demonstrated feedback inhibition of heteromeric ACCase in plant suspension cells after exogenous addition of oleic acid Tween esters (115,122). To determine if gene and protein expression are influenced by exogenous fatty acids, the absolute transcript and protein abundance of ACCase were monitored in *Arabidopsis* suspension cells over a time course of Tween 80 feeding.

To accomplish this, we applied an AQUA-MRM assay for simultaneous quantitative monitoring of absolute changes in protein abundance of all of the target proteins. Heavy-labeled AQUA peptides were designed against the target ACCase and BADC proteins, and MRM methods were optimized for each peptide (Chapter 3). Quantitative RT-PCR analysis was also performed on the same samples to compare changes in absolute transcript and protein levels.

Results revealed significant changes in some components of ACCase at the protein and transcript levels. First, α-CT, BC, and BCCP1 protein and transcript were significantly reduced three hours after Tween addition, suggesting heteromeric ACCase expression is down-regulated in response to Tween supplementation. BCCP2 displayed contrasting results, with no significant change in protein abundance and an increase in transcript expression after three hours of Tween feeding. However, BCCP2 was 30- and 20-fold less abundant than the BCCP1 isoform, in transcript and protein, respectively, confirming previous studies regarding the overall abundance of BCCP isoforms (122,123). One study demonstrated BCCP1 was expressed in all developing tissues of

Arabidopsis, while BCCP2 protein was only observed in developing seed and was two-fold less abundant than BCCP1 (122). Moreover, *Arabidopsis* BCCP2 knockout lines showed no effect on plant growth or fatty acid accumulation (123). Furthermore, expression of BCCP2 is controlled by the WRINKLED1 (WRI1) transcription factor (124,125). However, α-CT, BC, and BCCP1 appear to be under different transcriptional regulation, which could provide an additional explanation for the contrasting transcript and protein levels observed between BCCP2 and the other ACCase subunits.

The observed changes in transcript expression were much more pronounced than those of the protein abundance in response to Tween 80 feeding. However, this is not the first instance of poor correlation between transcript expression and protein abundance. For instance, a study of the relationship between transcript expression and protein abundance revealed poor statistical correlation of over 150 mRNAs and proteins in yeast cells (122). A later study performed in developing *Arabidopsis* seed displayed only a 56% concurrence between transcript and protein levels (56). Since ACCase is a protein complex, and the plastid stroma is not accessible to proteasome-mediated targeted protein degradation, it is expected that the half-lives of the protein subunits is above average. Therefore, protein changes are unlikely to mirror rapid transcriptional perturbations and could explain the large transcriptional response observed here in response to Tween. To wit, affecting the levels of stable proteins requires a dramatic transcriptional response. Thus,

the discrepancy between transcript and protein levels for the ACCase subunits may be due to a slow rate of protein turnover, coupled with a lag in translation.

In addition to the known catalytic subunits of ACCase, the newly-identified BADC subunits were also quantified at both the transcript and protein levels. Transcript levels of all three BADC isoforms increased over eight-fold with 3 h of Tween feeding, while BADC1 and BADC2 protein abundance was unchanged. Unfortunately, BADC3 protein abundance was below the limit of detection in the AQUA-MRM assays. Nevertheless, BADC3 transcript levels were obtained.

One of the primary goals of this study was to assess stoichiometric changes of BADC and BCCP proteins in response to fatty acid replete media. After observing the total abundance of BADC and BCCP proteins in the time course after Tween addition, it appears that BCCP protein abundance steadily decreases over time, while BADC abundance remains relatively constant and slightly increases at three hours (Figure 23A). This indicates that changes in BCCP abundance, as well as the other subunits, may affect the incorporation of BADC into the ACCase complex. Slight changes to each could have a collective effect on BADC/BCCP stoichiometry to promote BADC incorporation into holo ACCase. To demonstrate this, total BADC/BCCP abundance ratios were calculated over the course of 10 mM Tween feeding (Figure 23B). These results revealed a two-fold increase in the BADC/BCCP ratio three hours after 10 mM Tween treatment compared to the initial time point and negative control. This result suggests that the BADC/BCCP ratio could play a role in the down-

regulation of ACCase activity, and consequently, *de novo* FAS in response to cellular sensing of fatty acid replete media.

Changes in ACCase and BADC protein abundance were also quantified during *Arabidopsis* silique development. Previous studies have indicated bell-shaped patterns of expression for transcripts to the heteromeric ACCase subunits during the maturation phase of seed development (56,124), while seed oil accumulation displays a positive linear profile. For AQUA-MRM analysis, *Arabidopsis* siliques were collected at seven, nine, eleven, and thirteen DAF. A comparison was also performed using previously reported microarray data from seeds collected at seven, nine, eleven, and thirteen DAF (56) and qPCR at 6, 8, 10, 12, and 14 DAF.

The AQUA-MRM results revealed significant increases in BC and BCCP2 protein abundance at eleven DAF compared to the initial stage (seven DAF). BCCP1 protein abundance peaked at nine DAF, and similar to the results observed in the Tween feeding assays, BCCP1 protein abundance was 2-4-fold higher than that of BCCP2. This again suggests that BCCP1 is the dominant isoform involved in ACCase activity during seed development as previously noted (108,123). Furthermore, BADC protein abundance was relatively unchanged during silique development, and BADC1 abundance was ten-fold higher than that of BADC2 in all stages analyzed

Since the rates of protein turnover and synthesis of the ACCase subunits can affect coordination of complex formation, and ultimately, the overall activity of the complex during silique development, a comparison of protein abundance with

qPCR and previously-reported microarray analyses (56) was performed. Results from these comparisons indicated the majority of the ACCase subunits displayed relatively weak correlation of transcript and protein levels, which varied at different stages of development. Furthermore, the relative transcript levels of qPCR and microarray analysis displayed differences, which could be attributed to expression differences between developing siliques (used for protein and qPCR) and seed (microarray), or possibly variation in growth conditions between the two studies. Collectively, these comparisons suggest that steady state protein and transcript levels are discordant, which is likely a reflection of the rates of protein synthesis or turnover. These results could have implications for activity of the ACCase complex at different stages of silique development.

A secondary objective of this study was to compare the absolute levels of each ACCase subunit *in vivo*. These data represent steady state levels of each protein, and coupled to an understanding of ACCase quaternary structure, could allow for hypotheses about subunit stoichiometry and the possibility for excess "pools" of subunits. From structural models of the *E.coli* heteromeric ACCase we infer that the CT is comprised of a heterotetramer of α-CT and β-CT subunits. The composition of the BC-BCCP subcomplex has been demonstrated previously in *E. coli* as two BC subunits for every four BCCP subunits (1:2 ratio) (126), while an earlier report in soybean suggested the ratios of BC:BCCP are 1:1 (127). The absolute protein quantitation results from silique development indicated a 1:1 ratio of BC:BCCP at seven and nine DAF, and this ratio increased to 2:1 and 4:1 at eleven and thirteen DAF, respectively. Interestingly, the

Arabidopsis suspension cells also displayed a 4:1 (BC:BCCP) ratio at all time points analyzed. While this stoichiometric ratio is possible, it would mean BC is present in excess. However, the current assembly model does not account for the new subunit to ACCase, BADC, which also interacts with BC. When BADC and BCCP levels are summed, the ratio of BC:BCCP/BADC drops to 1:3 at seven DAF and 1:2 at nine DAF and increases to 2:3 and 1:1 at eleven and thirteen DAF, respectively. Although these ratios are expected to be even lower after addition of the BADC3 isoform, they are still a more accurate representation of the true stoichiometry of the ACCase complex during silique development. These results could ultimately present a new stoichiometric model for the BC-BCCP-BADC subcomplex, however, BADC3 would need to be included for this model to be complete.

The proteomics results also revealed quantitative information regarding abundance of the α-CT subunit. α-CT was approximately 75% less abundant than total BCCP at all developmental stages analyzed and up to 90% less abundant than BC. The α-CT subunit was also 75-90% lower than the other subunits of ACCase in the Tween feeding assays performed with *Arabidopsis* cell culture. However, the levels of β-CT will need to be quantified to determine if the abundance levels are comparable to α-CT, which would verify that the α-CT subunit is indeed “limiting.”

Stoichiometric changes to BADC and BCCP protein during silique development revealed BADC abundance was constant, while total BCCP abundance was highest at nine DAF and decreased over the later stages (Figure

25A). The observed ratios of BADC/BCCP total protein abundance indicated a 2:1 ratio at early stages of development and a 3:1 ratio BCCP at later stages of development (Figure 25B). These results suggest that BADC proteins could be incorporating into the ACCase complex at later stages of development.

CHAPTER V

SUMMARY

Since 14-3-3 implications in phosphorus stress have been reported (75,128), phenotypic analysis of *Arabidopsis* 14-3-3 χ T-DNA mutants was initially pursued from the perspective of this stress condition. These analyses revealed altered primary root lengths as well as primary root phosphate levels of 14-3-3 χ mutant lines in response to phosphate availability in the growth media, indicating the lack of 14-3-3 χ disrupts phosphate mobilization, ultimately leading to changes in root growth. As 14-3-3 interactions with plasma membrane H^+-ATPase (AHA) have been well-established in eukaryotes, further characterization of this phenotype was performed with a focus on AHA.

Both transcript and proteomic analysis of AHA in 14-3-3 χ mutant lines revealed altered expression when grown in phosphate-rich media. Furthermore, investigations of 14-3-3 χ interactions with AHA using co-immunoprecipitation assays established interactions in both phosphate-rich and phosphate-deficient media. Since AHA proteins have implications in phosphate stress adaptation (73) and are activated by 14-3-3s (26,47,79,85), it is likely that in the absence of 14-3-3 χ expression, other isoforms initiate the role of AHA activation. However, previous reports *in vitro* have demonstrated that AHA/14-3-3 association and subsequent activation is strongest with isoform χ (7,91), suggesting AHA

interactions with isoforms other than χ may result in lower activation. This provides an explanation for the observed altered expression of AHA in the 14-3-3 χ mutant lines, which would compensate for the reduced AHA activity. It can be speculated that up-regulation of AHA would presumably elevate the proton gradient across the plasma membrane, driving an increase of inorganic phosphate import into the root. A previous study reported increased root phosphate levels in soybean AHA overexpression lines (73), supporting the observed root phosphate phenotypes in *Arabidopsis* 14-3-3 χ mutant lines. Although these observed phenotypes are not directly related to seed development, AHA isoforms are expressed in the seed tissue (129), providing a plausible explanation for the high abundance of 14-3-3 proteins in seed development.

These established phenotypes for the 14-3-3 χ mutant lines were then used to investigate the effects of 14-3-3 χ phosphorylation *in vivo*. Stable expression of phosphomimetic 14-3-3 χ^{S72D} in the mutant background was unable to complement all phosphate-dependent phenotypes, while stable expression of the non-mutated 14-3-3 χ resulted complemented all phenotypes, suggesting phosphorylation at this Ser^{72} reduces the function of 14-3-3 χ.

Considering the altered activities observed for 14-3-3 χ^{S72D} both *in vitro* and *in vivo*, we hypothesized that phosphorylation of 14-3-3 χ was affecting interactions with client proteins either through dimer destabilization or altered structural conformation. A previous report indicated that 14-3-3 dimerization occurs between amino acid residues within the first four alpha helices of each

monomer (130). Interestingly, Ser^{72} of 14-3-3 χ is located within the third helix, indicating phosphorylation of this residue could result in destabilization of dimer formation. 14-3-3 χ^{S72D} dimerization was assessed using non-denaturing gel electrophoresis, which revealed a 12-fold increase in the monomer/dimer ratio compared to non-mutated 14-3-3 χ. Additionally, pull-down assays with 14-3-3 χ^{S72D} revealed a 77% reduction in interactions with *Arabidopsis* AHA, possibly attributed to the observed phenotypes in the phosphomimic transgenic lines.

In a search for regulatory proteins involved in malonyl-CoA formation for de novo fatty acid synthesis the BADC proteinswere discovered by co-immunoprecipitation assays using antibodies specific for different subunits of the heteromeric acetyl-CoA carboxylase complex (ACCase) (Salie et al., unpublished). ACCase is an enzyme complex that catalyzes the committed step of *de novo* fatty acid biosynthesis in the plastid and is comprised of four subunits, which work together to convert acetyl-CoA to malonyl-CoA. Interestingly, the BADC proteins resemble one of these subunits, biotin carboxyl carrier protein (BCCP), in size, sequence, and structure. However, a major difference between these proteins is that BADCs are not biotinylated unlike BCCPs. Since biotinylation is an essential component of ACCase activity, these observations provided the foundation for our hypothesis that BADC proteins could be inhibitors of the ACCase complex. We hypothesized that incorporation of BADC into the complex through displacement of BCCP would ultimately reduce the number of biotinylation sites available in the complex.

To further investigate this hypothesis we employed a targeted proteomics based approach called multiple reaction monitoring (MRM), coupled with the use of heavy-labeled AQUA peptides as internal standards to absolutely quantify proteins in biological samples. Using a triple quadrupole instrument enables targeting and isolation of specific precursor and fragment masses of interest, which allows for sensitive detection of low abundant peptides in a complex sample. By designing AQUA peptides for each ACCase subunit and BADC protein, we were able to develop a targeted assay to determine absolute changes in protein abundance of ACCase and BADC proteins, which could provide insight into BADC regulation of the ACCase complex.

AQUA-MRM method development involves rigorous steps of optimization to ensure reproducibility and accuracy of protein quantitation. These steps include assessment of retention times and fragmentation patterns, optimization of collision energies, and determination of linear ranges of detection for each target peptide. An accuracy evaluation was also performed using ACCase and BADC recombinant protein to obtain standard curves for each of the target peptides. This analysis determined the linear accuracy of each peptide and provided line equations which could be used as correction factors for protein quantitation in the biological analysis. Once developed, this method could then be used to test our hypothesis of BADC inhibition of ACCase in biologically-relevant experiments.

Monitoring BADC inhibition of ACCase, required the use of an experimental system in which ACCase inhibition had previously been established. One study had displayed feedback inhibition of ACCase after

addition of Tween esters to *Brassica napus* suspension cells (111). This study reported a 40% decrease in ACCase three hours after tween addition by monitoring fatty acid incorporation of ^{14}C-acetate. These results initiated development of a similar experiment in *Arabidopsis* suspension cells to quantify absolute changes in ACCase and BADC proteins in response to Tween feeding using our developed AQUA-MRM assay. We also performed a parallel quantitative RT-PCR analysis to determine changes in absolute transcript levels of the ACCase and BADC genes.

Results from this experiment indicated transcript expression drastically changed in response to Tween feeding compared to protein abundance levels. Slight changes in protein expression were observed after addition of Tween. In agreement with transcript levels, α-CT, BC, and BCCP1 protein decreased in response to Tween feeding, while BADC abundance did not change. However, transcript levels of all BADC genes were up-regulated in response to Tween feeding. Interestingly, total BADC protein abundance was relatively stable after Tween feeding, while total BCCP expression steadily decreased over time after Tween feeding. Furthermore, the overall stoichiometric ratio of BADC/BCCP expression increased two-fold, three hours after tween addition when compared to the initial time point. These observations of altered BADC/BCCP stoichiometry suggest BADC competition with BCCP in response to feedback inhibition.

In addition to feedback inhibition, changes in absolute protein abundance and transcript expression were quantified during *Arabidopsis* silique development. In general, these results revealed subtle changes in abundance

and expression profiles for the ACCase and BADC proteins, however, BCCP2 and BC protein abundance substantially increased eleven days after flowering (DAF) compared to the seven DAF time point. These expression trends were similar to other transcriptomics studies performed in developing seed (57,124). Furthermore, comparison of protein levels to qPCR analysis and microarray results from one of these reports (56) revealed insights into rates of protein synthesis and turnover for the ACCase subunits. Interestingly, α-CT abundance was up to 75% lower than the BCCP subunits and up to 90% less than the BC subunit, possibly indicating that this is a limiting subunit of the ACCase complex. However, β-CT abundance levels will need to be analyzed to confirm this observation.

Our investigation of the regulatory mechanisms of fatty acid production in oilseed species is not yet complete. The AQUA-MRM assay we developed for quantitation of the ACCase complex can be applied to study the stoichiometry of metabolic complexes, which may provide novel insights for metabolic engineering.

REFERENCE LIST

1. van Heusden, G. P., Griffiths, D. J., Ford, J. C., Chin, A. W. T. F., Schrader, P. A., Carr, A. M., and Steensma, H. Y. (1995) The 14-3-3 proteins encoded by the BMH1 and BMH2 genes are essential in the yeast Saccharomyces cerevisiae and can be replaced by a plant homologue. *European journal of biochemistry / FEBS* 229, 45-53
2. Yaffe, M. B., Rittinger, K., Volinia, S., Caron, P. R., Aitken, A., Leffers, H., Gamblin, S. J., Smerdon, S. J., and Cantley, L. C. (1997) The structural basis for 14-3-3:phosphopeptide binding specificity. *Cell* 91, 961-971
3. Coblitz, B., Shikano, S., Wu, M., Gabelli, S. B., Cockrell, L. M., Spieker, M., Hanyu, Y., Fu, H., Amzel, L. M., and Li, M. (2005) C-terminal recognition by 14-3-3 proteins for surface expression of membrane receptors. *The Journal of biological chemistry* 280, 36263-36272
4. Johnson, C., Crowther, S., Stafford, M. J., Campbell, D. G., Toth, R., and MacKintosh, C. (2010) Bioinformatic and experimental survey of 14-3-3-binding sites. *The Biochemical journal* 427, 69-78
5. Lambeck, I., Chi, J. C., Krizowski, S., Mueller, S., Mehlmer, N., Teige, M., Fischer, K., and Schwarz, G. (2010) Kinetic analysis of 14-3-3-inhibited Arabidopsis thaliana nitrate reductase. *Biochemistry* 49, 8177-8186
6. Ferl, R. J., Lu, G., and Bowen, B. W. (1994) Evolutionary implications of the family of 14-3-3 brain protein homologs in Arabidopsis thaliana. *Genetica* 92, 129-138
7. Pallucca, R., Visconti, S., Camoni, L., Cesareni, G., Melino, S., Panni, S., Torreri, P., and Aducci, P. (2014) Specificity of epsilon and non-epsilon isoforms of arabidopsis 14-3-3 proteins towards the H+-ATPase and other targets. *PloS one* 9, e90764
8. Taoka, K., Ohki, I., Tsuji, H., Furuita, K., Hayashi, K., Yanase, T., Yamaguchi, M., Nakashima, C., Purwestri, Y. A., Tamaki, S., Ogaki, Y., Shimada, C., Nakagawa, A., Kojima, C., and Shimamoto, K. (2011) 14-3-3 proteins act as intracellular receptors for rice Hd3a florigen. *Nature* 476, 332-335
9. Sehnke, P. C., Chung, H. J., Wu, K., and Ferl, R. J. (2001) Regulation of starch accumulation by granule-associated plant 14-3-3 proteins. *Proceedings of the National Academy of Sciences of the United States of America* 98, 765-770
10. Swatek, K. N., Wilson, R. S., Ahsan, N., Tritz, R. L., and Thelen, J. J. (2014) Multisite phosphorylation of 14-3-3 proteins by calcium-dependent protein kinases. *The Biochemical journal* 459, 15-25
11. Bunney, T. D., van Walraven, H. S., and de Boer, A. H. (2001) 14-3-3 protein is a regulator of the mitochondrial and chloroplast ATP synthase. *Proceedings of the National Academy of Sciences of the United States of America* 98, 4249-4254
12. Gampala, S. S., Kim, T. W., He, J. X., Tang, W., Deng, Z., Bai, M. Y., Guan, S., Lalonde, S., Sun, Y., Gendron, J. M., Chen, H., Shibagaki, N., Ferl, R. J., Ehrhardt, D., Chong, K., Burlingame, A. L., and Wang, Z. Y. (2007) An essential role for 14-3-3 proteins in brassinosteroid signal transduction in Arabidopsis. *Developmental cell* 13, 177-189
13. Igarashi, D., Ishida, S., Fukazawa, J., and Takahashi, Y. (2001) 14-3-3 proteins regulate intracellular localization of the bZIP transcriptional activator RSG. *The Plant cell* 13, 2483-2497

14. Ishida, S., Fukazawa, J., Yuasa, T., and Takahashi, Y. (2004) Involvement of 14-3-3 signaling protein binding in the functional regulation of the transcriptional activator REPRESSION OF SHOOT GROWTH by gibberellins. *The Plant cell* 16, 2641-2651
15. Swatek, K. N., Graham, K., Agrawal, G. K., and Thelen, J. J. (2011) The 14-3-3 isoforms chi and epsilon differentially bind client proteins from developing Arabidopsis seed. *Journal of proteome research* 10, 4076-4087
16. Paul, A. L., Sehnke, P. C., and Ferl, R. J. (2005) Isoform-specific subcellular localization among 14-3-3 proteins in Arabidopsis seems to be driven by client interactions. *Molecular biology of the cell* 16, 1735-1743
17. Gao, J., van Kleeff, P. J., Oecking, C., Li, K. W., Erban, A., Kopka, J., Hincha, D. K., and de Boer, A. H. (2014) Light modulated activity of root alkaline/neutral invertase involves the interaction with 14-3-3 proteins. *The Plant journal : for cell and molecular biology* 80, 785-796
18. Pan, S., Sehnke, P. C., Ferl, R. J., and Gurley, W. B. (1999) Specific interactions with TBP and TFIIB in vitro suggest that 14-3-3 proteins may participate in the regulation of transcription when part of a DNA binding complex. *The Plant cell* 11, 1591-1602
19. Lopez-Girona, A., Furnari, B., Mondesert, O., and Russell, P. (1999) Nuclear localization of Cdc25 is regulated by DNA damage and a 14-3-3 protein. *Nature* 397, 172-175
20. Brunet, A., Kanai, F., Stehn, J., Xu, J., Sarbassova, D., Frangioni, J. V., Dalal, S. N., DeCaprio, J. A., Greenberg, M. E., and Yaffe, M. B. (2002) 14-3-3 transits to the nucleus and participates in dynamic nucleocytoplasmic transport. *The Journal of cell biology* 156, 817-828
21. Ito, J., Heazlewood, J. L., and Millar, A. H. (2006) Analysis of the soluble ATP-binding proteome of plant mitochondria identifies new proteins and nucleotide triphosphate interactions within the matrix. *Journal of proteome research* 5, 3459-3469
22. May, T., and Soll, J. (2000) 14-3-3 proteins form a guidance complex with chloroplast precursor proteins in plants. *The Plant cell* 12, 53-64
23. Marra, M., Fullone, M. R., Fogliano, V., Pen, J., Mattei, M., Masi, S., and Aducci, P. (1994) The 30-kilodalton protein present in purified fusicoccin receptor preparations is a 14-3-3-like protein. *Plant physiology* 106, 1497-1501
24. Oecking, C., Eckerskorn, C., and Weiler, E. W. (1994) The fusicoccin receptor of plants is a member of the 14-3-3 superfamily of eukaryotic regulatory proteins. *FEBS letters* 352, 163-166
25. Fuglsang, A. T., Visconti, S., Drumm, K., Jahn, T., Stensballe, A., Mattei, B., Jensen, O. N., Aducci, P., and Palmgren, M. G. (1999) Binding of 14-3-3 protein to the plasma membrane H(+)-ATPase AHA2 involves the three C-terminal residues Tyr(946)-Thr-Val and requires phosphorylation of Thr(947). *The Journal of biological chemistry* 274, 36774-36780
26. Ottmann, C., Marco, S., Jaspert, N., Marcon, C., Schauer, N., Weyand, M., Vandermeeren, C., Duby, G., Boutry, M., Wittinghofer, A., Rigaud, J. L., and Oecking, C. (2007) Structure of a 14-3-3 coordinated hexamer of the plant plasma membrane H+ -ATPase by combining X-ray crystallography and electron cryomicroscopy. *Molecular cell* 25, 427-440
27. Assmann, S. M. (1993) Signal transduction in guard cells. *Annual review of cell biology* 9, 345-375
28. Kinoshita, T., and Shimazaki, K. (1999) Blue light activates the plasma membrane H(+)-ATPase by phosphorylation of the C-terminus in stomatal guard cells. *The EMBO journal* 18, 5548-5558

29. Sottocornola, B., Visconti, S., Orsi, S., Gazzarrini, S., Giacometti, S., Olivari, C., Camoni, L., Aducci, P., Marra, M., Abenavoli, A., Thiel, G., and Moroni, A. (2006) The potassium channel KAT1 is activated by plant and animal 14-3-3 proteins. *The Journal of biological chemistry* 281, 35735-35741
30. Sottocornola, B., Gazzarrini, S., Olivari, C., Romani, G., Valbuzzi, P., Thiel, G., and Moroni, A. (2008) 14-3-3 proteins regulate the potassium channel KAT1 by dual modes. *Plant Biol (Stuttg)* 10, 231-236
31. Bihler, H., Eing, C., Hebeisen, S., Roller, A., Czempinski, K., and Bertl, A. (2005) TPK1 is a vacuolar ion channel different from the slow-vacuolar cation channel. *Plant physiology* 139, 417-424
32. Latz, A., Becker, D., Hekman, M., Muller, T., Beyhl, D., Marten, I., Eing, C., Fischer, A., Dunkel, M., Bertl, A., Rapp, U. R., and Hedrich, R. (2007) TPK1, a Ca(2+)-regulated Arabidopsis vacuole two-pore K(+) channel is activated by 14-3-3 proteins. *The Plant journal : for cell and molecular biology* 52, 449-459
33. Latz, A., Mehlmer, N., Zapf, S., Mueller, T. D., Wurzinger, B., Pfister, B., Csaszar, E., Hedrich, R., Teige, M., and Becker, D. (2012) Salt stress triggers phosphorylation of the Arabidopsis vacuolar K+ channel TPK1 by calcium dependent protein kinases (CDPKs). *Molecular plant*
34. Mehlmer, N., Wurzinger, B., Stael, S., Hofmann-Rodrigues, D., Csaszar, E., Pfister, B., Bayer, R., and Teige, M. (2010) The Ca(2+)-dependent protein kinase CPK3 is required for MAPK-independent salt-stress acclimation in Arabidopsis. *The Plant journal : for cell and molecular biology*
35. Daugherty, C. J., Rooney, M. F., Miller, P. W., and Ferl, R. J. (1996) Molecular organization and tissue-specific expression of an Arabidopsis 14-3-3 gene. *The Plant cell* 8, 1239-1248
36. Schmid, M., Davison, T. S., Henz, S. R., Pape, U. J., Demar, M., Vingron, M., Scholkopf, B., Weigel, D., and Lohmann, J. U. (2005) A gene expression map of Arabidopsis thaliana development. *Nature genetics* 37, 501-506
37. Winter, D., Vinegar, B., Nahal, H., Ammar, R., Wilson, G. V., and Provart, N. J. (2007) An "Electronic Fluorescent Pictograph" browser for exploring and analyzing large-scale biological data sets. *PloS one* 2, e718
38. Diaz, C., Kusano, M., Sulpice, R., Araki, M., Redestig, H., Saito, K., Stitt, M., and Shin, R. (2011) Determining novel functions of Arabidopsis 14-3-3 proteins in central metabolic processes. *BMC systems biology* 5, 192
39. Lancien, M., and Roberts, M. R. (2006) Regulation of Arabidopsis thaliana 14-3-3 gene expression by gamma-aminobutyric acid. *Plant, cell & environment* 29, 1430-1436
40. Sato, T., Maekawa, S., Yasuda, S., Domeki, Y., Sueyoshi, K., Fujiwara, M., Fukao, Y., Goto, D. B., and Yamaguchi, J. (2011) Identification of 14-3-3 proteins as a target of ATL31 ubiquitin ligase, a regulator of the C/N response in Arabidopsis. *The Plant journal : for cell and molecular biology* 68, 137-146
41. Catala, R., Lopez-Cobollo, R., Mar Castellano, M., Angosto, T., Alonso, J. M., Ecker, J. R., and Salinas, J. (2014) The Arabidopsis 14-3-3 protein RARE COLD INDUCIBLE 1A links low-temperature response and ethylene biosynthesis to regulate freezing tolerance and cold acclimation. *The Plant cell* 26, 3326-3342
42. Mayfield, J. D., Folta, K. M., Paul, A. L., and Ferl, R. J. (2007) The 14-3-3 Proteins mu and upsilon influence transition to flowering and early phytochrome response. *Plant physiology* 145, 1692-1702

43. Kinoshita, T., and Shimazaki, K. (2001) Analysis of the phosphorylation level in guard-cell plasma membrane H+-ATPase in response to fusicoccin. *Plant & cell physiology* 42, 424-432
44. Tseng, T. S., and Briggs, W. R. (2010) The Arabidopsis rcn1-1 mutation impairs dephosphorylation of Phot2, resulting in enhanced blue light responses. *The Plant cell* 22, 392-402
45. Tseng, T. S., Whippo, C., Hangarter, R. P., and Briggs, W. R. (2012) The role of a 14-3-3 protein in stomatal opening mediated by PHOT2 in Arabidopsis. *The Plant cell* 24, 1114-1126
46. Oecking, C., Piotrowski, M., Hagemeier, J., and Hagemann, K. (1997) Topology and target interaction of the fusicoccin-binding 14-3-3 homologs of Commelina communis. *The Plant Journal* 12, 441-453
47. Alsterfjord, M., Sehnke, P. C., Arkell, A., Larsson, H., Svennelid, F., Rosenquist, M., Ferl, R. J., Sommarin, M., and Larsson, C. (2004) Plasma membrane H(+)-ATPase and 14-3-3 isoforms of Arabidopsis leaves: evidence for isoform specificity in the 14-3-3/H(+)-ATPase interaction. *Plant & cell physiology* 45, 1202-1210
48. Huber, S. C., Huber, J. L., Campbell, W. H., and Redinbaugh, M. G. (1992) Comparative studies of the light modulation of nitrate reductase and sucrose-phosphate synthase activities in spinach leaves. *Plant physiology* 100, 706-712
49. Bachmann, M., Huber, J. L., Athwal, G. S., Wu, K., Ferl, R. J., and Huber, S. C. (1996) 14-3-3 proteins associate with the regulatory phosphorylation site of spinach leaf nitrate reductase in an isoform-specific manner and reduce dephosphorylation of Ser-543 by endogenous protein phosphatases. *FEBS letters* 398, 26-30
50. Mayfield, J. D., Paul, A. L., and Ferl, R. J. (2012) The 14-3-3 proteins of Arabidopsis regulate root growth and chloroplast development as components of the photosensory system. *Journal of experimental botany* 63, 3061-3070
51. Brechenmacher, L., Kim, M. Y., Benitez, M., Li, M., Joshi, T., Calla, B., Lee, M. P., Libault, M., Vodkin, L. O., Xu, D., Lee, S. H., Clough, S. J., and Stacey, G. (2008) Transcription profiling of soybean nodulation by Bradyrhizobium japonicum. *Molecular plant-microbe interactions : MPMI* 21, 631-645
52. Radwan, O., Wu, X., Govindarajulu, M., Libault, M., Neece, D. J., Oh, M. H., Berg, R. H., Stacey, G., Taylor, C. G., Huber, S. C., and Clough, S. J. (2012) 14-3-3 proteins SGF14c and SGF14l play critical roles during soybean nodulation. *Plant physiology* 160, 2125-2136
53. He, Y., Wu, J., Lv, B., Li, J., Gao, Z., Xu, W., Baluska, F., Shi, W., Shaw, P. C., and Zhang, J. (2015) Involvement of 14-3-3 protein GRF9 in root growth and response under polyethylene glycol-induced water stress. *Journal of experimental botany* 66, 2271-2281
54. van Kleeff, P. J., Jaspert, N., Li, K. W., Rauch, S., Oecking, C., and de Boer, A. H. (2014) Higher order Arabidopsis 14-3-3 mutants show 14-3-3 involvement in primary root growth both under control and abiotic stress conditions. *Journal of experimental botany* 65, 5877-5888
55. Mayank, P., Grossman, J., Wuest, S., Boisson-Dernier, A., Roschitzki, B., Nanni, P., Nuhse, T., and Grossniklaus, U. (2012) Characterization of the phosphoproteome of mature Arabidopsis pollen. *The Plant journal : for cell and molecular biology* 72, 89-101
56. Hajduch, M., Hearne, L. B., Miernyk, J. A., Casteel, J. E., Joshi, T., Agrawal, G. K., Song, Z., Zhou, M., Xu, D., and Thelen, J. J. (2010) Systems analysis of seed filling in Arabidopsis: using general linear modeling to assess concordance of transcript and protein expression. *Plant physiology* 152, 2078-2087

57. Agrawal, G. K., and Thelen, J. J. (2006) Large scale identification and quantitative profiling of phosphoproteins expressed during seed filling in oilseed rape. *Molecular & cellular proteomics : MCP* 5, 2044-2059
58. Dou, Y., Liu, X., Yin, Y., Han, S., Lu, Y., Liu, Y., and Hao, D. (2015) Affinity chromatography revealed insights into unique functionality of two 14-3-3 protein species in developing maize kernels. *Journal of proteomics* 114, 274-286
59. Hajduch, M., Casteel, J. E., Tang, S., Hearne, L. B., Knapp, S., and Thelen, J. J. (2007) Proteomic analysis of near-isogenic sunflower varieties differing in seed oil traits. *Journal of proteome research* 6, 3232-3241
60. Shin, R., Alvarez, S., Burch, A. Y., Jez, J. M., and Schachtman, D. P. (2007) Phosphoproteomic identification of targets of the Arabidopsis sucrose nonfermenting-like kinase SnRK2.8 reveals a connection to metabolic processes. *Proceedings of the National Academy of Sciences of the United States of America* 104, 6460-6465
61. Benschop, J. J., Mohammed, S., O'Flaherty, M., Heck, A. J., Slijper, M., and Menke, F. L. (2007) Quantitative phosphoproteomics of early elicitor signaling in Arabidopsis. *Molecular & cellular proteomics : MCP* 6, 1198-1214
62. Jones, A. M., MacLean, D., Studholme, D. J., Serna-Sanz, A., Andreasson, E., Rathjen, J. P., and Peck, S. C. (2009) Phosphoproteomic analysis of nuclei-enriched fractions from Arabidopsis thaliana. *Journal of proteomics* 72, 439-451
63. Nakagami, H., Sugiyama, N., Mochida, K., Daudi, A., Yoshida, Y., Toyoda, T., Tomita, M., Ishihama, Y., and Shirasu, K. (2010) Large-scale comparative phosphoproteomics identifies conserved phosphorylation sites in plants. *Plant physiology* 153, 1161-1174
64. Reiland, S., Messerli, G., Baerenfaller, K., Gerrits, B., Endler, A., Grossmann, J., Gruissem, W., and Baginsky, S. (2009) Large-scale Arabidopsis phosphoproteome profiling reveals novel chloroplast kinase substrates and phosphorylation networks. *Plant physiology* 150, 889-903
65. Sugiyama, N., Nakagami, H., Mochida, K., Daudi, A., Tomita, M., Shirasu, K., and Ishihama, Y. (2008) Large-scale phosphorylation mapping reveals the extent of tyrosine phosphorylation in Arabidopsis. *Molecular systems biology* 4, 193
66. Lachaud, C., Prigent, E., Thuleau, P., Grat, S., Da Silva, D., Briere, C., Mazars, C., and Cotelle, V. (2013) 14-3-3-regulated Ca(2+)-dependent protein kinase CPK3 is required for sphingolipid-induced cell death in Arabidopsis. *Cell death and differentiation* 20, 209-217
67. Denison, F. C., Gokirmak, T., and Ferl, R. J. (2014) Phosphorylation-related modification at the dimer interface of 14-3-3omega dramatically alters monomer interaction dynamics. *Archives of biochemistry and biophysics* 541, 1-12
68. Fuller, B., Stevens, S. M., Jr., Sehnke, P. C., and Ferl, R. J. (2006) Proteomic analysis of the 14-3-3 family in Arabidopsis. *Proteomics* 6, 3050-3059
69. Poirier, Y., and Bucher, M. (2002) Phosphate transport and homeostasis in Arabidopsis. *The Arabidopsis book / American Society of Plant Biologists* 1, e0024
70. Hernandez, G., Ramirez, M., Valdes-Lopez, O., Tesfaye, M., Graham, M. A., Czechowski, T., Schlereth, A., Wandrey, M., Erban, A., Cheung, F., Wu, H. C., Lara, M., Town, C. D., Kopka, J., Udvardi, M. K., and Vance, C. P. (2007) Phosphorus stress in common bean: root transcript and metabolic responses. *Plant physiology* 144, 752-767
71. Raghothama, K. G. (2000) Phosphate transport and signaling. *Current opinion in plant biology* 3, 182-187

72. Karthikeyan, A. S., Varadarajan, D. K., Mukatira, U. T., D'Urzo, M. P., Damsz, B., and Raghothama, K. G. (2002) Regulated expression of Arabidopsis phosphate transporters. *Plant physiology* 130, 221-233
73. Shen, H., Chen, J., Wang, Z., Yang, C., Sasaki, T., Yamamoto, Y., Matsumoto, H., and Yan, X. (2006) Root plasma membrane H+-ATPase is involved in the adaptation of soybean to phosphorus starvation. *Journal of experimental botany* 57, 1353-1362
74. Cao, A., Jain, A., Baldwin, J. C., and Raghothama, K. G. (2007) Phosphate differentially regulates 14-3-3 family members and GRF9 plays a role in Pi-starvation induced responses. *Planta* 226, 1219-1230
75. Xu, W., Shi, W., Jia, L., Liang, J., and Zhang, J. (2012) TFT6 and TFT7, two different members of tomato 14-3-3 gene family, play distinct roles in plant adaption to low phosphorus stress. *Plant, cell & environment* 35, 1393-1406
76. Toroser, D., Athwal, G. S., and Huber, S. C. (1998) Site-specific regulatory interaction between spinach leaf sucrose-phosphate synthase and 14-3-3 proteins. *FEBS letters* 435, 110-114
77. Moorhead, G., Douglas, P., Morrice, N., Scarabel, M., Aitken, A., and MacKintosh, C. (1996) Phosphorylated nitrate reductase from spinach leaves is inhibited by 14-3-3 proteins and activated by fusicoccin. *Current biology : CB* 6, 1104-1113
78. Baunsgaard, L., Fuglsang, A. T., Jahn, T., Korthout, H. A., de Boer, A. H., and Palmgren, M. G. (1998) The 14-3-3 proteins associate with the plant plasma membrane H(+)-ATPase to generate a fusicoccin binding complex and a fusicoccin responsive system. *The Plant journal : for cell and molecular biology* 13, 661-671
79. Jaspert, N., and Oecking, C. (2002) Regulatory 14-3-3 proteins bind the atypical motif within the C terminus of the plant plasma membrane H(+)-ATPase via their typical amphipathic groove. *Planta* 216, 136-139
80. Olsson, A., Svennelid, F., Ek, B., Sommarin, M., and Larsson, C. (1998) A phosphothreonine residue at the C-terminal end of the plasma membrane H+-ATPase is protected by fusicoccin-induced 14-3-3 binding. *Plant physiology* 118, 551-555
81. Svennelid, F., Olsson, A., Piotrowski, M., Rosenquist, M., Ottman, C., Larsson, C., Oecking, C., and Sommarin, M. (1999) Phosphorylation of Thr-948 at the C terminus of the plasma membrane H(+)-ATPase creates a binding site for the regulatory 14-3-3 protein. *The Plant cell* 11, 2379-2391
82. Fuglsang, A. T., Borch, J., Bych, K., Jahn, T. P., Roepstorff, P., and Palmgren, M. G. (2003) The binding site for regulatory 14-3-3 protein in plant plasma membrane H+-ATPase: involvement of a region promoting phosphorylation-independent interaction in addition to the phosphorylation-dependent C-terminal end. *The Journal of biological chemistry* 278, 42266-42272
83. Camoni, L., Iori, V., Marra, M., and Aducci, P. (2000) Phosphorylation-dependent interaction between plant plasma membrane H(+)-ATPase and 14-3-3 proteins. *The Journal of biological chemistry* 275, 9919-9923
84. Fullone, M. R., Visconti, S., Marra, M., Fogliano, V., and Aducci, P. (1998) Fusicoccin effect on the in vitro interaction between plant 14-3-3 proteins and plasma membrane H+-ATPase. *The Journal of biological chemistry* 273, 7698-7702
85. Jelich-Ottmann, C., Weiler, E. W., and Oecking, C. (2001) Binding of regulatory 14-3-3 proteins to the C terminus of the plant plasma membrane H+ -ATPpase involves part of its autoinhibitory region. *The Journal of biological chemistry* 276, 39852-39857

86. Giacometti, S., Camoni, L., Albumi, C., Visconti, S., De Michelis, M. I., and Aducci, P. (2004) Tyrosine phosphorylation inhibits the interaction of 14-3-3 proteins with the plant plasma membrane H+-ATPase. *Plant Biol (Stuttg)* 6, 422-431
87. Li, H., Wong, W. S., Zhu, L., Guo, H. W., Ecker, J., and Li, N. (2009) Phosphoproteomic analysis of ethylene-regulated protein phosphorylation in etiolated seedlings of Arabidopsis mutant ein2 using two-dimensional separations coupled with a hybrid quadrupole time-of-flight mass spectrometer. *Proteomics* 9, 1646-1661
88. Walhout, A. J., Temple, G. F., Brasch, M. A., Hartley, J. L., Lorson, M. A., van den Heuvel, S., and Vidal, M. (2000) GATEWAY recombinational cloning: application to the cloning of large numbers of open reading frames or ORFeomes. *Methods in enzymology* 328, 575-592
89. Earley, K. W., Haag, J. R., Pontes, O., Opper, K., Juehne, T., Song, K., and Pikaard, C. S. (2006) Gateway-compatible vectors for plant functional genomics and proteomics. *The Plant journal : for cell and molecular biology* 45, 616-629
90. Clough, S. J., and Bent, A. F. (1998) Floral dip: a simplified method for Agrobacterium-mediated transformation of Arabidopsis thaliana. *Plant Journal* 16, 735-743
91. Rosenquist, M., Sehnke, P., Ferl, R. J., Sommarin, M., and Larsson, C. (2000) Evolution of the 14-3-3 protein family: does the large number of isoforms in multicellular organisms reflect functional specificity? *Journal of molecular evolution* 51, 446-458
92. Yocum, A. K., and Chinnaiyan, A. M. (2009) Current affairs in quantitative targeted proteomics: multiple reaction monitoring-mass spectrometry. *Briefings in functional genomics & proteomics* 8, 145-157
93. Gerber, S. A., Rush, J., Stemman, O., Kirschner, M. W., and Gygi, S. P. (2003) Absolute quantification of proteins and phosphoproteins from cell lysates by tandem MS. *Proceedings of the National Academy of Sciences of the United States of America* 100, 6940-6945
94. Bakalarski, C. E., and Kirkpatrick, D. S. (2016) A Biologist's Field Guide to Multiplexed Quantitative Proteomics. *Molecular & cellular proteomics : MCP*
95. Brun, V., Masselon, C., Garin, J., and Dupuis, A. (2009) Isotope dilution strategies for absolute quantitative proteomics. *Journal of proteomics* 72, 740-749
96. Rifai, N., Gillette, M. A., and Carr, S. A. (2006) Protein biomarker discovery and validation: the long and uncertain path to clinical utility. *Nature biotechnology* 24, 971-983
97. Yocum, A. K., Gratsch, T. E., Leff, N., Strahler, J. R., Hunter, C. L., Walker, A. K., Michailidis, G., Omenn, G. S., O'Shea, K. S., and Andrews, P. C. (2008) Coupled global and targeted proteomics of human embryonic stem cells during induced differentiation. *Molecular & cellular proteomics : MCP* 7, 750-767
98. Jenkins, R. E., Kitteringham, N. R., Hunter, C. L., Webb, S., Hunt, T. J., Elsby, R., Watson, R. B., Williams, D., Pennington, S. R., and Park, B. K. (2006) Relative and absolute quantitative expression profiling of cytochromes P450 using isotope-coded affinity tags. *Proteomics* 6, 1934-1947
99. Tao, H., Zhang, Y., Cao, X., Deng, Z., and Liu, T. (2016) Absolute quantification of proteins in the fatty acid biosynthetic pathway using protein standard absolute quantification. *Synthetic and Systems Biotechnology*
100. Lange, V., Picotti, P., Domon, B., and Aebersold, R. (2008) Selected reaction monitoring for quantitative proteomics: a tutorial. *Molecular systems biology* 4, 222-222
101. Trauchessec, M., Jaquinod, M., Bonvalot, A., Brun, V., Bruley, C., Ropers, D., de Jong, H., Garin, J., Bestel-Corre, G., and Ferro, M. (2014) Mass spectrometry-based workflow for

accurate quantification of Escherichia coli enzymes: how proteomics can play a key role in metabolic engineering. *Molecular & cellular proteomics : MCP* 13, 954-968
102. Davis, M. S., Solbiati, J., and Cronan, J. E., Jr. (2000) Overproduction of acetyl-CoA carboxylase activity increases the rate of fatty acid biosynthesis in Escherichia coli. *The Journal of biological chemistry* 275, 28593-28598
103. Desai, P. N., Shrivastava, N., and Padh, H. (2010) Production of heterologous proteins in plants: Strategies for optimal expression. *Biotechnology advances* 28, 427-435
104. Thelen, J. J., and Ohlrogge, J. B. (2002) Metabolic engineering of fatty acid biosynthesis in plants. *Metab Eng* 4, 12-21
105. Olsen, J. V., Ong, S. E., and Mann, M. (2004) Trypsin cleaves exclusively C-terminal to arginine and lysine residues. *Molecular & cellular proteomics : MCP* 3, 608-614
106. Swaney, D. L., Wenger, C. D., and Coon, J. J. (2010) The value of using multiple proteases for large-scale mass spectrometry-based proteomics. *Journal of proteome research* 9, 1323-1329
107. Liu, H., Zhang, J., Sun, H., Xu, C., Zhu, Y., and Xie, H. (2011) The Prediction of Peptide Charge States for Electrospray Ionization in Mass Spectrometry. *Procedia Environmental Sciences* 8, 483-491
108. Thelen, J. J., and Ohlrogge, J. B. (2002) Both antisense and sense expression of biotin carboxyl carrier protein isoform 2 inactivates the plastid acetyl-coenzyme A carboxylase in Arabidopsis thaliana. *Plant Journal* 32, 419-431
109. Kuhn, E., Wu, J., Karl, J., Liao, H., Zolg, W., and Guild, B. (2004) Quantification of C-reactive protein in the serum of patients with rheumatoid arthritis using multiple reaction monitoring mass spectrometry and 13C-labeled peptide standards. *Proteomics* 4, 1175-1186
110. Al Feteisi, H., Achour, B., Barber, J., and Rostami-Hodjegan, A. (2015) Choice of LC-MS Methods for the Absolute Quantification of Drug-Metabolizing Enzymes and Transporters in Human Tissue: a Comparative Cost Analysis. *The AAPS Journal* 17, 438-446
111. Andre, C., Haslam, R. P., and Shanklin, J. (2012) Feedback regulation of plastidic acetyl-CoA carboxylase by 18:1-acyl carrier protein in Brassica napus. *Proceedings of the National Academy of Sciences of the United States of America* 109, 10107-10112
112. Savage, L. J., and Ohlrogge, J. B. (1999) Phosphorylation of pea chloroplast acetyl-CoA carboxylase. *The Plant journal : for cell and molecular biology* 18, 521-527
113. Konishi, T., and Sasaki, Y. (1994) Compartmentalization of two forms of acetyl-CoA carboxylase in plants and the origin of their tolerance toward herbicides. *Proceedings of the National Academy of Sciences of the United States of America* 91, 3598-3601
114. Konishi, T., Shinohara, K., Yamada, K., and Sasaki, Y. (1996) Acetyl-CoA carboxylase in higher plants: most plants other than gramineae have both the prokaryotic and the eukaryotic forms of this enzyme. *Plant & cell physiology* 37, 117-122
115. Rocks, O., Peyker, A., Kahms, M., Verveer, P. J., Koerner, C., Lumbierres, M., Kuhlmann, J., Waldmann, H., Wittinghofer, A., and Bastiaens, P. I. (2005) An acylation cycle regulates localization and activity of palmitoylated Ras isoforms. *Science* 307, 1746-1752
116. Ohlrogge, J., Savage, L., Jaworski, J., Voelker, T., and Post-Beittenmiller, D. (1995) Alteration of acyl-acyl carrier protein pools and acetyl-CoA carboxylase expression in Escherichia coli by a plant medium chain acyl-acyl carrier protein thioesterase. *Archives of biochemistry and biophysics* 317, 185-190
117. Nikolau, B. J., and Hawke, J. C. (1984) Purification and characterization of maize leaf acetyl-coenzyme A carboxylase. *Archives of biochemistry and biophysics* 228, 86-96

118. Davis, M. S., and Cronan, J. E., Jr. (2001) Inhibition of Escherichia coli acetyl coenzyme A carboxylase by acyl-acyl carrier protein. *Journal of bacteriology* 183, 1499-1503
119. Jiang, P., and Cronan, J. E., Jr. (1994) Inhibition of fatty acid synthesis in Escherichia coli in the absence of phospholipid synthesis and release of inhibition by thioesterase action. *Journal of bacteriology* 176, 2814-2821
120. Shintani, D. K., and Ohlrogge, J. B. (1995) Feedback Inhibition of Fatty-Acid Synthesis in Tobacco Suspension Cells. *Plant Journal* 7, 577-587
121. Alonso, A. P., Piasecki, R. J., Wang, Y., LaClair, R. W., and Shachar-Hill, Y. (2010) Quantifying the labeling and the levels of plant cell wall precursors using ion chromatography tandem mass spectrometry. *Plant physiology* 153, 915-924
122. Shintani, D. K., and Ohlrogge, J. B. (1995) Feedback inhibition of fatty acid synthesis in tobacco suspension cells. *The Plant Journal* 7, 577-587
123. Ottmann, C., Yasmin, L., Weyand, M., Veesenmeyer, J. L., Diaz, M. H., Palmer, R. H., Francis, M. S., Hauser, A. R., Wittinghofer, A., and Hallberg, B. (2007) Phosphorylation-independent interaction between 14-3-3 and exoenzyme S: from structure to pathogenesis. *The EMBO journal* 26, 902-913
124. Subbaiah, C. C., Palaniappan, A., Duncan, K., Rhoads, D. M., Huber, S. C., and Sachs, M. M. (2006) Mitochondrial localization and putative signaling function of sucrose synthase in maize. *The Journal of biological chemistry* 281, 15625-15635
125. Muthusamy, B., Hanumanthu, G., Suresh, S., Rekha, B., Srinivas, D., Karthick, L., Vrushabendra, B. M., Sharma, S., Mishra, G., Chatterjee, P., Mangala, K. S., Shivashankar, H. N., Chandrika, K. N., Deshpande, N., Suresh, M., Kannabiran, N., Niranjan, V., Nalli, A., Prasad, T. S., Arun, K. S., Reddy, R., Chandran, S., Jadhav, T., Julie, D., Mahesh, M., John, S. L., Palvankar, K., Sudhir, D., Bala, P., Rashmi, N. S., Vishnupriya, G., Dhar, K., Reshma, S., Chaerkady, R., Gandhi, T. K., Harsha, H. C., Mohan, S. S., Deshpande, K. S., Sarker, M., and Pandey, A. (2005) Plasma Proteome Database as a resource for proteomics research. *Proteomics* 5, 3531-3536
126. Moreira, J. M., Shen, T., Ohlsson, G., Gromov, P., Gromova, I., and Celis, J. E. (2008) A combined proteome and ultrastructural localization analysis of 14-3-3 proteins in transformed human amnion (AMA) cells: definition of a framework to study isoform-specific differences. *Molecular & cellular proteomics : MCP* 7, 1225-1240
127. Janicka, S., and Augustyniak, H. (2006) [Multifunctional 14-3-3 proteins of plant cell]. *Postepy biochemii* 52, 303-312
128. Cao, A., Jain, A., Baldwin, J., and Raghothama, K. (2007) Phosphate differentially regulates 14-3-3 family members and GRF9 plays a role in Pi-starvation induced responses. *Planta* 226, 1219-1230
129. Harper, J. F., Manney, L., and Sussman, M. R. (1994) The plasma membrane H(+)-ATPase gene family in Arabidopsis: genomic sequence of AHA10 which is expressed primarily in developing seeds. *Molecular & general genetics : MGG* 244, 572-587
130. Gardino, A. K., Smerdon, S. J., and Yaffe, M. B. (2006) Structural determinants of 14-3-3 binding specificities and regulation of subcellular localization of 14-3-3-ligand complexes: a comparison of the X-ray crystal structures of all human 14-3-3 isoforms. *Seminars in cancer biology* 16, 173-182

VITA

Rashaun S. Wilson was born on October 15th, 1988, in Manhattan, KS to Gerri Balthazor and Cody Wilson. She received her Bachelors of Science in Biochemistry and Chemistry at Kansas State University in 2011 under the mentorship of Dr. Christopher Culbertson. She received a PhD in Biochemistry at the University of Missouri, Columbia in the spring of 2016 under the guidance of Dr. Jay Thelen. She will be continuing her scientific career as a postdoctoral associate at the Yale/NIDA Neuroproteomics Center in New Haven, CT.